Development of an electrochemical platform for the hemofiltration of platinum-based organometallic drugs

by

Adam Kolodziej

UNIVERSITY OF BIRMINGHAM

A thesis submitted to the University of Birmingham for the degree of

DOCTOR OF PHILOSOPHY

School of Chemistry

College of Engineering and Physical Sciences

University of Birmingham

August 2019

Abstract

Cancerous diseases remain a major threat to human population causing millions of deaths every year. Chemotherapy, being a major treatment method, lacks selectivity towards cancerous cells what causes severe side effect in patients who underwent this treatment. Lower quality of life after chemotherapy stimulated research on technologies that could eliminate some of these drawbacks, but no breakthrough has been achieved yet. The overall aim of this project is to develop a novel concept of the electrochemical hemofiltration system for the removal of platinum-based anti-cancer drugs. Since this PhD thesis represents the first approach to develop the electrochemical hemofiltration system, it is mostly composed of systematic studies of aspects that are of key importance for the successful and safe performance of the system.

The thesis is structured is the following way. Chapter 1 introduces a reader to the tackled problem and the state-of-the-art solutions. Chapter 2 presents the aims this thesis is aimed to accomplish. Chapter 3 includes a brief description of experimental techniques that were applied in the research project presents the aims this thesis is aimed to accomplish. Chapter 4 describes the electrochemical behaviour of cisplatin, a common anti-cancer drug, on the surface of gold. Chapter 5 describes factors that determine the stability of sulphur-based modifiers assembled on gold surface. Chapter 6 presents extensive studies on the coordination of cisplatin and other Pt-based molecules in both, homogeneous and heterogeneous phase. Finally, Chapter 7 concludes on the impact this work has on the electrochemical hemofiltration concept along with an insight into future directions of the project.

This thesis provides proof-of-concept experiments that show a great potential of surface-modified electrode in capturing and quantification of Pt-based drugs in physiological medium.

Acknowledgements

The preparation of this thesis would not have been possible without many people I am indebted to. Firstly, I would like to thank Dr. Paramaconi Rodriguez for the opportunity of joining his group and the great training I have received. It has been a 3 years long lesson of critical thinking, in-depth analysis and fundamental understanding of electrochemistry I have thoroughly enjoyed. I am also extremely grateful to my second supervisor, Dr. Francisco Fernandez-Trillo who has provided me with the excellent experience of looking at the electrochemistry from non-electrochemist perspective and exposure to the great world of polymer chemistry/microbiology.

I have been very fortunate to be surrounded to great colleagues in the laboratory as well as in the office. I am especially thankful to Javi Monzo for introducing me to the School of Chemistry, teaching me Spanish, and being a great support throughout these times. It would not be the same without the rest of the gang: Nacho Insua Lopez, Daniel Crisan, Nico Perez Soto, Oliver Creese, Zelu Brioso Jimenez, Manal Alanazi, Krystian Ubych, Matthew Lawrence, Carlos Guillen Posteguillo, Pavan Adoni, Tom Leigh, Yayun Pu, and Lizzie Sargeant. It has been a great pleasure to work with you.

Finally, I am very grateful to my family as I would not be where I am now without them. To my parents who have supported my enthusiasm for science since early days. To my wife, Aleksandra who has continuously motivated me and kept my lunchbox full. To my son, Mieszko, who has joined us at a very advanced stage of my PhD but totally changed my perspective on the undertaken research.

Table of content

Chapter 1: Introduction

1.1. Introduction to cancer treatment and challenges

Cancer is a group of diseases that is considered as a major threat to human population. According to the recent statistics released by the Cancer Research UK, there are over 360 000 of new cases of cancer every year in the UK. In the same time, 160 000 people die because of cancers, what stands for 28% of all deaths in the country.[1] On a global scale, there are over 14 million of new cases, and over 8 million of deaths caused by cancers. Fatal cases are mostly related to cancers of lung, liver, stomach, bowel – these account for almost 50 % of cancer-related deaths.[2]

The most straight-forward definition of a cancer is an abnormal cell growth.[3] It all starts with a single cell that was mutated, either due to genetic alterations or to exposure to carcinogens. This cell further divides to form more cells with altered properties[4, 5] what eventually leads to their domination among healthy cells[6].

Depending on the nature of cancer, different modes of treatment are available. In case of the least unfortunate benign tumour, surgery is the most feasible option as it removes tumour cells in a mechanical way. In case of malignant tumours, which are known to spread around body tissues, treatment options are more sophisticated and involve, but are not limited to following methods:

i) Radiation therapy – relies on the application of high doses of radiation that makes damage to DNA. It is non-specific towards cancer cells; therefore, it is usually applied locally. Cells exposed to radiation stop dividing and are removed from the body. The main drawback of radiation therapy is the radiation itself;

human body can tolerate only a limited dose of radiation, so in case of the cancer recovery an alternative treatment is often needed. Due to being non-specific, radiotherapy causes number of side-effects with no substantial impact on the quality of patient's life.[7]

ii) Immunotherapy – it is a new way of treating cancers that aims on aiding the immune system to fight the cancer out. It works through the injection of a substance that enhances the response of an immune system to a cancer via many mechanisms, such as better recognition of cancer cells.[8]

iii) Hormone therapy – it is used to treat certain types of cancer that use hormones to grow. It relies on the application of drugs that block production or change the behaviour of certain hormones, therefore, stopping cancer cells from further division. Side effects of this method are related to changes in hormone economy. [9]

iv) Chemotherapy – relies on the application of drugs that kill cell while they divide. There are many types of drugs that can fight different types of cancer. Chemotherapy is known to be versatile but also to cause severe side effects substantially affecting the quality of patients' life. Since chemotherapy is of paramount relevance to this thesis, it is discussed in more details in the following paragraph.[10]

The applicability of most used treatment methods towards different types of tumours is shown in Figure 1.1.

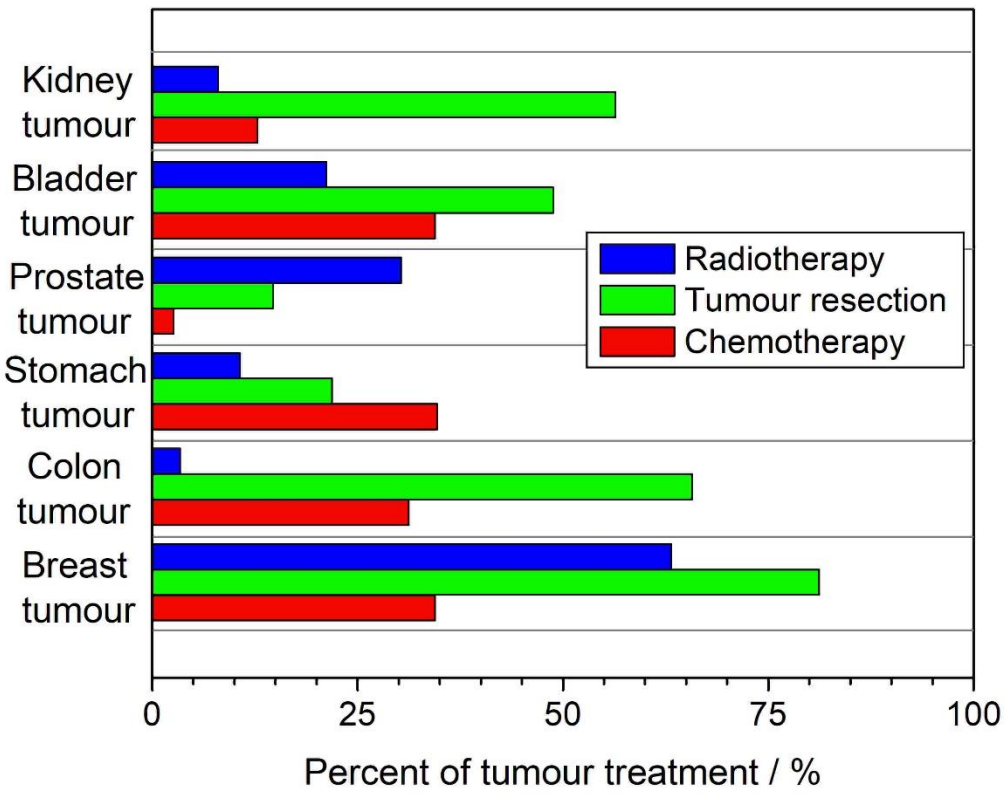

Figure 1.1. Statistical representation of methods used for the treatment of certain tumours. Data based on the report published by Cancer Research UK for the period of 2013 - 2014.[11]

1.1.1. Chemotherapy

The history of chemotherapy is dated back to the beginning of XX century when chemical warfare was used during two great World Wars.[12] It was found out that mustard gas and its nitrogen (nitrogen mustard) analogue have DNA crosslinking properties what results in the apoptosis (death) of quickly dividing cells.[13] It was first theorized, and later proven

clinically that mustard blue injected to a person suffering from a cancer results in a substantial reduction of cancer mass.[14]

Following years have brought a few advancements in the field, such as introduction of aminopterin, 6-mercaptopurine, fluorouracil or the concept of combination chemotherapy. Nevertheless, the breakthrough was achieved Barnett Rosenberg who studied the effect of electric field on the bacterial growth.[15] Initial promising results showed an inhibition of cell division. This was later attributed to the presence of Pt-containing species in the culture medium due to the electrochemical dissolution of Pt electrodes that were used to provide electric field.[16] This serendipitous result gave a rise to a brand-new family of anticancer drugs based on platinum.[17]

The first of Pt-based anticancer drugs, called cisplatin was approved for the use in humans in 1978.[18] The mechanism of action leading to the anticancer activity of cisplatin was extensively discussed in the literature.[19, 20] It all starts with an administration of the drug to the patient, what is followed by the diffusion of cisplatin and extensive binding to tissues based on sulphur-rich proteins. It is believed that a major part of a dose behaves this way, what leads to cisplatin inactivation and accumulation before it reaches cellular targets.

Since administered intravenously, cisplatin is carried through the body by blood with high chloride concentration (~ 100 mM). It allows cisplatin to reach outer cell walls in the non-dissociated form and enter cells via two mechanisms, passive or active diffusion (Fig. 1.2A).[21] Once inside cells, due to significantly lower concentration of chlorides (a few mM) cisplatin hydrolyses to form water-substituted analogues that bind to DNA and form many inter- and intra-strand adducts[22] based on DNA's building block, with a preference given to highly nucleophilic guanine and adenine (Fig. 1.2B).[23]

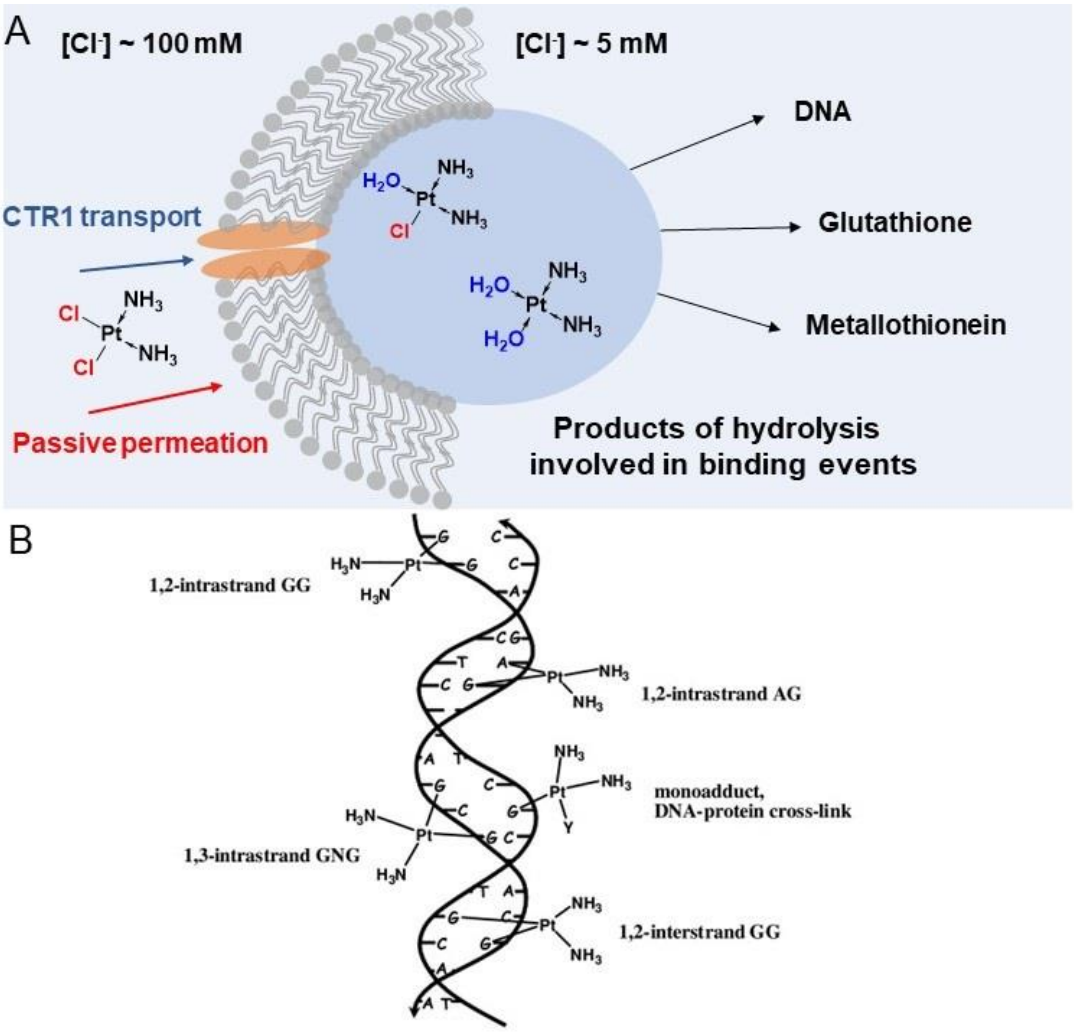

Figure 1.2. (A) Schematic representation of cisplatin's cellular transport. Reproduced with permission from Springer Nature: Nature Reviews Cancer, ref.[24] copyright (2007). (B) Different modes of cisplatin binding to DNA strands. Reproduced with permission from reference[25]. Copyright (2009) Elsevier.

This, rather simple, molecule had an enormous impact on chemotherapy bringing the cure rate up to 90 % for certain types of cancer. It also stimulated the pursuit for new transition metal-containing drugs based not only on Pt but on most elements that belong to this group, such as Pd, Ru, Au.[26-28]

Potential Pt-containing anticancer drugs were explored in vast amounts and some of them were finally approved for the use in humans, although sometimes with territorial restrictions (Fig. 1.3).[29, 30]

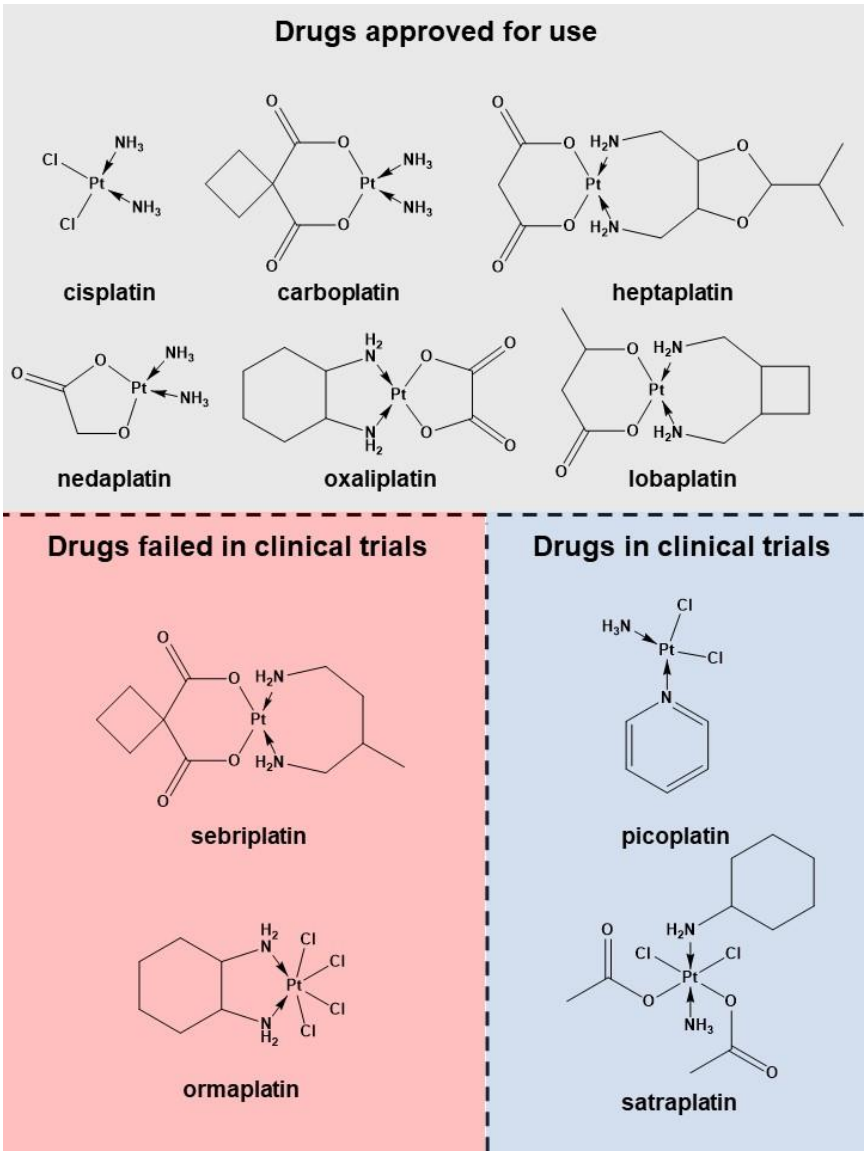

Figure 1.3. Examples of Pt-based anticancer drugs that (A) are commercially available, (B) failed in clinical trials, (C) undergo clinical trials. Figure based on the reference[30].

Nowadays, chemotherapy remains the relevant treatment method (Fig. 1.1) for numerous tumour types.

1.1.2. Associated side effects

As mentioned before, there are many obstacles that cisplatin needs to come through to reach its destination, and only a small fraction of the initial dose succeeds. The rest of cisplatin ends up being bound to glutathione[31], metallothioneins[32], phospholipids[33] and phospatidylserine[34] and remains in the body a long time after chemotherapy.[35]

The accumulation of cisplatin is dependent on many factors, such as dosage, administration, and individuals' conditions of a patient. In line with that, observed side effects are not consistent across the whole hospitalized group. Most of patients experience gastrointestinal symptoms, such as vomiting and nausea. In addition to those, but with lower abundance, patients suffer from neurotoxicity[36], nephrotoxicity[37], ototoxicity[38].

It is important to mention that many of cisplatin-induced side-effects are dose-dependent; their occurrence can be limited to a certain extent[39], but an overdose may be fatal[40]. This finding provoked a search for new ways of regulating cisplatin economy in patients' bodies.

In order to minimize the size effects, research across different disciplines have tried to develop methods to reduce platinum-based drugs toxicity. Some of the key aspects of those attempts are summarized in the next section.

1.1.3. Methods of reducing drug-induced toxicity

A relatively vast amount of work was devoted to the application of sodium thiosulfate (STS) as cisplatin-induced toxicity regulator. As fundamentally studied[41], STS coordinates Pt(II) centres via sulphur atom to form adducts with various stoichiometries. These adducts lose their toxicity along with anticancer properties. It is presumed that STS binds to toxic products of cisplatin hydrolysis leaving some of them unbound to induce apoptosis of cancer cells. Importantly, no change in Pt oxidation state nor the formation of toxic H_2S were observed during the application of sodium thiosulfate. On the other hand, the decrease in the concentration of active hydrolysed species leads to the lower efficiency of chemotherapy.[42] Many studies used STS to regulate the toxicity, increase the drug dose and as a rescue agent in case of an overdose.[43-46] Recently, the use of sodium thiosulfate was shown to be useful in the prevention of hearing loss caused by cisplatin.[47, 48]

Some improvements were achieved using a strategy based on intra-arterial chemotherapy. Ideally, it would benefit from a higher concentration of a drug nearby cancer and lower toxicity as compared to systemic administration.[49, 50] Nevertheless, certain studies revealed that neither the therapy efficiency is much higher, nor the toxicity is substantially lower.[51]

Certain organs, such as liver, offer a great opportunity of regional or localized therapy thanks to their anatomy. Hemoperfusion (HP) makes a use of it by delivering high doses of drugs to affected sites without exposing the entire body to the same drug level. In short, anticancer agent is administered through the hepatic artery, perfuses the liver and leaves the through hepatic veins. The blood rich in drugs goes through the activated carbon-based column with the aim of reducing the drug content before being returned back to the

body.[52, 53] Even though the preliminary results revealed a great efficiency of reducing exposure to toxic species up to 90%,[54] the method was not extensively applied as it causes a number of side effects[55] with the most severe related to the release of carbon particles to blood.[56] To overcome these disadvantages, carbon materials were coated with biocompatible membranes[57, 58], but this in turn lowered the efficiency of drug adsorption.[59]

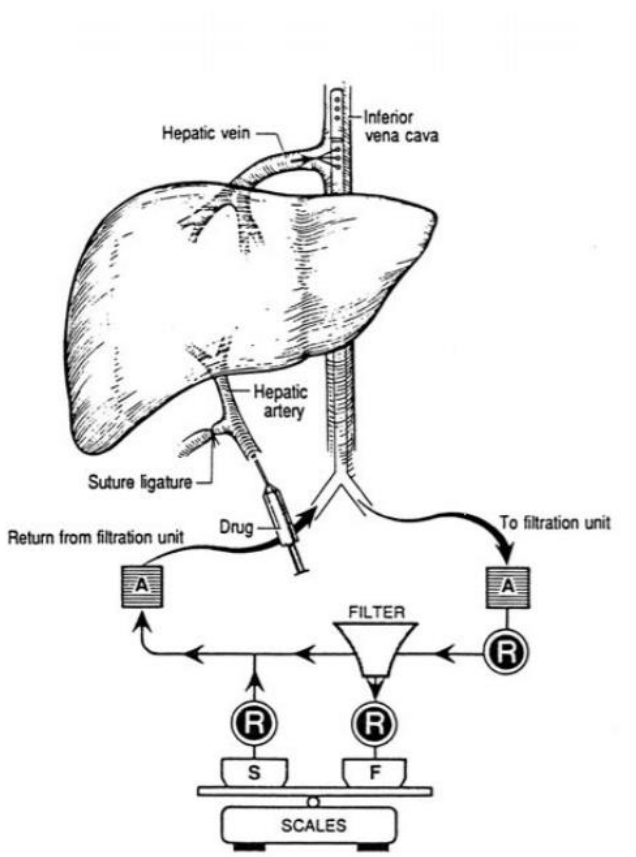

Figure 1.4. Schematic representation of the extracorporeal hemofiltration circuit. A - air trap, R – roller pump, F – filtrate, S – solution. Reprinted with permission from reference[60]. Copyright (1990) Springer Nature.

Since no versatile solution to overcome anti-cancer drug toxicity was found, this thesis presents a novel concept of the electrochemical hemofiltration of these drugs. I believe that the application of electrochemistry to the (post)chemotherapy may solve some challenges, as well as provide new opportunities for the monitoring of drug removal progress.

1.2. Introduction to electrochemistry in cancer research

Electrochemical methods were found to be useful in widely considered cancer diagnostics, covering aspects of biomarker, drugs and cancer cell detection. It is important to state here that electrochemistry was used as a method of cancer treatment *per se*. Attempts based on the insertion of two Pt electrodes inside cancer tissues and application of high voltage were reported.[61] Although one could rationalize the positive effect of such a therapy by the analogy to Barnett Rosenberg's initial experiments[62], the actual mechanism of action was not established. Nevertheless, this approach is very distant from the work presented in this thesis and is not to be discussed further; readers are referred to the appropriate review article[63].

1.2.1. Detection of cancer biomarkers and cancer cells

Detection of biomarkers and cells that indicate the presence of cancer is of utmost importance for the healthcare systems around the globe since early diagnosis leads to higher likelihood of successful therapy and lower treatment cost. Cancerous cells express larger amounts of certain molecules; therefore, their level is important during cancer

diagnosis. Commonly used techniques, such as enzyme-linked immunosorbent assay (ELISA), involve extensive laboratory-based labour and can detect concentrations that correspond to rather advanced stages of cancer.[64, 65]

On the other hand, electrochemistry offers great perspectives for highly sensitive and user-friendly devices. High number of research articles reported the use of a variety of electrochemical tools including amperometric[66], potentiometric[67] and impedimetric[68] techniques but also electrochemical luminescence[69]. By far, the most popular way of biomarkers recognition is through the attachment of specific antibodies to the electrode surface through various surface modification approaches (Fig. 1.5).[68, 70]

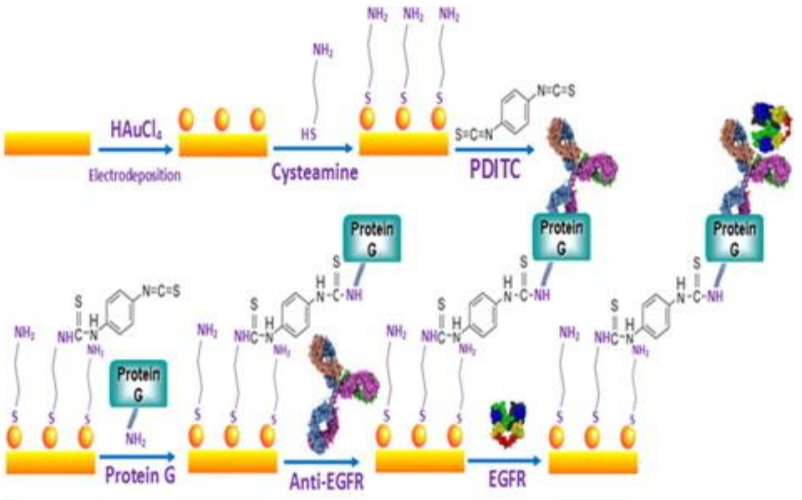

Figure 1.5. Schematic representation of the modification strategy used to prepare cancer biomarker sensor. Reproduced with permission from reference[68]. Copyright (2013) Elsevier.

This field is very vibrant, and a vast amount of work is related to the optimization of sensor performance through signal amplification[71] or use of magnetic particles[72], nevertheless, these go far beyond the scope of this thesis.

1.2.2. Detection of anti-cancer drugs

Electrochemistry was used to determine the concentration of anti-cancer drugs in relevant media as well as to monitor their interactions with human body components. This part, although the least explored in the literature, is the most relevant for the research undertaken in this project due to the number of concepts developed.

Molecular interactions between anticancer drugs and naturally occurring compounds are important for several reasons. Firstly, in-depth understanding of these interactions underpins the development of more specific drugs.[73] Secondly, it allows rational treatment in case of potential overdoses.[74] Thirdly, these interactions open doors for the quantification of drug concentration once a suitable analytical technique is chosen. Drug concentration can be obviously directly measured via chromatographic techniques[75], but these are not suitable further optimization in terms of cost, labour and miniaturisation. Electrochemistry, on the other hand, can offer this perspective but requires a measurable change in the electrical properties of the studied system to be applicable. This could be realised if a drug has electroactive properties – a defined signal would confirm the presence of the drug and the charge involved in the faradaic process would allow quantification. Nevertheless, a vast majority of anticancer drugs do not possess these properties, therefore, could interact with an electrode only in non-specific way, for instance through adsorption what would be difficult to quantify. Due to the relevance of this matter and extensive knowledge already gathered using other techniques, such as mass spectrometry[76], nuclear magnetic resonance[77] and vibrational spectroscopy[78], many electrochemical approaches to study drug-biomolecule interactions were developed.

As previously mentioned, DNA is the goal for the anticancer drug since this interaction is responsible for the chemotherapeutic effect. Consequently, several articles have been devoted to DNA-drug interactions visualised using electrochemical methods, typically through the change in electron transfer reaction of a redox probe. Many anticancer agents, such as 4,4'-dihydroxy chalcone[79], daunomycin[80], lycorine[81], mitoxantrone[82], mitomycin C[83], actinomycin D[84], echinomycin[85] and cisplatin[86] were found to interact with DNA and these interactions were monitored using electrochemistry. Some of those work rely on the elegant approach related to the hybridization of DNA, which was extensively reviewed elsewhere.[87] In short, binding of a drug to DNA strands results in the conformational change which may impede the charge transfer through the double helix (Fig. 1.6A) as described by Gooding and co-workers.[86] Alternatively, if the electrode is modified with a single DNA strand, a binding event may change the orientation of the strand with respect to the surface (Fig. 1.6B).[88]

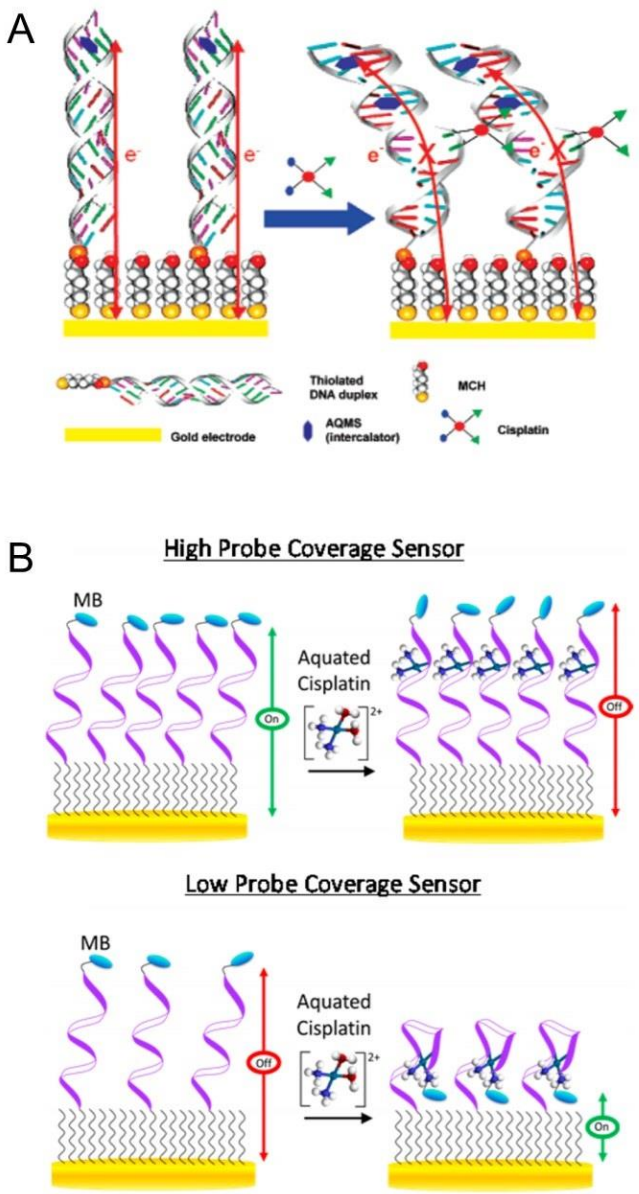

Figure 1.6. A concept of cisplatin sensing through (A) change in charge transfer resistance in a double helix (B) change in the conformation of a single strand DNA. (A) is reprinted with permission from reference[86]. Copyright (2007) American Chemical Society. (B) is reprinted with permission from reference[88]. Copyright (2017) American Chemical Society.

Successful electrochemical monitoring of drug-DNA interactions was subsequently turned into sensor concepts, where the drug concentration could be determined by a change in

electrochemical signal.[88-91] It is important to mention that sensing strategies did not exclusively rely on DNA-modified electrodes, but also on the quantification of solution-based interaction.[91]

The use of DNA has certain limitations related to the cost what provoked the search for less sophisticated drug recognition centres. To this end, many materials were used to detect anti-cancer drugs. Nature-inspired gluthathione-s-transferase (GST) was applied as an electrode's modification and provided a versatile system for a broad range of drugs.[92] Additionally, 5-fluorouracil was quantitatively detected on glucose-modified carbon electrode.[93] More works were devoted to the application of carbon nanostructures, such as graphene and carbo nanotubes to a variety of drugs including regorafenib, dacarbazine, doxorubicin, methotrexate and cisplatin.[94-97] On the top of that, polymeric materials such as dendrimers[98], metal-organic frameworks[99] and molecularly-imprinted systems[100] were used to sense anti-cancer drugs. Critically speaking, although many of those materials show some potential in the detection of relevant drugs, their mechanisms of action are rather unclear. This feature can be as a disadvantage since limited knowledge may impede the rational design of sensor that could work with real samples.[101] Therefore, there is a great opportunity to discover materials that can act with a specificity similar to DNA while being cheap and easily manufactured.

1.3. References

1. https://www.cancerresearchuk.org/health-professional/cancer-statistics-for-the-uk, (accessed 04/10/2018).
2. https://www.cancerresearchuk.org/health-professional/cancer-statistics/worldwide-cancer, (accessed 04/10/2018).
3. https://www.macmillan.org.uk/information-and-support/understanding-cancer/what-is-cancer.html#18623, (accessed 04/10/2018).
4. G. I. Evan and K. H. Vousden, *Nature*, 2001, **411**, 342-348.
5. P. A. Futreal, L. Coin, M. Marshall, T. Down, T. Hubbard, R. Wooster, N. Rahman and M. R. Stratton, *Nat. Rev. Cancer*, 2004, **4**, 177-183.
6. M. Greaves and C. C. Maley, *Nature*, 2012, **481**, 306-313.
7. https://www.cancer.gov/about-cancer/treatment/types/radiation-therapy, 20/07/2019).
8. https://www.cancer.gov/about-cancer/treatment/types/immunotherapy, (accessed 20/07/2019).
9. https://www.cancer.gov/about-cancer/treatment/types/hormone-therapy).
10. https://www.cancer.gov/about-cancer/treatment/types/chemotherapy, (accessed 20/07/2019).
11. https://www.cancerresearchuk.org/health-professional/cancer-statistics/diagnosis-and-treatment, 21/07/2019).
12. V. T. DeVita and E. Chu, *Cancer Res.*, 2008, **68**, 8643-8653.
13. E. B. Krumbhaar and H. D. Krumbhaar, *J. Med. Res.*, 1919, **40**, 497-508.
14. A. Gilman, *Fed. Proc.*, 1946, **5**, 285-292.
15. B. Rosenberg, L. Van Camp and T. Krigas, *Nature*, 1965, **205**, 698-699.
16. B. Rosenberg, L. Van Camp, J. E. Trosko and V. H. Mansour, *Nature*, 1969, **222**, 385-386.
17. F. M. Muggia, A. Bonetti, J. D. Hoeschele, M. Rozencweig and S. B. Howell, *J. Clin. Oncol.*, 2015, **33**, 4219-4226.
18. B. Rosenberg, in *Cisplatin*, eds. A. W. Prestayko, S. T. Crooke and S. K. Carter, Academic Press, 1980, pp. 9-20.
19. S. Dasari and P. Bernard Tchounwou, *Eur. J. Pharmacol.*, 2014, **740**, 364-378.

20. M. A. Fuertes, J. Castilla, C. Alonso and J. M. Pérez, *Curr. Med. Chem.*, 2003, **10**, 257-266.
21. N. D. Eljack, H.-Y. M. Ma, J. Drucker, C. Shen, T. W. Hambley, E. J. New, T. Friedrich and R. J. Clarke, *Metallomics*, 2014, **6**, 2126-2133.
22. F. J. P. Hoebers, D. Pluim, A. A. M. Hart, M. Verheij, A. J. M. Balm, G. Fons, C. R. N. Rasch, J. H. M. Schellens, L. J. A. Stalpers, H. Bartelink and A. C. Begg, *Cancer Chemother. Pharmacol.*, 2008, **61**, 1075-1081.
23. B. Chiavarino, M. E. Crestoni, S. Fornarini, D. Scuderi and J.-Y. Salpin, *J. Am. Chem. Soc.*, 2013, **135**, 1445-1455.
24. L. Kelland, *Nat. Rev. Cancer*, 2007, **7**, 573-584.
25. A. M. Pizarro and P. J. Sadler, *Biochimie*, 2009, **91**, 1198-1211.
26. K. Benjamin Garbutcheon-Singh, M. P Grant, B. W Harper, A. M. Krause-Heuer, M. Manohar, N. Orkey and J. R Aldrich-Wright, *Curr. Top. Med. Chem.*, 2011, **11**, 521-542.
27. P. C. A. Bruijnincx and P. J. Sadler, *Curr. Opin. Chem. Biol.*, 2008, **12**, 197-206.
28. M. J. Hannon, *Pure Appl. Chem.*, 2007, **79**, 2243-2261.
29. E. Wong and C. M. Giandomenico, *Chem. Rev.*, 1999, **99**, 2451-2466.
30. N. J. Wheate, S. Walker, G. E. Craig and R. Oun, *Dalton Trans.*, 2010, **39**, 8113-8127.
31. Y. Kasherman, S. Sturup and D. Gibson, *J. Med. Chem.*, 2009, **52**, 4319-4328.
32. D. Hagrman, J. Goodisman, J. C. Dabrowiak and A.-K. Souid, *Drug Metab. Dispos.*, 2003, **31**, 916-923.
33. G. Speelmans, W. H. H. M. Sips, R. J. H. Grisel, R. W. H. M. Staffhorst, A. M. J. Fichtinger-Schepman, J. Reedijk and B. de Kruijff, *Biochim. Biophys. Acta Biomembr.*, 1996, **1283**, 60-66.
34. G. Speelmans, R. W. H. M. Staffhorst, K. Versluis, J. Reedijk and B. de Kruijff, *Biochemistry*, 1997, **36**, 10545-10550.
35. P. Tothill, H. S. Klys, L. M. Matheson, K. McKay and J. F. Smyth, *Eur. J. Cancer*, 1992, **28**, 1358-1361.
36. A. Avan, T. J. Postma, C. Ceresa, A. Avan, G. Cavaletti, E. Giovannetti and G. J. Peters, *Oncologist*, 2015, **20**, 411-432.

37. R. P. Miller, R. K. Tadagavadi, G. Ramesh and W. B. Reeves, *Toxins*, 2010, **2**, 2490-2518.
38. L. P. Rybak, D. Mukherjea, S. Jajoo and V. Ramkumar, *Tohoku J. Exp. Med.*, 2009, **219**, 177-186.
39. K. K. Soni, H. K. Kim, B. R. Choi, K. K. Karna, J. H. You, J. S. Cha, Y. S. Shin, S. W. Lee, C. Y. Kim and J. K. Park, *Drug Des. Devel. Ther.*, 2016, **10**, 3959-3968.
40. C. Charlier, P. Kintz, N. Dubois and G. Plomteux, *J. Anal. Toxicol.*, 2004, **28**, 138-140.
41. M. Sooriyaarachchi, J. Gailer, N. V. Dolgova, I. J. Pickering and G. N. George, *J. Inorg. Biochem.*, 2016, **162**, 96-101.
42. M. Inoue, C. Shimizu, H. Shimizu and O. Tanizawa, *Gynecol. Oncol.*, 1991, **40**, 34-37.
43. C. E. Pfeifle, S. B. Howell, R. D. Felthouse, T. B. Woliver, P. A. Andrews, M. Markman and M. P. Murphy, *J. Clin. Oncol.*, 1985, **3**, 237-244.
44. D. R. Gandara, V. J. Wiebe, E. A. Perez, R. W. Makuch and M. W. DeGregorio, *Crit. Rev. Oncol. Hematol.*, 1990, **10**, 353-365.
45. R. Goel, S. M. Cleary, C. Horton, S. Kirmani, I. Abramson, C. Kelly and S. B. Howell, *J. Natl. Cancer Inst.*, 1989, **81**, 1552-1560.
46. N. Kusunoki, Y. Ku, M. Tominaga, T. Iwasaki, T. Fukumoto, S. Muramatsu, T. Sugimoto, S. Tsuchida, M. Takamatsu, Y. Suzuki and Y. Kuroda, *Ann. Surg. Oncol.*, 2001, **8**, 449-457.
47. D. R. Freyer, L. Chen, M. D. Krailo, K. Knight, D. Villaluna, B. Bliss, B. H. Pollock, J. Ramdas, B. Lange, D. Van Hoff, M. L. Van Soelen, J. Wiernikowski, E. A. Neuwelt and L. Sung, *Lancet Oncol.*, 2017, **18**, 63-74.
48. P. R. Brock, R. Maibach, M. Childs, K. Rajput, D. Roebuck, M. J. Sullivan, V. Laithier, M. Ronghe, P. Dall'Igna, E. Hiyama, B. Brichard, J. Skeen, M. E. Mateos, M. Capra, A. A. Rangaswami, M. Ansari, C. Rechnitzer, G. J. Veal, A. Covezzoli, L. Brugières, G. Perilongo, P. Czauderna, B. Morland and E. A. Neuwelt, *N. Engl. J. Med.*, 2018, **378**, 2376-2385.
49. J. M. Collins, *J. Clin. Oncol.*, 1984, **2**, 498-504.
50. H. Chen and J. Gross, *Cancer Treat. Rep.*, 1980, **64**, 31-40.
51. J. B. Vermorken, *Int. J. Gynecol. Cancer*, 1993, **3**, 129-142.

52. H. Yatzidis, *Proc. Eur. Dial. Transplat. Assoc.*,1964, **1**, 83-87.
53. J. Tijssen, A. Bantjes, A. W. van Doorn, J. Feijen, B. van Dijk, C. R. Vonk and I. C. Dijkhuis, *Artif. Organs*, 1979, **3**, 11-14.
54. J. F. Pingpank, S. K. Libutti, R. Chang, B. J. Wood, Z. Neeman, A. W. Kam, W. D. Figg, S. Zhai, T. Beresneva and G. D. Seidel, *J. Clin. Oncol.*, 2005, **23**, 3465-3474.
55. J. L. Rosenbaum, M. S. Kramer, R. M. Raja, M. J. Krug and C. G. Bolisay, *Clin. Toxicol.*, 1980, **17**, 493-500.
56. T. M. S. Chang, *Nat. Rev. Drug Discov.*, 2005, **4**, 221-235.
57. S. Elkheshen, H. Zia, T. Needham, A. Badawy and L. Luzzi, *J. Microencapsul.*, 1992, **9**, 41-51.
58. S. El-Kheshen, H. Zia, A. Badawi, T. Needham and L. Luzzi, *J. Microencapsul.*, 1995, **12**, 505-514.
59. C. Legallais, A. Gautier, M. Dufresne, B. Carpentier and R. Baudoin, *J. Chromatogr. B*, 2008, **861**, 171-176.
60. R. A. Graham, Z. H. Siddik and D. C. Hohn, *Cancer Chemother. Pharmacol.,* 1990, **26**, 210-214.
61. B. Nordenström, *Am. J. Clin. Oncol.*, 1989, **12**, 530-536.
62. C. Monneret, *Ann. Pharm. Fr.*, 2011, **69**, 286-295.
63. E. Nilsson, H. von Euler, J. Berendson, A. Thörne, P. Wersäll, I. Näslund, A.-S. Lagerstedt, K. Narfström and J. M. Olsson, *Bioelectrochemistry*, 2000, **51**, 1-11.
64. J. Wang, *Biosens. Bioelectron.*, 2006, **21**, 1887-1892.
65. B. V. Chikkaveeraiah, A. A. Bhirde, N. Y. Morgan, H. S. Eden and X. Chen, *ACS Nano*, 2012, **6**, 6546-6561.
66. X. Yu, B. Munge, V. Patel, G. Jensen, A. Bhirde, J. D. Gong, S. N. Kim, J. Gillespie, J. S. Gutkind, F. Papadimitrakopoulos and J. F. Rusling, *J. Am. Chem. Soc.*, 2006, **128**, 11199-11205.
67. Y. T. Wang, Z. Q. Zhang, V. Jain, J. J. Yi, S. Mueller, J. Sokolov, Z. X. Liu, K. Levon, B. Rigas and M. H. Rafailovich, *Sensor. Actuat. B-Chem.*, 2010, **146**, 381-387.
68. R. Elshafey, A. C. Tavares, M. Siaj and M. Zourob, *Biosens. Bioelectron.*, 2013, **50**, 143-149.
69. N. P. Sardesai, J. C. Barron and J. F. Rusling, *Anal. Chem.*, 2011, **83**, 6698-6703.

70. C. Hao, F. Yan, L. Ding, Y. D. Xue and H. X. Ju, *Electrochem. Commun.*, 2007, **9**, 1359-1364.
71. R. Malhotra, V. Patel, J. P. Vaque, J. S. Gutkind and J. F. Rusling, *Anal. Chem.*, 2010, **82**, 3118-3123.
72. M. Y. Li, Y. M. Sun, L. Chen, L. Li, G. Z. Zou, X. L. Zhang and W. R. Jin, *Electroanalysis*, 2010, **22**, 333-337.
73. M. Misiak, F. Mantegazza and G. L. Beretta, *Curr. Pharm. Des.*, 2016, **22**, 6596-6611.
74. R. Y. Tsang, T. Al-Fayea and H. J. Au, *Drug Safety*, 2009, **32**, 1109-1122.
75. S. Nussbaumer, P. Bonnabry, J. L. Veuthey and S. Fleury-Souverain, *Talanta*, 2011, **85**, 2265-2289.
76. A. J. Tomlinson, L. M. Benson, K. L. Johnson and S. Naylor, *J. Chromatogr. B Biomed. Appl.*, 1993, **621**, 239-248.
77. J. Vinje and E. Sletten, *Anti-Cancer Agents Med. Chem.*, 2007, **7**, 35-54.
78. D. K. Jangir, S. Charak, R. Mehrotra and S. Kundu, *J. Photochem. Photobiol., B*, 2011, **105**, 143-148.
79. B. Meric, K. Kerman, D. Ozkan, P. Kara, A. Erdem, O. Kucukoglu, E. Erciyas and M. Ozsoz, *J. Pharm. Biomed. Anal.*, 2002, **30**, 1339-1346.
80. J. Wang, M. Ozsoz, X. H. Cai, G. Rivas, H. Shiraishi, D. H. Grant, M. Chicharro, J. Fernandes and E. Palecek, *Bioelectrochem. Bioenerg.*, 1998, **45**, 33-40.
81. H. Karadeniz, B. Gulmez, F. Sahinci, A. Erdem, G. I. Kaya, N. Unver, B. Kivcak and M. Ozsoz, *J. Pharm. Biomed. Anal.*, 2003, **33**, 295-302.
82. A. M. O. Brett, T. R. A. Macedo, D. Raimundo, M. H. Marques and S. H. P. Serrano, *Biosens. Bioelectron.*, 1998, **13**, 861-867.
83. D. Marin, P. Perez, C. Teijeiro and E. Palecek, *Biophys. Chem.*, 1998, **75**, 87-95.
84. S. Wang, T. Z. Peng and C. F. Yang, *J. Electroanal. Chem.*, 2003, **544**, 87-92.
85. F. Jelen, A. Erdem and E. Palecek, *Bioelectrochemistry*, 2002, **55**, 165-167.
86. E. L. S. Wong and J. J. Gooding, *J. Am. Chem. Soc.*, 2007, **129**, 8950-8951.
87. J. J. Gooding, *Electroanalysis*, 2002, **14**, 1149-1156.
88. Y. Wu and R. Y. Lai, *Anal. Chem.*, 2017, **89**, 9984-9989.
89. J. Wang, X. H. Cai, G. Rivas, H. Shiraishi and N. Dontha, *Biosens. Bioelectron.*, 1997, **12**, 587-599.

90. A. M. O. Brett, S. H. P. Serrano, T. A. Macedo, D. Raimundo, M. H. Marques and M. A. LaScalea, *Electroanalysis*, 1996, **8**, 992-995.
91. Y. Yoshimoto, T. Yasukawa and F. Mizutani, *Analyst*, 2009, **134**, 2113-2117.
92. E. M. Materon, P. J. J. Huang, A. Wong, A. A. P. Ferreira, M. D. T. Sotomayor and J. W. Liu, *Biosens. Bioelectron.*, 2014, **58**, 232-236.
93. S. D. Bukkitgar and N. P. Shetti, *ChemistrySelect*, 2016, **1**, 771-777.
94. M. Venu, S. Venkateswarlu, Y. V. M. Reddy, A. S. Reddy, V. K. Gupta, M. Yoon and G. Madhavi, *ACS Omega*, 2018, **3**, 14597-14605.
95. S. Dehdashtian, N. Behbahanian and K. M. Taherzadeh, *J. Iran. Chem. Soc.*, 2018, **15**, 931-941.
96. Y. J. Guo, Y. H. Chen, Q. Zhao, S. M. Shuang and C. Dong, *Electroanalysis*, 2011, **23**, 2400-2407.
97. L. Q. Ye, M. W. Xiang, Y. W. Lu, Y. T. Gao and P. F. Pang, *Int. J. Electrochem. Sci.*, 2014, **9**, 1537-1546.
98. A. Erdem, H. Karadeniz and A. Caliskan, *Analyst*, 2011, **136**, 1041-1045.
99. A. Florea, Z. Z. Guo, C. Cristea, F. Bessueille, F. Vocanson, F. Goutaland, S. Dzyadeyych, R. Sandulescu and N. Jaffrezic-Renault, *Talanta*, 2015, **138**, 71-76.
100. A. Kumar, P. K. Pathak and B. B. Prasad, *ACS Appl. Mater. Interfaces*, 2019, **11**, 16065-16074.
101. J. J. Gooding, *ACS Sensors*, 2018, **3**, 1609-1609.

Chapter 2: Aim and Objectives

As described in Chapter 1, chemotherapy using Pt-based drugs is currently one of the main treatment routes of solid tumours. However, this treatment results in severe side effects what efficiently reduces the maximum dose that can be administered and implies lower cure rates. One of the main challenges is to increase the cure rate of the treatment while reducing the side effects. This can be realised by the development of a localized treatment that allows the extraction of Pt-based drugs from the physiological fluids to prevent them from recirculation in the healthy areas of the body.

The main goal of this thesis is to design and implement a novel electrochemical platform that enables the extraction of Pt-based drugs from physiological fluids using surface modified electrodes.

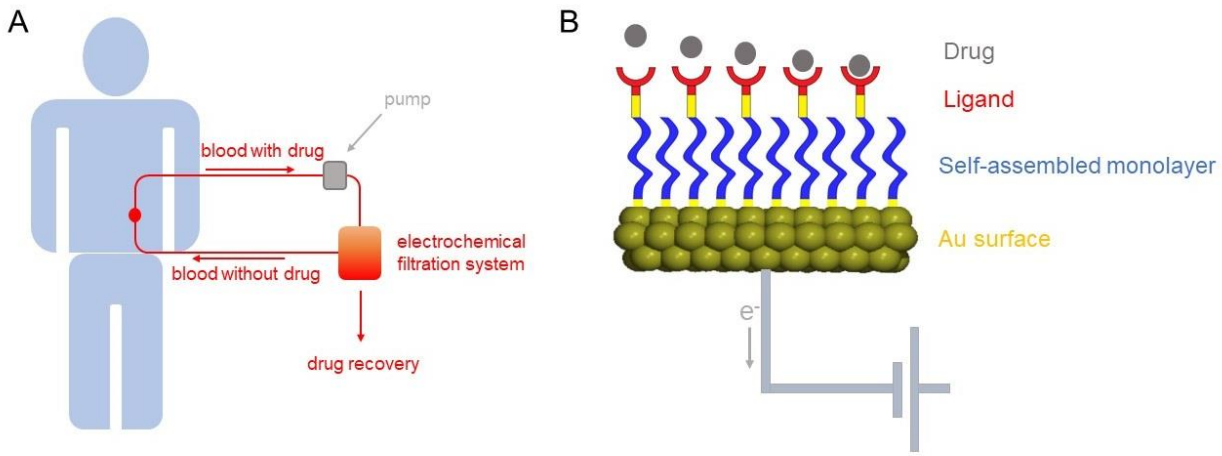

Figure 2.1. (A) Schematic representation of the electrochemical filtration system with (B) the design of the working electrode.

Considering the unique nature of this PhD project and its novelty, there are several aims that must be accomplished in order to develop this concept in the coherent way.

The aim of **Chapter 4** is to understand of the behaviour of cisplatin on bare gold. This aspect is crucial since non-specific interactions may lead to the deposition of metallic platinum on gold. Platinum is a great electrocatalyst and exposure of blood components to this metal is highly undesirable.

The aim of **Chapter 5** is to evaluate of the stability of surface-modifying layers. This is of great relevance since it prevents drugs and blood components from interacting with bare gold what may cause deposition of platinum and fouling of the electrode with sulphur-containing species. Therefore, determination of the potential where the modifying layer is stable is the key feature for the safe performance of the proposed system.

The aim of **Chapter 6** is to identify an efficient Pt-coordinating ligand and immobilise it on the surface of the electrode. It is a key aspect of the electrochemical hemofiltration system to be able bind drugs in the time-efficient manner, therefore a well-coordinating ligand offering possibilities to be attached to the electrode is of greatest importance.

Chapter 3: Experimental techniques

3.1. Electrochemistry

Electrochemistry is a vibrant part of chemistry that describes an interplay between chemical and electrical phenomena. Since seminal developments, such as Faraday's laws, Volta's cell and Heyrovsky's electrode, it has attracted a broad attention from the community as it provides means to develop the new class of alternative energy source, including fuel cells, batteries and electrochemical capacitors.[1-3] Apart from those, electrochemistry has been widely applied in developing a broad spectrum of sensor technologies[4], and more recently has found the application in a vast scope of organic syntheses[5, 6]. Therefore, many aspects of electrochemistry have been investigated along with the development of new experimental techniques. This section aims to introduce basic concepts of electrochemistry that are necessary to understand the content of the thesis.

3.1.1. Fundamental aspects of electrochemistry

The major interest of electrochemical science lies at the interface between two phases. In most cases the interface consists of a solid electronic conductor (an electrode) and a liquid ionic conductor (an electrolyte), nevertheless, solid-solid[7] or liquid-liquid[8] interfaces have been also studied. When the electrochemical potential is applied to the system, the current passes through the circuit and the charge transfer between two phases is of utmost importance – it underpins all interests in electrochemistry.

Electrochemical processes are driven by the energy of the electrons within the working electrode (WE). By applying a sufficiently negative potential to the WE, the energy of the electrons will increase to the extent where it is more favourable to transfer the charge to species in the solution. This process is also known as a flow reduction (cathodic) current. By analogy, application of a sufficiently positive potential to the WE result in charge transfer from species in the solution to the electrode, and a flow of oxidation (anodic) current. The nature of these processes is well presented by a diagram shown in Figure 3.1.

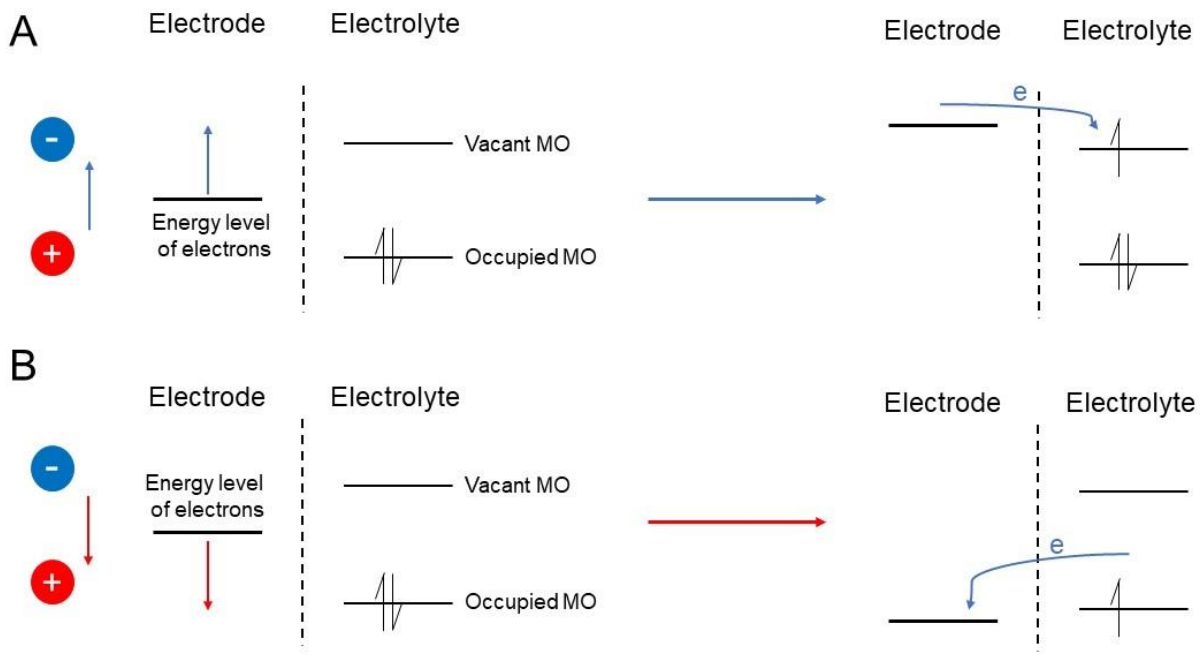

Figure 3.1. Schematic representation of (A) reduction (B) oxidation process of species in solution. Reproduced with permission from reference[9]. Copyright (2000) John Wiley & Sons.

It is important to mention, that once the electrodes are immersed in a conducting medium, but with source of power not yet connected, there is no control over the potential of the WE with respect to the RE. The potential acquired by the working electrode is called an open-circuit potential and reflects on the thermodynamic equilibrium in the system. Application of an external source of power changes the potential of the WE and pushes the system away from the equilibrium. Change in the value of the electrochemical potential may drive many processes at the solid/liquid interface that can be defined as non-faradaic (capacitive) or faradaic (related to the electron transfer).

Capacitive processes are responsible for the accumulation of charge (ions) in the electric double-layer (EDL) region that forms on a conductor exposed to a conducting medium. Although these processes are not of primary interest, except supercapacitor and capacitive desalination communities, they take place in parallel to electron transfer reactions and must be considered.

Non-faradaic processes are strictly connected with the concept of the Ideal Polarized Electrode (IPE). Ideally, no charge transfer across the interface is possible on such electrode regardless the potential applied. Real electrodes can realize this concept only in a limited potential range, where no charge transfer takes place. Within this potential range, the electrode behaves as an element of the electronic circuit – capacitor. As in a capacitor, at a given potential applied to the electrode (equivalent to a metal plate in a capacitor), an accumulation of charge q^M exists on the electrode surface. This excess of charge (either positive or negative) is neutralised by solution-based species (equivalent to electrons and holes in a dielectric layer) bearing the charge q^S, so the equation 3.1 is real.

$$q^M = -q^S \qquad (3.1)$$

An array of species that contribute to the solution-based charge excess is defined as electric double-layer and forms a complex structure made up of a few layers (Fig. 3.2). The inner one, called Inner Helmholtz Plane (IHP) is composed of specifically adsorbing ions. Further away an Outer Helmholtz Plane (OHP) is placed and defines the nearest distance that can be achieved by solvated ions with respect to the surface of the electrode. These ions are weakly attracted through electrostatic forces and for irregular diffusive layer.

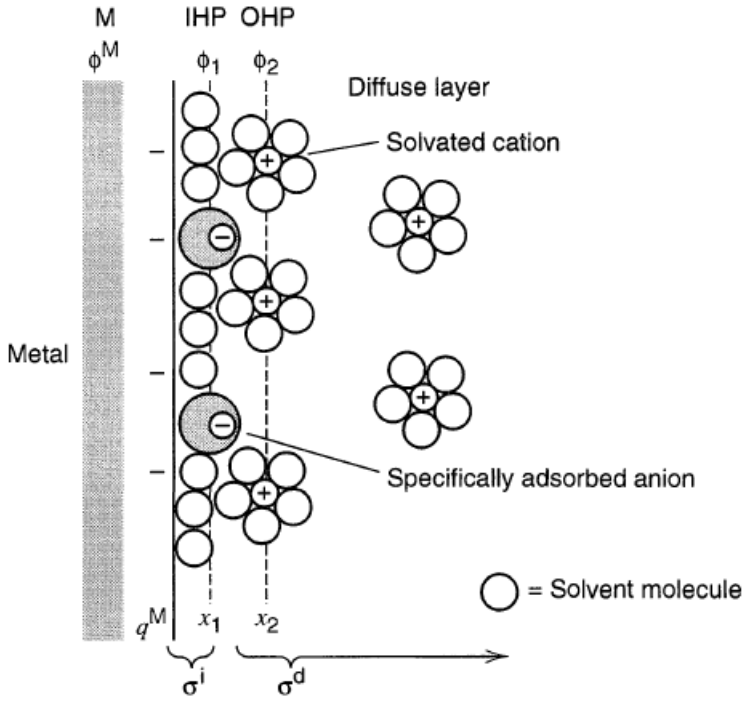

Figure 3.2. Schematic representation of an electric double-layer structure. Reprinted with permission from reference[9]. Copyright (2000) John Wiley & Sons

Understanding of these fundamental aspects of electrochemistry is crucial for the interpretation of any electrochemical data included in this PhD thesis.

3.1.2. The importance of mass transfer

Since most modern electrochemistry is focused on the solid/liquid interface, the importance of mass transfer processes cannot be underestimated due to number of fundamental and applied reasons.

Molecules are transferred through migration (move of charged particles in the electric field), convection (by applying mechanical stirring) and diffusion (movement caused by a difference in concentrations in two points in space). All three components of mass transfer are typically present while performing an electrochemical experiment. Nevertheless, experimental systems can be designed to make some of these components negligible. The use of inert electrolyte as a supporting electrolyte results is a reduced contribution from migration, while preventing stirring lowers the impact of convection.

When it comes to diffusion, initially, the concentration of species in the solution is even at any considered point so there is no diffusional gradient present. Once the electrochemical potential is set so the species are consumed, a concentration gradient is formed which causes a flux of molecules from the bulk to the electrode. According to the Fick's first law, the flux is proportional to the concentration gradient (Eq. 3.2).

$$-J(x,t) = D\frac{\partial c(x,t)}{\partial x} \qquad (3.2)$$

To put it in simple words, equation 3.2 describes the number of molecules of pass through a certain location in a unit of time. This was later further developed to the Fick's second law, which predicts the concentration of species as a function of time (Eq. 3.3).

$$\frac{\partial c(x,t)}{\partial t} = D\left(\frac{\partial^2 c(x,t)}{\partial x}\right) \qquad (3.3)$$

This differential equation solved for certain conditions (initial concentration is homogeneous, surface concentration is equal to zero) results in the Cottrell equation (Eq. 3.4) which describes the current output for a planar electrode under diffusion-limited conditions as a function of time (Fig. 3.3).

$$I = \frac{nFA\sqrt{D}}{\sqrt{\pi t}} \qquad (3.4)$$

where n – number of electrons, F – Faraday's constant, A – electrode's geometric surface area, D – diffusion coefficient, t – time.

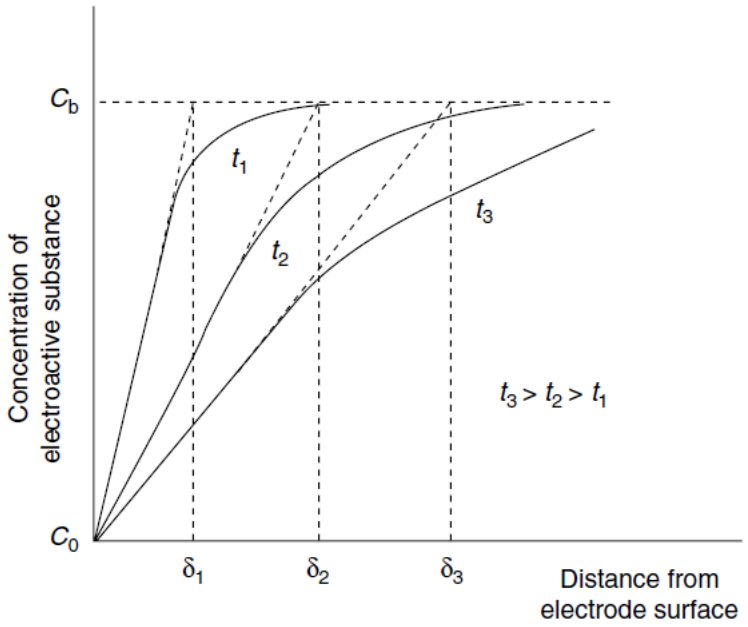

Figure 3.3. Profiles of concentrations after a potential step experiments for different times and distances from the surface. Reproduced with permission from reference[10]. Copyright (2006) John Wiley & Sons.

Understanding basic concepts of diffusion is important for interpretation of the data, where molecules diffuse towards the surface of the electrode (such as adsorption of Pt-based drugs) or are desorbed from the surface (such as reductive desorption of thiols and disulfides).

2.1.3. Extended charge transfer

In the discussion above, the molecules are adsorbed on or approach surfaces very closely for the electron transfer processes to take place. Electrochemistry on thiol-modified electrodes requires additional introduction. This is related to the fact that thiols covering the surface of the electrode typically form an insulating layer. This leads to the scenario where electroactive species are located at a certain distance from the surface what implies effects on the electron transfer rate. In such a case, the electron transfer is described as electron tunnelling. The probability of this process to happen is proportional to the distance that electron needs to pass and the factor describing the energy barrier (Eq. 3.5).[9]

$$Probability \propto \exp(-\beta x) \qquad (3.5)$$

where β – tunnelling constant, x – distance over which tunnelling occurs.

Extended charge transfer is of great importance when it comes to the rational design of electrode's modification for applications in electrochemical sensors. On one hand, one wants to prepare a compact, defect-free monolayer which is normally facilitated using long carbon chain thiols. On the other hand, a too thick modification may substantially reduce the ability of the system to perform charge transfer processes. The concept of extended charge transfer can be well visualised by the examples from the literature. Michael Weaver

studied the effect of the length of the linker that separated an electroactive cobalt centre from the surface of the electrode.[11] He reported that the rate of the reaction decreases exponentially with the distance between the surface and the redox probe. As a follow-up, a robust strategy for studying tunnelling effect was proposed using a ferrocene as a redox probe.[12] Authors observed similar outcomes of increasing the length of a linker (Fig. 3.4)

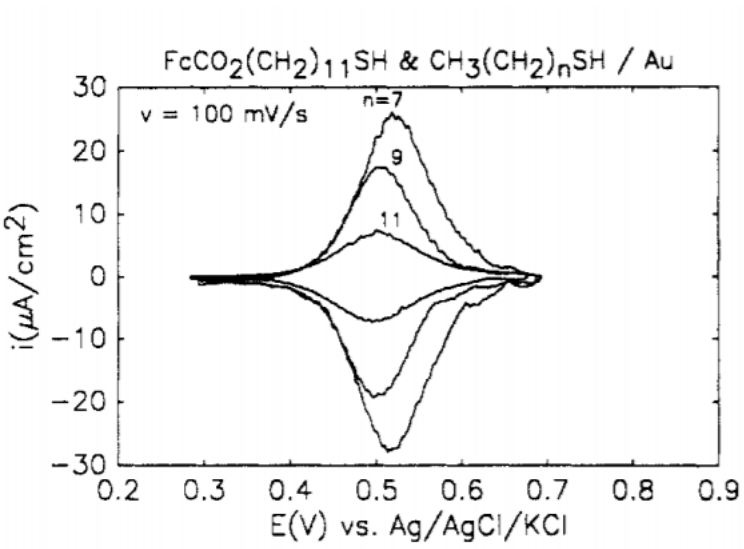

Figure 3.4. The effect of the length of a methylene linker on the cyclic voltammetry profiles of $FcCO_2(CH_2)_nSH$ adsorbed on Au electrode. Reprinted with permission from reference[12]. Copyright (1990) American Chemical Society.

Understanding the basic concepts of extended charge transfer was of great relevance at the stage of designing the molecular architecture to be employed in the electrochemical hemofiltration system.

3.1.4. Electrochemical techniques

Cyclic voltammetry

Cyclic voltammetry is a widely used electrochemical technique. It is a potentiodynamic method that relies on sweeping the potential of the WE between two values at a constant rate (Fig. 3.5A) and recording the output current (Fig. 3.5B). The current response is dependent on many factors, from the experimental point of view – a choice of electrode (material, geometry, crystallographic structure) and electrolyte (nature of supporting electrolyte, presence of redox species, concentration). The choice of the experimental set-up implies on the details related to adsorption (interactions between the material of the WE and the supporting electrolyte), diffusional (mass transfer to the working electrode) and other processes.

In the simplified case scenario, as shown in Fig. 3.5B, the voltammetric profile of a working electrode in a redox-free electrolyte (Fig. 3.5B, dotted line) resembles a rectangular shape, what corresponds to the charging and discharging of EDL via electrostatic forces. Once a redox-active molecule is present in the solution, the voltammetric profiles acquire new features related to the faradaic processes (Fig. 3.5B, solid line). In the simplest, thermodynamically and chemically reversible, case we observe a pair of peaks corresponding to the oxidation and subsequent reduction of a redox probe, where both peaks integrate to the same value of charge, and their centres are separated by 59 mV – for a 1 electron transfer reaction. For these processes peak positions are independent of the scan rate values. Recorded currents increase proportionally with the square root of the scan rate value. This is related to the mass transfer-controlled process; at lower scan rates species have more time to diffuse to the electrode and undergo electrochemical

reaction (giving a current output), therefore the number of processed species is higher when compared to the case where the scan rate is high. Mass transfer effects are not present in the case where the species of interest are adsorbed on the surface of the electrode. Recorded current is directly proportional to the scan rate value. Cathodic and anodic peaks are ideally separated by 0 mV, nevertheless, this is often not the case, especially at higher scan rates, due to limitations in electron transfer kinetics.

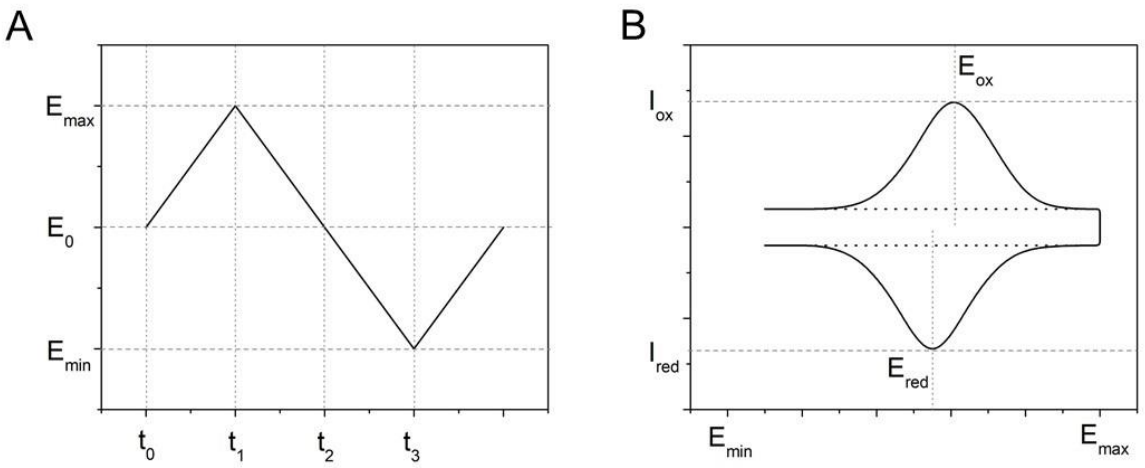

Figure 3.5. (A) A function that describes a potential change over time in cyclic voltammetry experiment. (B) Schematic voltammetric profiles of purely capacitive behaviour (dotted line) with contribution from thermodynamically reversible redox process (solid line).

These considerations are not representative for most cases as electrochemical reactions are rarely thermodynamically reversible and often couple to other electrochemical/chemical processes what implies more complex voltammetric shapes. For irreversible and quasi-reversible processes, the peaks are reduced in size and their separation increases significantly due to sluggish electron transfer exchange. The best

example of the irreversible process from the perspective of this thesis is the electrochemical reduction of cisplatin on bare gold (Chapter 4). In the forward scan a well-defined signal is observed but no back response in observed in the backward scan.

This technique was applied throughout this thesis, therefore, familiarity with cyclic voltammetry is needed to understand majority of the undertaken work.

Chronoamperometry

Chronoamperometry is an electrochemical technique that involves the application of a constant potential over time and measuring the current output. In its basic form, it relies on setting a potential that drives processes at the interface. As can be seen, the change in potential value from the initial E_0 to E_1 (Fig. 3.6A) results in a substantial current output at t_1 (Fig. 3.6B). In the case of purely capacitive process, a current spike corresponds to the rapid charging of the EDL (dotted line). Once a redox-active molecule is present in the studied system (solid line), a current spike is followed by an exponentially decreasing current which is related to the diffusionally-limited supply of the redox probe that can undergo the electrochemical reaction. This behaviour is described by a Cottrell equation and has found many applications in determining the mass transfer effect in electro-analysis/catalysis.[13]

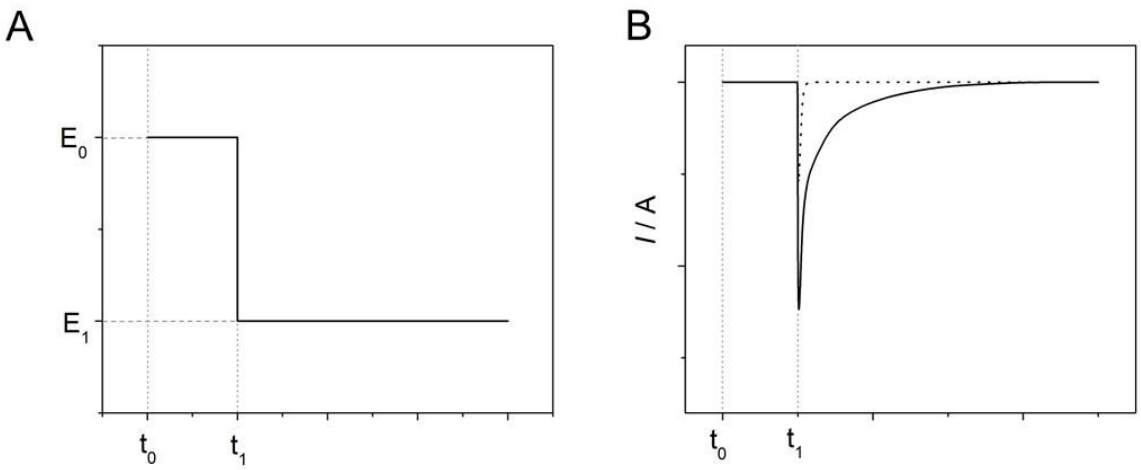

Figure 3.6. (A) A function that describes a potential change over time in chronoamperometry experiment. (B) Schematic chronoamperometric profiles of purely capacitive behaviour (dotted line) with a contribution from a redox process (solid line).

A single step chronoamperometry represents the basic application of this technique. A combination of two or more steps have been used to study more complex systems, such as adsorption of the reaction product, what leads to the change in the value of capacitance.[14] In that case, the use of multistep chronoamperometry facilitates the investigation of the change in the value of a capacitive current and allows a precise estimation of the charge involved in the redox process in both directions.

This technique was applied in the Chapter 5 of this thesis to study desorption of thiols and disulfides from gold surfaces at the constant potential.

Electrochemical impedance spectroscopy

The previously described electrochemical techniques provide a certain dose of information about the studied interface, yet this dose is limited due to the coupling of

capacitive and faradaic components. A more comprehensive characterization of the system requires separating these components. This can be achieved by the application of the Electrochemical Impedance Spectroscopy (EIS). It relies on the application of a small ac voltage perturbation (a few mV) to a certain dc potential in a broad frequency range. This results in ac current output which is phase-shifted with respect to the applied voltage function. This data can be presented in many ways, out of which Nyquist plot is the most seen in the literature (Fig. 3.7).

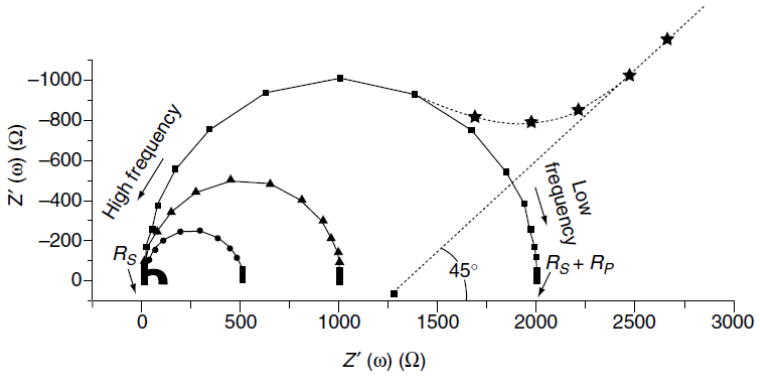

Figure 3.7. Example of a Nyquist plot. Reprinted with permission from reference[10]. Copyright (2006) John Wiley & Sons.

These plots provide information about the charge transfer processes (high frequencies) and diffusional properties (low frequencies) on studied systems and can be fitted to an electronic circuit.[15]

EIS is particularly useful technique when substantial changes in applied potential may affect the studied electrode.[16] Its application covers a wide range of practical aspects such as sensing[17, 18], corrosion[19], analysis of power sources[20-22], and fundamental matters such as interactions at the interface[23, 24] and ion-permeability[25, 26].

This technique was applied in the Chapter 6 of this thesis to investigate the impact of the modification of gold surfaces on the resistive properties of the working electrode.

3.2. *In-situ* electrochemical external reflection Fourier transform infrared spectroscopy[27]

In-situ electrochemical external reflection Fourier transform infrared spectroscopy (ER-FTIR) relies on the exposure of the electrochemically controlled surface to the source of infrared light and collecting spectra corresponding to any interactions taking place. Depending on the polarization of the light, one can study species that are both in the solution and adsorbed on the surface (p-polarized light) or only in solution (s-polarized light). Especially, p-polarized light in of great interest since it provides opportunities to investigate species adsorbed at the interface, such as contaminations and intermediates in catalysis[28] or in studying monolayers adsorbed on metal surfaces[29]. The experiments typically involve the collection of a background spectrum at the potential where no relevant process takes place. Subsequently, the potential is gradually changed, and as-collected spectra are background-subtracted. This creates an easy to follow plot where the evolution of peak intensities during potential modulation indicates the formation or depletion of species at the solid/liquid interface.

A typical experimental setup for such experiments is shown in Figure 3.8.

.

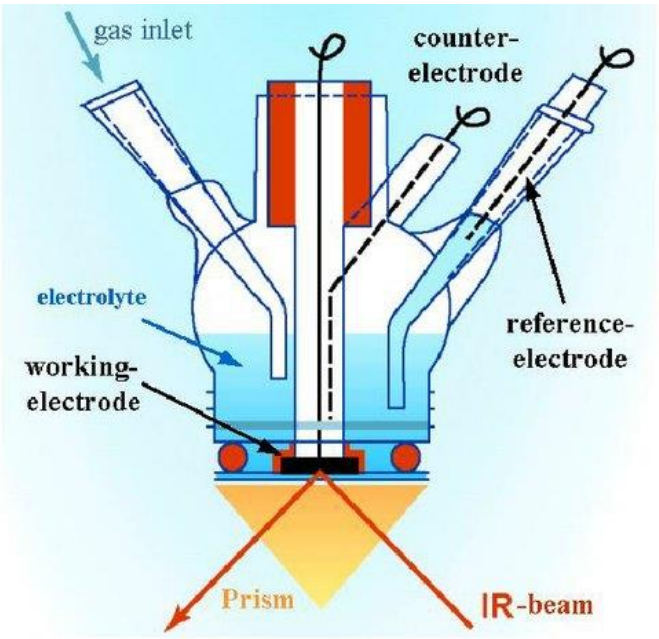

Figure 3.8. A schematic representation of the electrochemical cell used for the external reflection FTIR. Reprinted from reference[30].

This technique was applied in the Chapter 4 of this thesis to investigate the behaviour of cisplatin on gold electrodes.

3.3. Ultraviolet-visible Spectroscopy

Radiation in the range of ultraviolet (200 - 400 nm) and visible (400 – 700 nm) light is rather highly energetic, therefore, exposure of any molecules to this radiation may change their electronic state due to light-induced transitions. This transition can be easily visualised by the Figure 3.9.

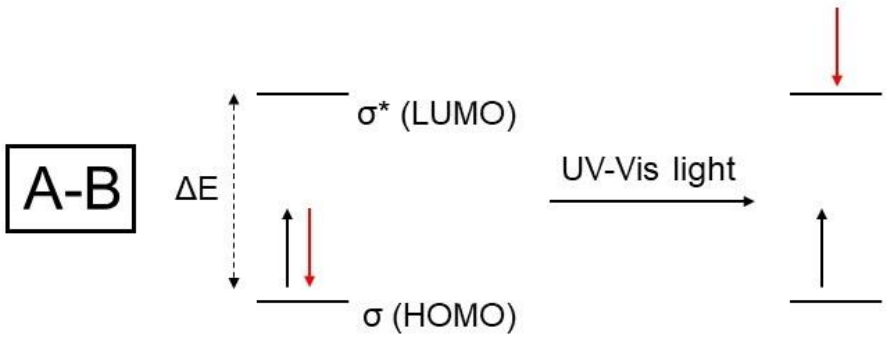

Figure 3.9. Schematic representation of the effect of UV-Vis radiation on the electronic state of a molecule. Reproduced with permission from reference[31]. Copyright (2017) Elsevier.

When the molecule (denoted as A-B) is in the ground state, an electron pair is located at the Highest Occupied Molecular Orbital (HOMO). If the molecule is exposed to the light with energy equal to the gap between HOMO and Lowest Unoccupied Molecular Orbital (LUMO), this portion of light is absorbed and used to bring the molecule to the excited state.

This simple concept opens the door for the qualitative and quantitative analysis (Fig. 3.10). The adsorption wavelength works as a fingerprint of a molecule[32]/functional group[33]/particle size[34] due to their unique absorption properties, what allows identification. In the same time the absorbance value is directly proportional to the concentration of studied species in accordance to the Beer-Lambert law[35] giving an opportunity for quantification.

$$A = \varepsilon l c \qquad (3.1)$$

where ε – molar absorption coefficient, l – path length, c – concentration.

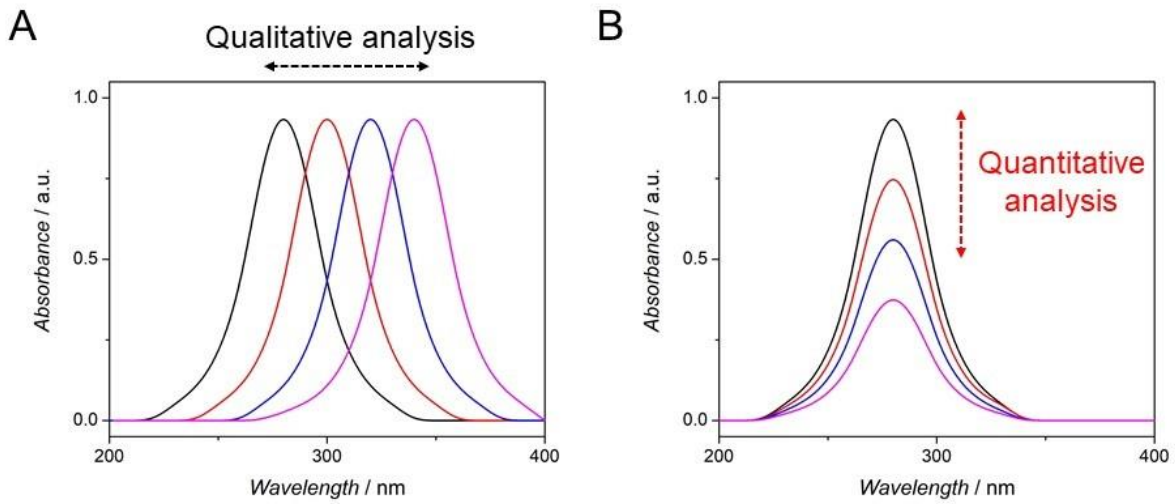

Figure 3.10. A schematic representation of UV-Vis spectroscopy results that can be used for (A) qualitative and (B) quantitative analysis.

This technique was applied in the Chapter 6 of this thesis to investigate interactions between ligands and Pt-based drugs, including kinetic profiles, as well as Job's and Hill's assays.

3.4. Nuclear magnetic resonance spectroscopy[36]

In order to obtain a more detailed information about the structure of the studied molecule, Nuclear Magnetic Resonance (NMR) Spectroscopy is of great use. This technique relies on the interactions of nuclei with external magnetic field. In short, many nuclei have a magnetic moment which is related to their structure-related nuclear spin (defined by a spin number) with odd number of neutrons and protons; nuclei having even number of protons and neutrons have magnetic moment equal to 0. The most commonly studied nuclei, such as ^{1}H, ^{13}C and ^{31}P have a spin number of ½, which means they can be in two different states of ½ and -½ , where nuclei are oriented in parallel (low energy) or in antiparallel

position (high energy) to the magnetic field. Naturally, it is more likely for them to be in the lower one (parallel to the magnetic field). Once a radiofrequency magnetic field is applied, nuclei can change their orientation to the antiparallel one. This transition called spin flip only happens when a specific frequency of the magnetic field that matches the energy gap between two energy levels is applied and adsorbed by the nuclei (Fig. 3.11).

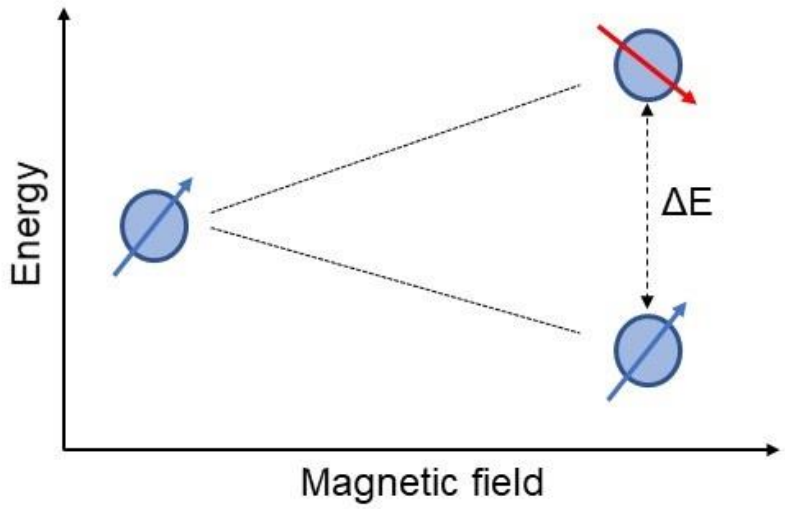

Figure 3.11. Schematic representation of the principle governing NMR. Reproduced with permission from reference[37]. Copyright (1995) John Wiley & Sons.

This technique was applied in the Chapter 6 of this thesis to investigate interactions between ligands and Pt-based drugs at a structural level.

3.5. X-ray photoelectron spectroscopy

X-ray Photoelectron Spectroscopy (XPS) is an analytical technique of great use in surface composition analysis. It relies on the photoelectric effect described by Albert Einstein in 1905.[38] In short, if photons (that can be characterized by energy/frequency and intensity) having energy high enough to overcome the so-called threshold frequency irradiate electrons, these can absorb the energy and be emitted as photoelectrons (Fig. 3.12). The kinetic energy of a photoelectron is equal to the energy of incident photon lowered by the energy that is consumed to overcome electron's binding energy. Binding energy defines the energy that is needed to remove electrons from the orbital and it is a characteristic value for any kind of species, including the same element at various oxidation states[39].

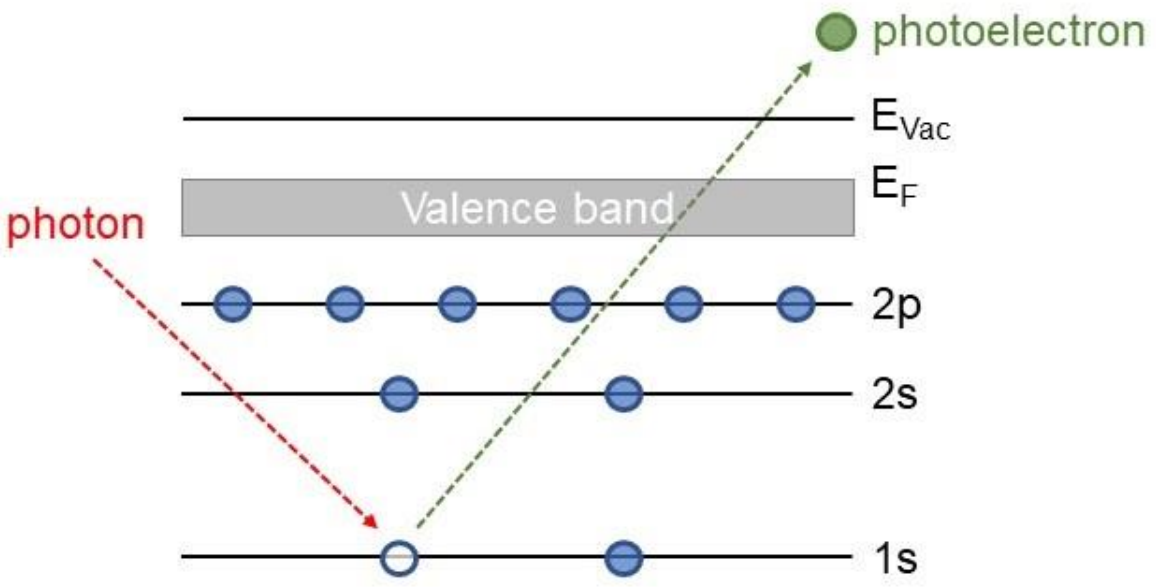

Figure 3.12. Schematic representation of the photoelectric effect that underpins the XPS development. Reproduced with permission from reference[40]. Copyright (2006) Springer.

XPS was found to be useful in characterizing the surface composition of materials, such as core-shell nanoparticles[41], as well as in monitoring of surface modifications[42].

This technique was applied in the Chapter 6 of this thesis to investigate the oxidation state of Pt species adsorbed on modified electrodes.

3.6. Contact angle measurement[43]

Surface properties can be also characterized by contact angle measurements. This technique, although mainly developed to study wettability various materials, is very useful in monitoring the progress of the surface modification process.[44] By observing changes in the contact angle values, one can assess the presence of desired functionalities on the surface. The experimental procedure is straight-forward and involves the application of a small liquid drop on the studied surface and subsequent angle measurement (Fig. 3.13).

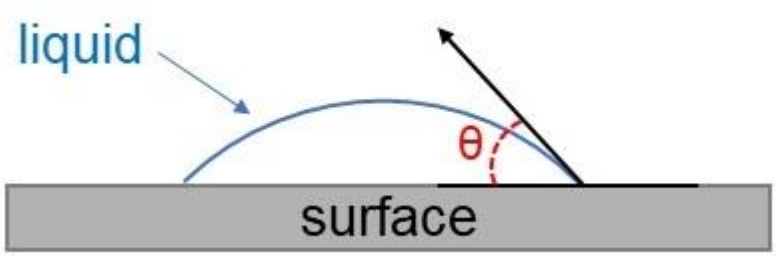

Figure 3.13. A principle of contact angle measurements. Reproduced with permission from reference[43]. Copyright (1999) Elsevier.

This technique was applied in the Chapter 6 of this thesis to monitor the change of contact angle during the surface modification.

3.7. References

1. K. V. Kordesch, *J. Electrochem. Soc.*, 1978, **125**, C77-C91.
2. B. Dunn, H. Kamath and J. M. Tarascon, *Science*, 2011, **334**, 928-935.
3. L. L. Zhang and X. S. Zhao, *Chem. Soc. Rev.*, 2009, **38**, 2520-2531.
4. E. Bakker and Y. Qin, *Anal. Chem.*, 2006, **78**, 3965-3983.
5. E. J. Horn, B. R. Rosen and P. S. Baran, *ACS Cent. Sci.*, 2016, **2**, 302-308.
6. M. Yan, Y. Kawamata and P. S. Baran, *Chem. Rev.*, 2017, **117**, 13230-13319.
7. P. Bai and M. Z. Bazant, *Nat. Commun.*, 2014, **5**.
8. F. Reymond, D. Fermin, H. J. Lee and H. H. Girault, *Electrochim. Acta*, 2000, **45**, 2647-2662.
9. A. J. Bard and L. R. Faulkner, *Electrochemical Methods: Fundamentals and Applications, 2nd Edition*, Wiley Textbooks, 2000.
10. J. Wang, *Analytical Electrochemistry*, Wiley, 2006.
11. T. T. T. Li and M. J. Weaver, *J. Am. Chem. Soc.*, 1984, **106**, 6107-6108.
12. C. E. D. Chidsey, C. R. Bertozzi, T. M. Putvinski and A. M. Mujsce, *J. Am. Chem. Soc.*, 1990, **112**, 4301-4306.
13. A. Yamada, Y. Kato, T. Yoshikuni, Y. Tanaka and N. Tanaka, *Anal. Chim. Acta*, 1979, **3**, 55-63.
14. A. Kolodziej, F. Fernandez-Trillo and P. Rodriguez, *J. Electroanal. Chem.*, 2018, **819**, 51-57.
15. D. Andre, M. Meiler, K. Steiner, H. Walz, T. Soczka-Guth and D. U. Sauer, *J. Power Sources*, 2011, **196**, 5349-5356.
16. J. W. Byeon, B. Jayaraj, S. Vishweswaraiah, S. Rhee, V. H. Desai and Y. H. Sohn, *Mat. Sci. Eng. A-Struct.*, 2005, **407**, 213-225.
17. F. Lisdat and D. Schafer, *Anal. Bioanal. Chem.*, 2008, **391**, 1555-1567.
18. C. M. Ruan, L. J. Yang and Y. B. Li, *Anal. Chem.*, 2002, **74**, 4814-4820.
19. P. L. Bonora, F. Deflorian and L. Fedrizzi, *Electrochim. Acta*, 1996, **41**, 1073-1082.
20. P. L. Taberna, P. Simon and J. F. Fauvarque, *J. Electrochem. Soc.*, 2003, **150**, A292-A300.
21. P. M. Gomadam and J. W. Weidner, *Int. J. Energy Res.*, 2005, **29**, 1133-1151.

22. D. Andre, M. Meiler, K. Steiner, C. Wimmer, T. Soczka-Guth and D. U. Sauer, *J. Power Sources*, 2011, **196**, 5334-5341.
23. X. X. Li, L. H. Shen, D. D. Zhang, H. L. Qi, Q. Gao, F. Ma and C. X. Zhang, *Biosens. Bioelectron.*, 2008, **23**, 1624-1630.
24. A. B. Kharitonov, L. Alfonta, E. Katz and I. Willner, *J. Electroanal. Chem.*, 2000, **487**, 133-141.
25. E. Boubour and R. B. Lennox, *Langmuir*, 2000, **16**, 4222-4228.
26. E. Boubour and R. B. Lennox, *J. Phys. Chem. B*, 2000, **104**, 9004-9010.
27. R. Mendelsohn, G. R. Mao and C. R. Flach, *Biochim. Biophys. Acta Biomembr.*, 2010, **1798**, 788-800.
28. S. C. Chang, L. W. H. Leung and M. J. Weaver, *J. Phys. Chem.*, 1990, **94**, 6013-6021.
29. S. Ye, Y. Sato and K. Uosaki, *Langmuir*, 1997, **13**, 3157-3161.
30. K. J. J. Mayrhofer, *Oxygen reduction and carbon monoxide oxidation on Pt-from model to real systems for fuel cell electrocatalysis*, PhD Thesis, 2005.
31. C. Burgess, in *UV-Visible Spectrophotometry of Water and Wastewater (Second Edition)*, eds. O. Thomas and C. Burgess, Elsevier, 2017, pp. 1-35.
32. O. Nekrassova, N. S. Lawrence and R. G. Compton, *Talanta*, 2003, **60**, 1085-1095.
33. C. Liu, J. T. Lin, S. H. Wang, J. C. Jiang and L. G. Lin, *Sensor. Actuat. B-Chem.*, 2005, **108**, 521-527.
34. W. Haiss, N. T. K. Thanh, J. Aveyard and D. G. Fernig, *Anal. Chem.*, 2007, **79**, 4215-4221.
35. R. W. Ricci, M. A. Ditzler and L. P. Nestor, *J. Chem. Educ.*, 1994, **71**, 983-985.
36. V. Mlynarik, *Anal. Biochem.*, 2017, **529**, 4-9.
37. H. Günther, *NMR Spectroscopy: Basic Principles, Concepts, and Applications in Chemistry*, Wiley, 1995.
38. A. Einstein, *Ann. Phys.*, 1905, **17**, 132-148.
39. G. Silversmit, D. Depla, H. Poelman, G. B. Marin and R. De Gryse, *J. Electron Spectrosc. Relat. Phenom.*, 2004, **135**, 167-175.
40. H.-L. Lee and N. T. Flynn, in *Handbook of Applied Solid State Spectroscopy*, ed. D. R. Vij, Springer US, Boston, MA, 2006, pp. 485-507.

41. E. Bennett, J. Monzo, J. Humphrey, D. Plana, M. Walker, C. McConville, D. Fermin, A. Yanson and P. Rodriguez, *ACS Catal.*, 2016, **6**, 1533-1539.
42. C. D. Bain, J. Evall and G. M. Whitesides, *J. Am. Chem. Soc.*, 1989, **111**, 7155-7164.
43. D. Y. Kwok and A. W. Neumann, *Adv. Colloid Interface Sci.*, 1999, **81**, 167-249.
44. K. M. Chen, W. B. Caldwell and C. A. Mirkin, *J. Am. Chem. Soc.*, 1993, **115**, 1193-1194.

Chapter 4: Preface

The goal of Chapter 4 is to determine the interaction of cisplatin on the surface of gold electrodes. As discussed in Chapter 2, the design of the working electrode includes a monolayer covering the surface of gold. Nevertheless, monolayers are often imperfect what may result in interactions between solution-based species and the surface. This scenario opens a discussion on what would be the interaction between cisplatin and a gold surface with particular attention to the deposition of metallic platinum on the surface. Platinum is known to be a highly catalytically active metal and its exposure to the blood stream could result in undesired transformations of blood components. This aspect is of paramount importance for the safe performance of the proposed hemofiltration system.

Therefore, this chapter describes the potential-dependent behaviour of cisplatin on bare gold surface highlighting the potential range that can be applied without the risk of electrochemical reduction of Pt^{2+} to metallic Pt. This aspect is of great importance for the safe performance of the electrochemical hemofiltration system. This is followed by the catalytic tests that prove the presence of Pt deposits on gold and are relevant for current discussions in the field of electrocatalysis.

Chapter 4: Phosphate-mediated electrochemical adsorption of cisplatin on gold electrodes

This chapter is a modified version of the research article published as:

A. Kolodziej, M. C. Figueiredo, M. T. M. Koper, F. Fernandez-Trillo, P. Rodriguez, *Electrochim. Acta*, 2017, **248**, 409-415.

Authors contribution

P.R, P.F.T and AK conceived the experiments and contributed to the experimental set-up and discussed the results. AK performed all experimental work. The *in-situ* FTIR experiments were performed by MCF at the university of Leiden. All authors contributed to the analysis of the results, discussion, writing and revision of the manuscript. All authors have given approval to the final version of the manuscript.

Acknowledgements

AK acknowledges the University of Birmingham for the financial support through a PhD scholarship at the School of Chemistry. PR and FFT would like to acknowledge the University of Birmingham for the financial support through the Birmingham fellowship program and the Wellcome Trust ISSF grant 184ISSFPP. FFT also thanks John Evans (John Evans Fellowship) for the financial support.

4.1. Abstract

This manuscript reports the potential-dependent adsorption and deposition of cisplatin on polycrystalline gold electrodes. It was found that this process is mediated by the adsorption of phosphate anions on the gold electrode and that the maximum coverage of Pt adsorbed is given by the maximum coverage of phosphate adsorbed at a given potential. The interaction of cisplatin with the phosphate groups was confirmed by in-situ FTIR spectroscopy under external reflexion configuration. Quantitative analysis suggests that the stoichiometry of the phosphate species and the cisplatin adsorbed is 1:1. Moreover, the relationship between the charge of the Pt deposited and the charge of the electrochemical surface area of the Pt deposited on the gold electrodes indicates that 3D nanoclusters of a few atoms of Pt were formed over the gold electrode upon the electrochemical reduction of the adsorbed cisplatin.

The Pt nanoclusters formed under these conditions were later evaluated for the oxidation of a monolayer of carbon monoxide. The Pt nanoclusters showed a high overpotential for the oxidation of this carbon monoxide monolayer and this high oxidation overpotential was attributed to the absence of adsorption sites for OH species on the Pt clusters: only at potentials where the OH species are adsorbed at the edge between the Pt nanocluster and the gold support, the oxidation of the carbon monoxide on the Pt nanoparticles takes place.

4.2. Introduction

The cost of Pt is one of the limitations in the broad commercialization of low temperature fuel cell and water electrolyzers.[1, 2] In the attempt to reduce the cost of the catalyst layer, the scientific community has established a race to decrease the loading of platinum through different strategies such as decreasing the particle size, metal alloying or the optimization of the efficiency of the Pt catalyst through metal supported interactions.[3, 4]

Among all the approaches, decreasing the size of the Pt particles has been one of the most exploited since previous works have reported a strong size-dependent electrocatalytic activity of Pt clusters and nanoparticles.[5, 6] To achieve control over the size and particle size distribution of the Pt nanoparticles and supported Pt clusters different physical and chemical approaches have been adopted.[7-10] One of these approaches, the so-called wet impregnation method, includes the spontaneous adsorption of platinum compounds (hexa- and tetra-chloroplatinates) on the support materials with subsequent reduction by chemical or electrochemical means.[11-13]

Significant efforts have been made to understand and control the initial stages of the adsorption of the Pt precursors and the formation of Pt clusters and films on different support materials. Scanning Tunnelling Microscopy has revealed that the formation of Pt nanoparticles (3 nm) from haloplatinate complexes is preceded by the formation of long order structures of haloplatinate complexes adlayers on Au(111) prepared by a simple immersion method in $HClO_4$.[14]

In other work[15], Bakos et al. reported the potential controlled adsorption of hexachloroplatinic acid on gold polycrystalline electrode in sulfuric acid solution. In this work, the authors reported a maximum coverage of 5% platinum on the gold surface

independently of the adsorption potential in a region between 0.77 V and 0.95 V RHE. Other works have described the formation of platinum deposits on Au(111) electrodes in sulfuric acid solutions.[16-18] Recent works provide full characterization of the structure of the platinum deposits as a function of the deposition time and multiple depositions processes. However, the origin and the understanding of the adsorption of the platinum was not discussed. This information is highly relevant since the adequate selection of the electrolyte will contribute in the optimization of the surface coverage of the platinum deposits.

The electrochemical adsorption and reduction of Pt is a complex process and will not only depend on the ligands coordinated to the Pt-centre [19] but also on the affinity of the Pt-centre or the ligands to the surface chemistry of the support where the platinum would be deposited. This manuscript reports for the first time the use of cisplatin ($Pt(NH_3)_2Cl_2$) and phosphate ions to control the coverage of platinum on gold electrodes. We demonstrate that Pt adsorption on gold electrodes can be mediated by phosphate ions adsorbed on gold and characterise the nature of the phosphate-mediated adsorption of cisplatin on a gold electrode. The potential-dependence of the phosphate-mediated adsorption of the Pt complex allows the control over the surface coverage of platinum atoms over the gold electrode. In addition, upon the reduction of the phosphate-mediated platinum complex, the surface modified electrodes were evaluated towards the electrochemical oxidation of carbon monoxide in acidic media.

4.3. Experimental methods

To ensure reproducible and clean conditions of experiments, all the glassware was soaked overnight in acidified solution of potassium permanganate, followed by a rinse with acidified solution of hydrogen peroxide and boiled five times with Milli-Q water (18.2 MΩ cm, 1 ppb total organic carbon).[20] A three compartment electrochemical cell was employed where a high surface area gold flag was used as the counter electrode and Hg/Hg_2SO_4 electrode as the reference electrode. All the results were converted to RHE scale as presented in the manuscript. The cyclic voltammetry measurements were performed on μAutoLab III potentiostat. Prior to experiments, Argon (6N, BOC) was used to deoxygenate electrolytic solutions.

Gold disk electrodes were prepared from high purity (Sigma Aldrich, 99.999%) gold wire. Prior to each experiment, the gold disk electrode was mechanically polished with alumina slurry, rinsed with water, flame-annealed and cooled down under argon atmosphere. The blank voltammetry of the gold electrode was registered prior each experiment to confirm the cleanness of the system (both electrode and electrolyte). The electrolyte and the solutions were prepared from Dulbecco's Phosphate Buffer Saline solution (DPBS, Lonza) or sulfuric acid (Merck Suprapur, 96%).

The adsorption of cisplatin (Biovision, ≥ 98%), on gold surface was completed by immersing the electrode in 2.6 mg L^{-1} solution of cisplatin in DPBS over the period of 60 seconds at the controlled potential. Excess of cisplatin solution, beyond the monolayer, was removed by rinsing with a copious amount of Milli-Q water.

The oxidation of a monolayer of carbon monoxide (BOC, Research grade) was performed as follow. The Pt-modified electrode was immersed in a sulfuric acid solution at 0.1 V vs

RHE. Carbon monoxide was bubbled in the electrochemical cell for 1 min. In order to avoid any possible contamination from the formation of metal carbonyls, the carbon monoxide was bubbled through a 1 mol L^{-1} solution of NaOH prior inflowing the electrochemical cell. The excess of CO was removed by bubbling Ar for 10 mins. The oxidation of the CO monolayer was recorded in a meniscus configuration between 0.1 V and 1.2 V vs RHE at 0.02 V s^{-1}. The peak convolution of the voltammetric profiles were performed using Peakfit v4.12 software, using smoothing, background correction and Lorentzian minimization.

In situ FTIRs experiments were performed with a Bruker Vertex 80V IR spectrophotometer equipped with a MCT detector. A spectroelectrochemical glass cell with a 60° CaF_2 prism was used, designed for the external reflection mode in a thin layer configuration. FTIR spectra were collected with p-polarized light from an average of 200 scans obtained with 4 cm^{-1} resolution at selected potentials, by applying single potential steps from a reference potential (E = 1.25 V vs RHE) in the negative-going direction up to 0.6 V vs RHE. Several sample spectra at different potentials were collected, and the difference with respect to the reference spectrum was evaluated as ΔR/R. In these difference spectra, negative bands (pointing down) correspond to the generation of species at the gold−electrolyte interface and positive bands (pointing up) to the consumption of species.

4.4. Results and Discussion

4.4.1. Potential-dependence of the electrochemical adsorption and reduction of cisplatin on gold electrodes in phosphate buffer

Cisplatin was pre-adsorbed on the gold electrode by immersing a flat gold polycrystalline electrode in a DPBS solution containing 2.6 mg L^{-1} of cisplatin during 1 min at different potentials ranging between 0.65 V and 1.65 V vs RHE. The currents measured during the adsorption process are shown in Figure SI4.1. Positive currents were recorded during the adsorption of Pt at potentials higher than 1.6 V vs RHE indicating the absence of any adsorption or reduction process (Fig. SI4.2). We attribute the lack of adsorption of cisplatin on the gold surface to the bulk oxidation and formation of gold oxide taking place at these potentials.[21] Large negative currents during the adsorption step at potentials below 0.7 V vs RHE indicated the bulk deposition of platinum. At the adsorption potential of 0.75 V vs RHE, a slightly negative current was recorded suggesting electrodeposition of Pt, however adsorption of cisplatin cannot be discarded. In the potential window between 0.8 V and 1.2 V vs RHE, low values of positive current were observed during the adsorption step. Figure 4.1A shows the cyclic voltammetry profiles in cisplatin-free DPBS solution of a gold polycrystalline electrode onto which cisplatin had been pre-adsorbed at different potentials.

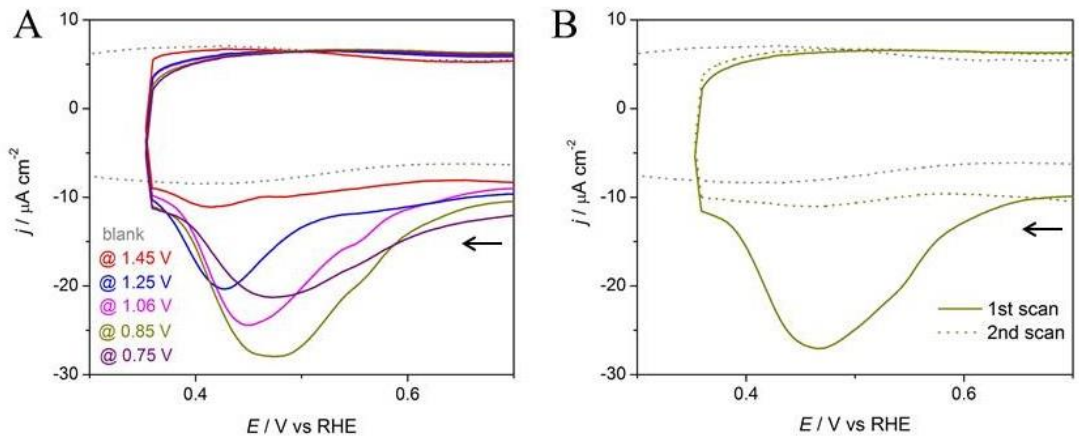

Figure 4.1. (A) Voltammetric profiles in a cisplatin free phosphate buffer solution of surface-modified Au(poly) electrode. Surface modified electrodes were obtained by immersing the electrode in 2.6 mg L^{-1} solution of cisplatin solution during 1 min at different potentials as indicated in the figure. The scan direction is indicated by the arrow in the figure. (B) Consecutive scans of a cisplatin-modified Au(poly) electrode at (@) 0.85 V vs RHE recorded in a cisplatin-free phosphate buffer solution. Scan rate υ = 0.05 V s^{-1}.

All the voltammetric profiles present an irreversible reduction signal in the region between 0.6 V and 0.35 V vs RHE. The absence of this reduction peak and the increase of the double layer in a 2nd scan (Figure 4.1B) confirmed that this reduction peak is associated to the electrochemical reduction of pre-adsorbed cisplatin into metallic Pt according to the reaction:

$$Pt(NH_3)_2Cl_2 + 2e \rightarrow Pt^0 + 2\ NH_3 + 2\ Cl^- \qquad (4.1)$$

The presence of Pt^0 at the surface was further confirmed by recording the voltammograms in a broader potential window (Fig. SI4.3) where two characteristic regions can be observed: the adsorption/desorption of protons and anions in the potential region between 0.05 V and 0.4 V vs RHE, and the oxide formation/reduction region in the potential region between 0.7 V and 1.4 V vs RHE.

Figure 4.1A also shows that the decrease towards more negative potentials of the pre-adsorption potential of the cisplatin resulted in a shift of the onset potential of the reduction of Pt^{+2} to Pt^{0} toward more positive potentials. In addition, the charge associated to the reduction process followed the same trend which confirmed an increase of the cisplatin pre-adsorbed as the adsorption potential decreased. The shift on the onset of the reduction potential and the increase of the total charge matched with the appearance of new features on the voltammetric profiles.

The voltammetric profiles of the reduction of cisplatin on the gold electrode in DPBS contain contributions for the nucleation and growth mechanism of the platinum deposits on the gold electrode. Since different adsorption sites on the surface have characteristic nucleation and growth signals, it should be possible to deconvolute the voltammetric profile to obtain information about the reduction of cisplatin on different sites present on the surface.[22, 23] Understanding each of these peaks might reveal the nature of the reduction process and therefore, furthers studies on single crystal electrodes with different orientations and step-densities will be performed in the future.

The reduction feature appearing between 0.6 V and 0.35 V vs RHE revealed an overlapping of 3 separate peaks (Fig. 4.2A-D). The charge associate to each of these peaks and the total charge corresponding to the reduction is presented as a function of the adsorption potential in Figure 4.3A. When the adsorption potential was as positive as 1.4 V vs RHE, a double peak centred at 0.42/0.5 V vs RHE was observed. At less positive adsorption potentials - 1.25 V, 1.06 V and 0.85 V vs RHE- a new reduction peak appeared at 0.55 V vs RHE, and the charge obtained from the three convoluted peaks increased when the adsorption potential became less positive (Fig. 4.3A). Since the overpotential for the nucleation and growth of Pt particles is dependent on the concentration, changes

in the surface concentration of pre-adsorbed cisplatin should result in a shift in the reduction potential of the platinum.[24]

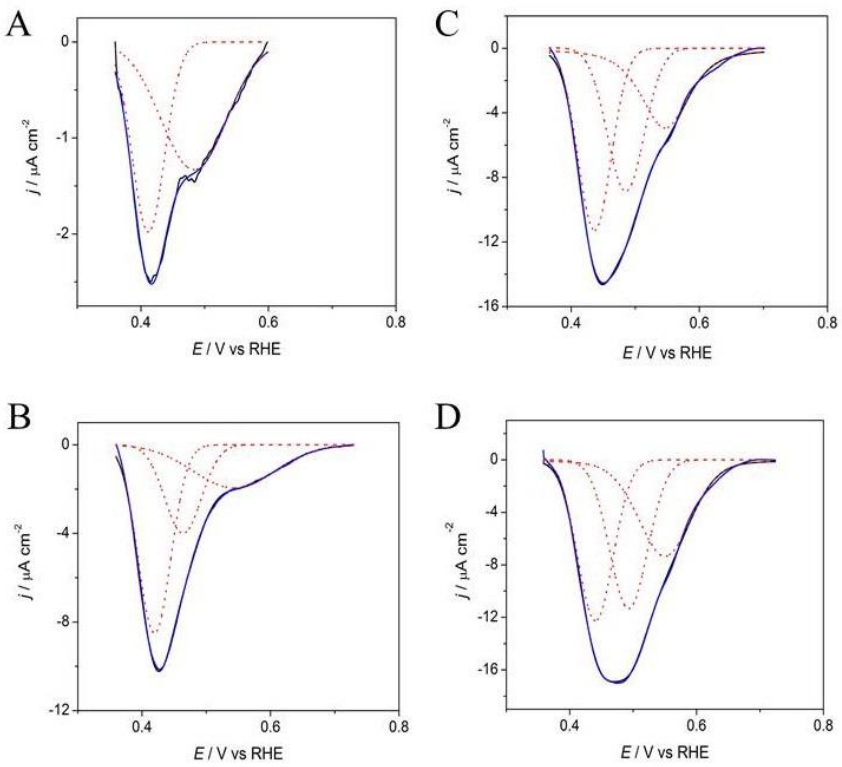

Figure 4.2. Voltammetric profiles taken from Fig. 4.1A (solid black line), deconvoluted peaks (dashed red lines) and fitting of the convoluted peaks (solid blue lines) after preadsorption at (A) 1.45 V (B) 1.25 V (C) 1.06 V vs RHE (D) 0.85 V vs RHE. Peaks were smoothed, background-corrected and deconvoluted using PeakFit v4.12 software. [1]

In order to determine the structure of the Pt deposited on the gold electrode as a function of the adsorption potential, the charge associated to the proton adsorption/desorption from

[1] The shape of the reductive peak is dependent on the surface structure and roughness of gold electrode In the supporting information (Fig. SI4.4) we show the changes in these features observed when studying the adsorption of cisplatin on gold wires with different surface roughness.

Figure SI4.3 was represented as a function of the number of atoms of Pt deposited on the gold electrode (Fig. 4.3B), which was calculated from the total charge of the reduction process (Fig. 4.3A). A linear relationship between reduction charge and the number of platinum atoms adsorbed (slope $6 \cdot 10^{-14}$ µC/atoms Pt) was observed when the adsorption was done between 0.8 V and 1.2 V vs RHE. The deviation of the linear relationship when the adsorption potential was 0.75 V vs RHE is due to the mixed mechanism observed at this potential (adsorption + bulk deposition). A similar observation has been reported by Bakos et al. for the adsorption of Pt in acidic media.[15] Given that the surface atom density of a Pt(111) is $1.50 \cdot 10^{15}$ atoms per 1 cm^2 , the hydrogen adsorption on the platinum deposited on the gold electrodes gives a charge density of 90 µC cm^{-2} which is significantly lower than the theoretical value of 240 µC cm^{-2} for a $1e^-/1H^+$ reaction over a Pt(111) structure.[25] The presence of 2D platinum deposits would result in a charge density closer to the theoretical value of 240 µC cm^{-2}. Given that we are using polycrystalline electrodes, we would expect the value of charge to be smaller and approximately 210 µC cm^{-2}. Thus, we can conclude from here that the reduction of the pre-adsorbed platinum in a potential window between 0.85 V and 1.45 V vs RHE resulted in the formation of 3D nanoclusters over the gold electrode. This result is highly relevant since the final structure of the adsorbed Pt will have an impact on the catalytic activity of the deposited platinum.

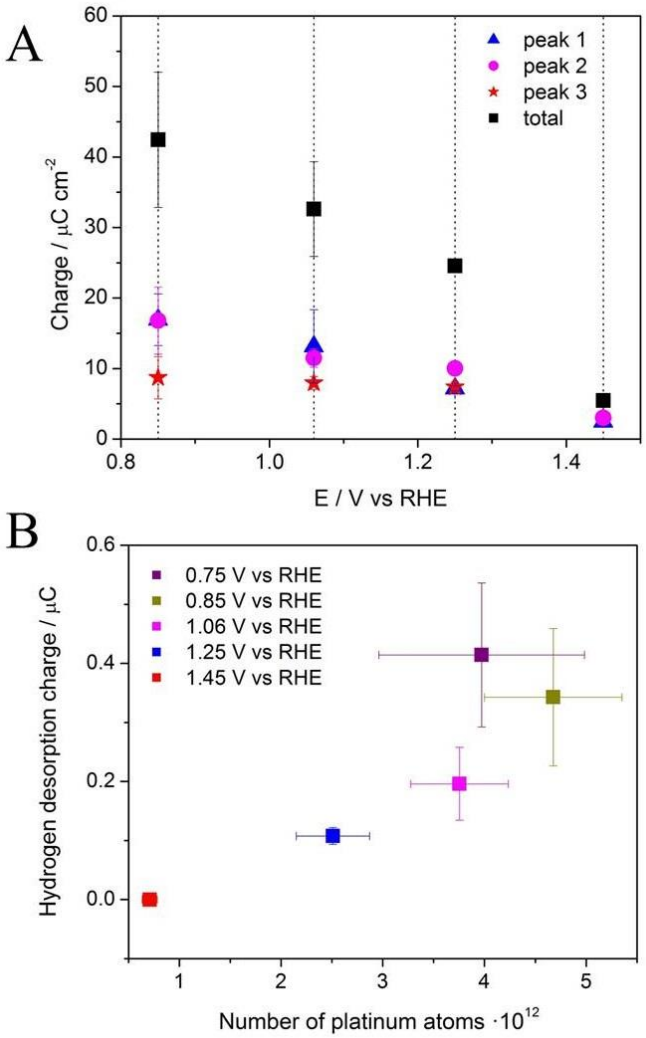

Figure 4.3. (A) Integrated charge from the deconvoluted peaks shown in Figure 3.2 as a function of the adsorption potentials (B) Integrated charge of the hydrogen desorption region from Figure SI4.3A as a function of the number of atoms of platinum adsorbed at each adsorption potential calculated from the total charge in Figure 4.3A.

Interestingly, the potential window where the adsorption of cisplatin was taking place (0.65 V - 1.4 V vs RHE) coincided with the potential limits of the adsorption/desorption of phosphates on gold electrode.[26] It has been reported that the adsorption of phosphate species appears at approx. 0.65 V vs RHE. At potentials higher than 1.2 V vs RHE, the adsorbed phosphate is displaced by the adsorption of OH that results in a decrease in

surface coverage by phosphate. At potentials higher than 1.5 V vs RHE the formation of AuO_x [26] blocks the adsorption of phosphates and therefore the adsorption of cisplatin.

Given the similarities between the reported potential window for the adsorption of phosphates on gold surfaces[26] and the potential window we identified for the adsorption of Pt in these type of surfaces, we suggest that this potential-controlled adsorption of cisplatin is mediated by phosphate anions that are pre-adsorbed on these gold electrodes (Fig. 4.4). Although the interaction of cisplatin with free-phosphate has not been reported to the date, the interactions between Pt-based anti-tumour agents and phosphate groups of organic molecules is well-known.[27-30] For instance, it has been reported that DNA's phosphate groups have high affinity to polynuclear Pt complexes acting as 'Phosphate Clamps' through hydrogen bonds.[28-30] In addition the interaction of cisplatin has been also reported for zirconium phosphate nanoplatelets and calcium phosphates, that can be used as potential delivery agents of cisplatin.[31, 32]

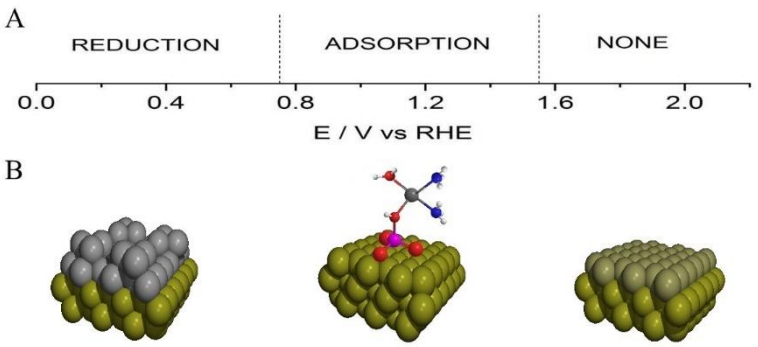

Figure 4.4. (A) Schematic representation of the potential-dependence for the phosphate-mediated adsorption of cisplatin on Au polycrystalline electrode. (B) Hard-sphere model corresponding to the phenomena observed at the range of potentials. Yellow spheres stand for gold, grey spheres stand for platinum, pale yellow spheres stand for gold oxide layer.

This observation implied that the coverage of Pt was limited by the coverage of the phosphate anions. It was thus important to identify the relationship between the adsorbed phosphate and the potential. Habib and Bockris have reported that the maximum coverage (i.e. $\theta = 2 \cdot 10^{-12}$ mol cm^{-2}) of phosphate ions on a polycrystalline gold electrode is obtained at approximately 0.8 V vs RHE.[33] An increase in the electrochemical potential results in lower coverage due to the competitive adsorption of OH species and the formation of the surface oxide, in agreement with previous reports[26] and our observations. We thus compared the number of phosphate molecules adsorbed per surface area on Au polycrystalline surfaces[33] with the number of Pt atoms adsorbed that we calculated as a function of the applied potential during the adsorption process (Table 4.1 and Appendix to Table 4.1 in SI). Overall, there is a good correlation between the number of Pt atoms and the number of phosphate anions, suggesting a 1:1 binding ratio between this phosphate anion and the molecule of cisplatin.

	Number of molecules on the surface / $\cdot 10^{-10}$ mol cm^{-2}		
$E_{adsorption}$ vs RHE	0.85 V	1.06 V	1.25 V
Cisplatin[2]*	**2.2 ± 0.3**	**1.8 ± 0.2**	**1.1 ± 0.2**
Phosphate anions[3]**	**2.0**	**1.5**	**0.7**

Table 4.1. Values of surface concentrations of cisplatin and phosphate anions at different potentials on Au polycrystalline electrode.

[2] Calculated from the value of charge consumed during electrochemical reduction of pre-adsorbed cisplatin assuming no other reductive processes taking place

[3] Concentrations of phosphate anions has been estimated from FTIR data and radiotracer data presented in the ref. 33.

4.4.2. In situ FTIR characterization of the adsorption mechanism of cisplatin

In order to demonstrate the mechanism of this phosphate-mediated adsorption of cisplatin on the gold electrode, in-situ FTIR experiments under external reflection configuration were performed. Figure 4.5 shows a series of potential-dependent FTIR spectra obtained with p-polarized light of Au polycrystalline flat electrodes in a DPBS solution. In both cases, the spectra were obtained with a reference potential at 1.25 V vs RHE. The left panel was obtained in absence of cisplatin while the right panels were obtained in presence of 8.67 µmol L^{-1} cisplatin.

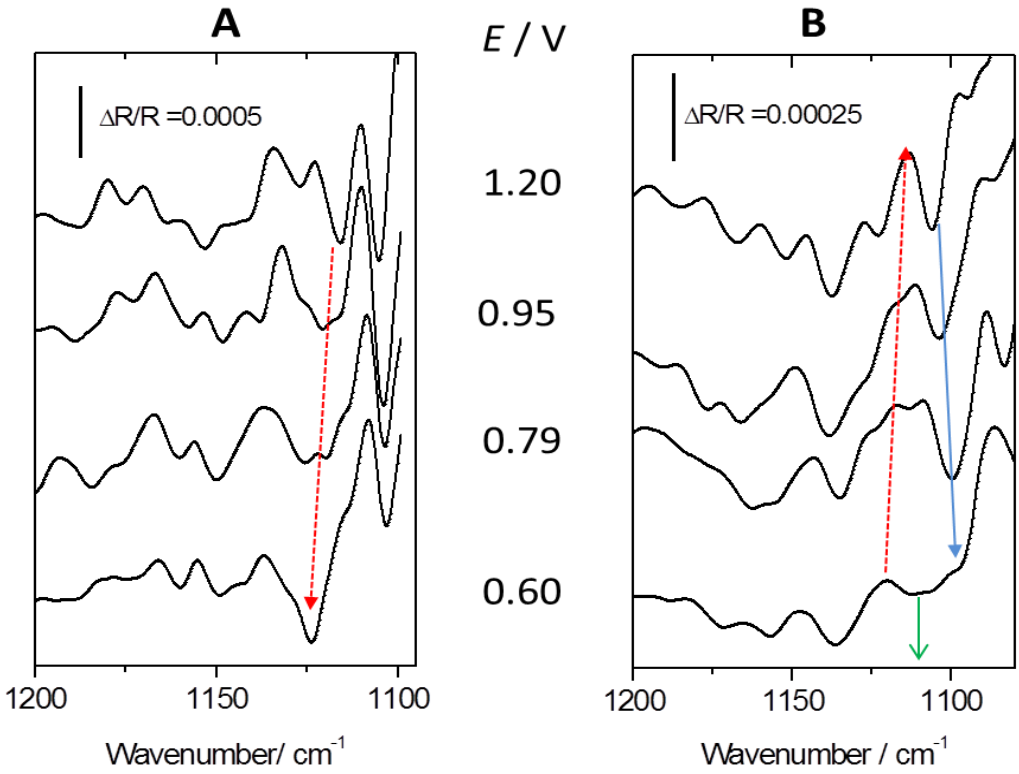

Figure 4.5. Potential difference FTIR spectra of Au flat polycrystalline electrode in DPBS solution in (A) absence and (B) presence of cisplatin. Both spectra were acquired in absence of cisplatin and are referred to the reference spectrum acquired at E_{ref} = 1.25 V vs RHE prior to the potential step-down to 0.6 V vs RHE.

The spectrum in Figure 4.5A shows two negative bands at approximately 1105 cm^{-1} and 1118 cm^{-1}. This bands were associated to the combination of the δ(OH)+ υ (PO) modes of the HPO_4^- according to Yaguchi et al.[26] The spectra below 1080 cm^{-1} was not accessible due to the strong adsorption of the CaF_2 prism. The band at 1118 cm^{-1} showed a blue shift with a stark tuning slope of 19 cm^{-1} V^{-1} demonstrating that this band corresponds to the adsorbed HPO_4^-. However, the negative band at 1105 cm^{-1} increased in intensity between 1.2 V and 0.95 V vs RHE and decreased at lower potentials. This behavior was in agreement with similar results presented by Yaguchi et al.[26] The bands between 1130 cm^{-1} and 1200 cm^{-1} were attributed to contributions of the fluctuation of the thin layer. Figure 4.5B shows the potential depended FTIR spectra of Au polycrystalline flat electrode in a DPBS solution in presence of cisplatin. The reference spectrum was collected in absence of cisplatin at 1.25 V. At 1.2 V vs RHE a negative band was observed at 1102 cm^{-1} associated to the υ(P-O-Pt) which increased in intensity between 1.2 V and 0.79 V vs RHE and showed a red shift with a stark tuning slope of 9 cm^{-1} V^{-1}. A negative band at 1120 cm^{-1} was also observable at 1.2 V vs RHE and disappeared at lower potentials. This band can be associated to the disappearance of the combination of the δ(OH)+ υ(PO) modes of the HPO_4^- due to the strong interaction of the Pt with the OH group in phosphate. A new negative band was observed at 0.6 V vs RHE which can be attributed to the adsorption of phosphate on the Pt deposited on the gold electrode. Overall, we believe these results are consistent with the concept of phosphate-mediated adsorption of Pt on Au surface proposed in Figure 4.4B.

4.4.3. Electrochemical oxidation of carbon monoxide on ultra-small loadings of Pt nanoparticles on gold electrodes.

In order to evaluate the catalytic activity of the platinum nanoparticles deposited on the gold electrodes, the electrochemical oxidation in acidic media of a monolayer of carbon monoxide was evaluated. The oxidation of a monolayer of carbon monoxide was chosen as a probe of the catalytic activity of the Pt deposit because of the lack of adsorption of CO on gold electrodes in acidic pH.[34, 35] Figure 4.6 shows voltammetric profiles of the oxidation of a monolayer of carbon monoxide in acidic media on two platinum modified electrodes obtained using the adsorption-reduction of cisplatin. Figure 4.6 also includes the voltammetric profiles of the oxidation of a monolayer of carbon monoxide on gold electrode modified with cisplatin deposited at 0.65 V, where reduction of Pt should be observed. As can be seen, the oxidation of carbon monoxide on the electrode prepared by deposition of Pt at 0.65 V vs RHE showed two oxidation peaks at 0.8 V and 1.0 V vs RHE. While the appearance of a peak at 0.8 V vs RHE is in agreement with the oxidation of carbon monoxide on supported platinum nanoparticles[36], the appearance of a second peak at significantly higher overpotentials suggested that the oxidation of carbon monoxide was taking place in two different reactions sites. Interestingly, when the electrode was modified by the phosphate-mediated adsorption and deposition of cisplatin, only this second peak at 1.01 V vs RHE was observed.

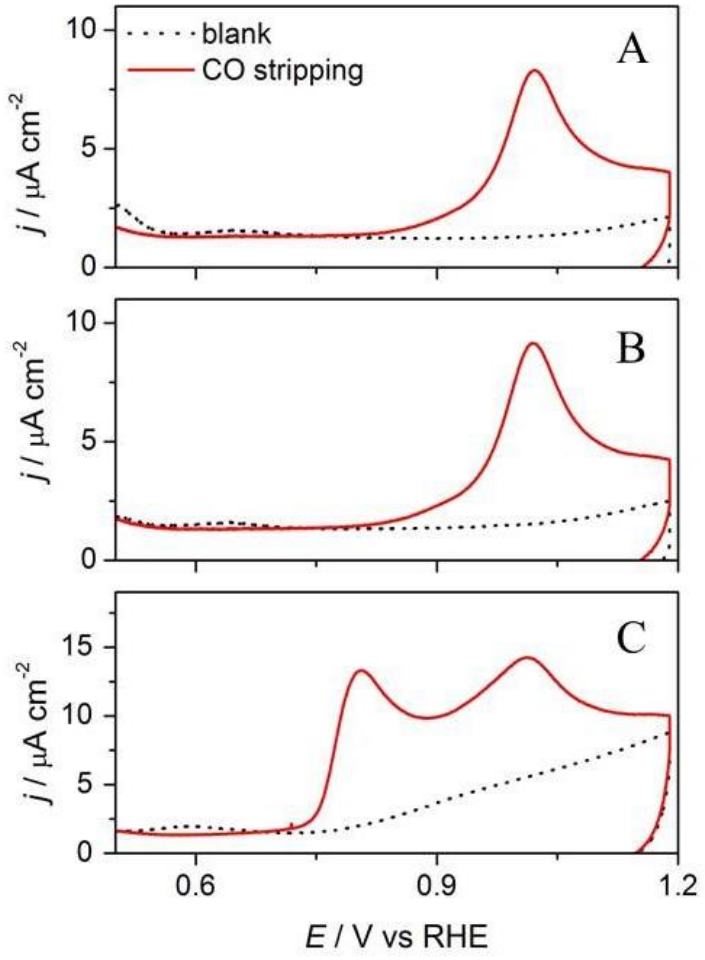

Figure 4.6. Voltammetric profiles in 0.5 M H_2SO_4 for the oxidation of a CO monolayer on the Pt-modified gold electrodes prepared at (A) 1.06 V vs RHE, (B) 0.75 V vs RHE, (C) 0.65 V vs RHE. Scan rate: 0.02 V s^{-1}.

For over more than 2 decades, understanding the mechanism of CO oxidation on Pt substrates has been subject of intensive discussions and several pathways have been proposed.[37-43] Important considerations, such as adsorption energies, have to be taken into account when comparing results on Pt single-crystal electrodes or with supported nanoparticles.[10, 36, 44] The electrochemical oxidation of CO results from a reaction between neighboring CO_{ads} and the OH generated by the activation of water following a Langmuir–Hinshelwood mechanism (L-H), as proposed by Gilman (Equation 4.2).[45]

$$Pt\text{-}CO_{ads} + Pt\text{-}OH_{ads} \rightarrow CO_2 + H^+ + e^- + 2Pt^* \quad (4.2)$$

In our system, the low coverage and the restricted mobility of CO in small Pt-islands significantly limits the likelihood of finding adsorbed ^-OH on nearby sites.[46] Interestingly, the blank voltammograms in Figure 4.6A-B did not show any contributions associated to the oxidation of the Pt catalyst. However, it is important to notice that the onset of the CO oxidation in Figure 4.6A-B coincided with the potential (> 0.95 V vs RHE) where the desorption of sulfates anions and the adsorption of OH species on the gold electrodes at the pH investigated has been reported.[47-49] Therefore, we propose here that the Pt nanoclusters obtained by the phosphate-mediated adsorption of cisplatin on gold are not active towards the CO oxidation on their own. The CO oxidation only takes place at overpotentials where OH replaces the adsorbed phosphate on the gold surface. We propose that on such small Pt nanoclusters, the reaction take place at the edges of the Pt particles following the overall reaction mechanism (Eq. 4.3).

$$Pt\text{-}CO_{ads} + Au\text{-}OH_{ads} \rightarrow CO_2 + H^+ + e^- + Pt^* + Au^* \quad (4.3)$$

4.5. Conclusions

The phosphate-mediated adsorption of cisplatin on gold electrodes has been investigated. This process is potential dependent and takes place in a potential region between 0.75 V vs RHE and 1.5 V vs RHE. At lower potentials than 0.75 V vs RHE the bulk deposition of Pt takes place and at higher potentials the phosphate replacement by the gold oxide

blocks the adsorption of platinum. The maximum coverage of cisplatin is reached at ≈ 0.8 V vs RHE which coincides with the maximum coverage of phosphate.

We propose an adsorption model where each cisplatin is bound to one adsorbed phosphate molecules. In-situ FTIR experiments confirmed this interaction of the platinum with the P-O group in the potential range where the adsorption takes place.

Upon electrochemical reduction of the phosphate mediated cisplatin, platinum 3D nanoclusters islands where obtained on the surface of gold electrodes. The platinum nanoclusters showed high overpotentials for the CO oxidation. The large overpotential was attributed to the low availability of free Pt-sites for the adsorption -OH species. We believe that the oxidation of the CO at high potentials >1.0 V vs RHE is triggered by the displacement of phosphate by OH on gold electrodes.

This manuscript represents the first report of the anion-mediated adsorption/deposition of Pt on an electrified surface. Our findings may open the door for the use of electrochemistry to prepare well-defined monolayers and sub-monolayers of metals using potential dependence adsorption of anions or other relevant ligands.[50] The ability to control the deposition of metal (sub)monolayers has important implications in the development of core-shell nanostructures for Fuel Cells applications and environmental remediation.[51-54] In future studies, the relationship between the crystal structure of the electrodes, the structure of the anion adlayer and the coverage and structure of the resulting Pt deposit will be studied.[55, 56].

4.6. References

1. A. Rabis, P. Rodriguez and T. J. Schmidt, *ACS Catal.*, 2012, **2**, 864-890.
2. M. Li, P. Liu and R. R. Adzic, *J. Phys. Chem. Lett.*, 2012, **3**, 3480-3485.
3. V. R. Stamenkovic, B. S. Mun, M. Arenz, K. J. J. Mayrhofer, C. A. Lucas, G. Wang, P. N. Ross and N. M. Markovic, *Nat. Mater.*, 2007, **6**, 241-247.
4. W.-P. Zhou, X. Yang, M. B. Vukmirovic, B. E. Koel, J. Jiao, G. Peng, M. Mavrikakis and R. R. Adzic, *J. Am. Chem. Soc.*, 2009, **131**, 12755-12762.
5. M. Arenz, K. J. Mayrhofer, V. Stamenkovic, B. B. Blizanac, T. Tomoyuki, P. N. Ross and N. M. Markovic, *J. Am. Chem. Soc.*, 2005, **127**, 6819-6829.
6. K. J. J. Mayrhofer, B. B. Blizanac, M. Arenz, V. R. Stamenkovic, P. N. Ross and N. M. Markovic, *J. Phys. Chem. B*, 2005, **109**, 14433-14440.
7. M. Bayati, J. M. Abad, C. A. Bridges, M. J. Rosseinsky and D. J. Schiffrin, *J. Electroanal. Chem.*, 2008, **623**, 19-28.
8. O. V. Cherstiouk, P. A. Simonov and E. R. Savinova, *Electrochim. Acta*, 2003, **48**, 3851-3860.
9. B. E. Hayden, D. Pletcher, J.-P. Suchsland and L. J. Williams, *Phys. Chem. Chem. Phys.*, 2009, **11**, 1564-1570.
10. F. Maillard, M. Eikerling, O. V. Cherstiouk, S. Schreier, E. Savinova and U. Stimming, *Faraday Discuss.*, 2004, **125**, 357-377.
11. A. E. Aksoylu, J. L. Faria, M. F. R. Pereira, J. L. Figueiredo, P. Serp, J. C. Hierso, R. Feurer, Y. Kihn and P. Kalck, *Appl. Catal., A*, 2003, **243**, 357-365.
12. J. T. Miller, M. Schreier, A. J. Kropf and J. R. Regalbuto, *J. Catal.*, 2004, **225**, 203-212.
13. Q.-H. Zhang, W.-D. Han, Y.-J. Hong and J.-G. Yu, *Catal. Today*, 2009, **148**, 335-340.
14. Y. Nagahara, M. Hara, S. Yoshimoto, J. Inukai, S.-L. Yau and K. Itaya, *J. Phys. Chem. B*, 2004, **108**, 3224-3230.
15. I. Bakos, S. Szabo and T. Pajkossy, *J. Solid State Electrochem.*, 2011, **15**, 2453-2459.
16. S. Strbac, S. Petrovic, R. Vasilic, J. Kovac, A. Zalar and Z. Rakocevic, *Electrochim. Acta*, 2007, **53**, 998-1005.

17. J. Kim, C. Jung, C. K. Rhee and T.-h. Lim, *Langmuir*, 2007, **23**, 10831-10836.
18. J. Kim, D. Shin, C. K. Rhee and S.-H. Yoon, *Langmuir*, 2014, **30**, 4203-4206.
19. C. R. K. Rao and D. C. Trivedi, *Coord. Chem. Rev.*, 2005, **249**, 613-631.
20. J. Souza-Garcia, A. Berná, E. A. Ticianelli, V. Climent and J. M. Feliu, *J. Electroanal. Chem.*, 2011, **660**, 276-284.
21. L. D. Burke and P. F. Nugent, *Gold Bull.*, 1997, **30**, 43-53.
22. R. Francke, V. Climent, H. Baltruschat and J. M. Feliu, *J. Electroanal. Chem.*, 2008, **624**, 228-240.
23. E. B. Molodkina, M. R. Ehrenburg, A. I. Danilov and J. M. Feliu, *Electrochim. Acta*, 2016, **194**, 385-393.
24. A. Milchev, *Electrocrystallization: fundamentals of nucleation and growth*, Springer Science & Business Media 2002.
25. A. J. Bard and C. G. Zoski, *Electroanalytical Chemistry: A Series of Advances: Volume 25*, CRC Press 2013.
26. M. Yaguchi, T. Uchida, K. Motobayashi and M. Osawa, *J. Phys. Chem. Lett.*, 2016, **7**, 3097-3102.
27. K. Taylor, R. Goel, F. Shirazi, M. Molepo, P. Popovic, D. Stewart and P. Wong, *Br. J. Cancer*, 1995, **72**, 1400-1405.
28. S. Komeda, T. Moulaei, M. Chikuma, A. Odani, R. Kipping, N. P. Farrell and L. D. Williams, *Nucleic Acids Res.*, 2011, **39**, 325-336.
29. S. Komeda, T. Moulaei, K. K. Woods, M. Chikuma, N. P. Farrell and L. D. Williams, *J. Am. Chem. Soc.*, 2006, **128**, 16092-16103.
30. A. Prisecaru, Z. Molphy, R. G. Kipping, E. J. Peterson, Y. Qu, A. Kellett and N. P. Farrell, *Nucleic Acids Res.*, 2014, **42(22)**, 13474-13487.
31. A. Barroug and M. J. Glimcher, *J. Orthopaed. Res.*, 2002, **20**, 274-280.
32. A. Diaz, M. L. Gonzalez, R. J. Perez, A. David, A. Mukherjee, A. Baez, A. Clearfield and J. L. Colon, *Nanoscale*, 2013, **5**, 11456-11463.
33. M. A. Habib and J. O. M. Bockris, *J. Electrochem. Soc.*, 1985, **132**, 108-114.
34. C.-H. Shue, L.-Y. Ou Yang, S.-L. Yau and K. Itaya, *Langmuir*, 2005, **21**, 1942-1948.
35. P. Rodriguez, N. Garcia-Araez and M. T. M. Koper, *Phys. Chem. Chem. Phys.*, 2010, **12**, 9373-9380.

36. J. Solla-Gullón, F. J. Vidal-Iglesias, E. Herrero, J. M. Feliu and A. Aldaz, *Electrochem. Commun.*, 2006, **8**, 189-194.
37. N. P. Lebedeva, M. T. M. Koper, J. M. Feliu and R. A. van Santen, *J. Electroanal. Chem.*, 2002, **524**, 242-251.
38. S. C. S. Lai, N. P. Lebedeva, T. H. M. Housmans and M. T. M. Koper, *Top. Catal.*, 2007, **46**, 320-333.
39. H. Wang, Z. Jusys, R. J. Behm and H. D. Abruña, *J. Phys. Chem. C*, 2012, **116**, 11040-11053.
40. M. J. S. Farias, E. Herrero and J. M. Feliu, *J. Phys. Chem. C*, 2013, **117**, 2903-2913.
41. G. García, A. González-Orive, M. Roca-Ayats, O. Guillén-Villafuerte, G. Á. Planes, M. V. Martínez-Huerta, A. Hernández-Creus and E. Pastor, *Int. J. Hydrogen Energy*, 2016, **41**, 19674-19683.
42. M. J. S. Farias, C. Busó-Rogero, F. J. Vidal-Iglesias, J. Solla-Gullón, G. A. Camara and J. M. Feliu, *Langmuir*, 2017, **33**, 865-871.
43. M. T. M. Koper, S. C. S. Lai and E. Herrero, in *Fuel Cell Catalysis*, John Wiley & Sons, Inc. , 2008, p. 159.
44. C. Coutanceau, P. Urchaga and S. Baranton, *Electrochem. Commun.*, 2012, **22**, 109-112.
45. S. Gilman, *J. Phys. Chem.*, 1964, **68**, 70-80.
46. K. A. Friedrich, F. Henglein, U. Stimming and W. Unkauf, *Electrochim. Acta*, 2000, **45**, 3283-3293.
47. Y. B. Skuratnik, A. E. Kozachinskii, A. P. Pchelnikov and V. V. Losev, *J. Electroanal. Chem.*, 1994, **366**, 311-316.
48. G. J. Edens, X. Gao and M. J. Weaver, *J. Electroanal. Chem.*, 1994, **375**, 357-366.
49. K. Ataka and M. Osawa, *Langmuir*, 1998, **14**, 951-959.
50. C. J. Serpell, J. Cookson, D. Ozkaya and P. D. Beer, *Nat. Chem.*, 2011, **3**, 478-483.
51. L. Peng, L. Gan, Y. Wei, H. Yang, J. Li, H. Du and F. Kang, *J. Phys. Chem. C*, 2016, **120**, 28664-28671.
52. F. Calle-Vallejo, M. T. M. Koper and A. S. Bandarenka, *Chem. Soc. Rev.*, 2013, **42**, 5210-5230.

53. J. Monzo, Y. Malewski, R. Kortlever, F. J. Vidal-Iglesias, J. Solla-Gullon, M. T. M. Koper and P. Rodriguez, *J. Mater. Chem. A*, 2015, **3**, 23690-23698.
54. J. J. L. Humphrey, D. Plana, V. Celorrio, S. Sadasivan, R. P. Tooze, P. Rodríguez and D. J. Fermín, *ChemCatChem*, 2016, **8**, 952-960.
55. N. Garcia-Araez, P. Rodriguez, H. J. Bakker and M. T. M. Koper, *J. Phys. Chem. C*, 2012, **116**, 4786-4792.
56. A. Cuesta, M. Kleinert and D. M. Kolb, *Phys. Chem. Chem. Phys.*, 2000, **2**, 5684-5690.

Chapter 4: Supporting information

4.7. Supporting figures

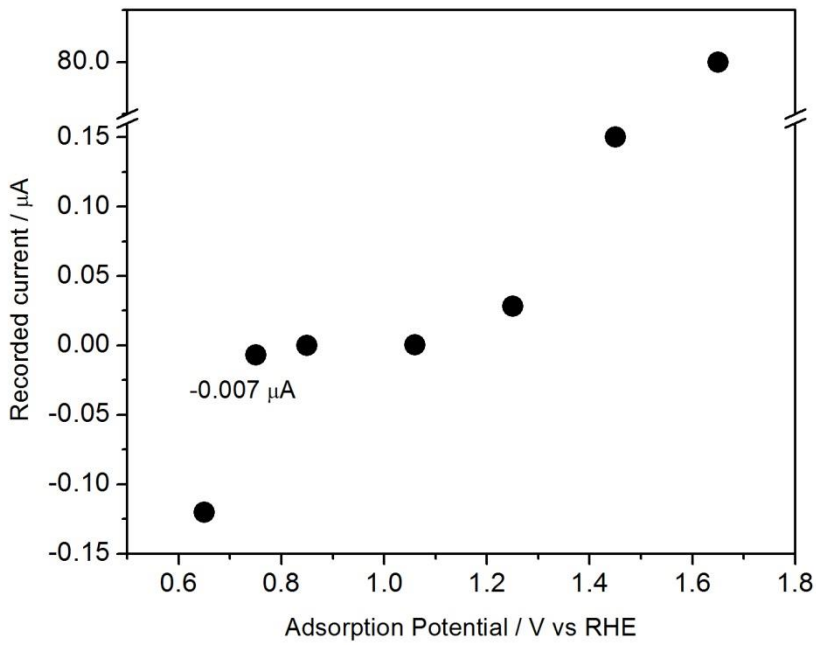

Figure SI4.1. Instant currents recorded during potential-controlled adsorption of cisplatin in DPBS.

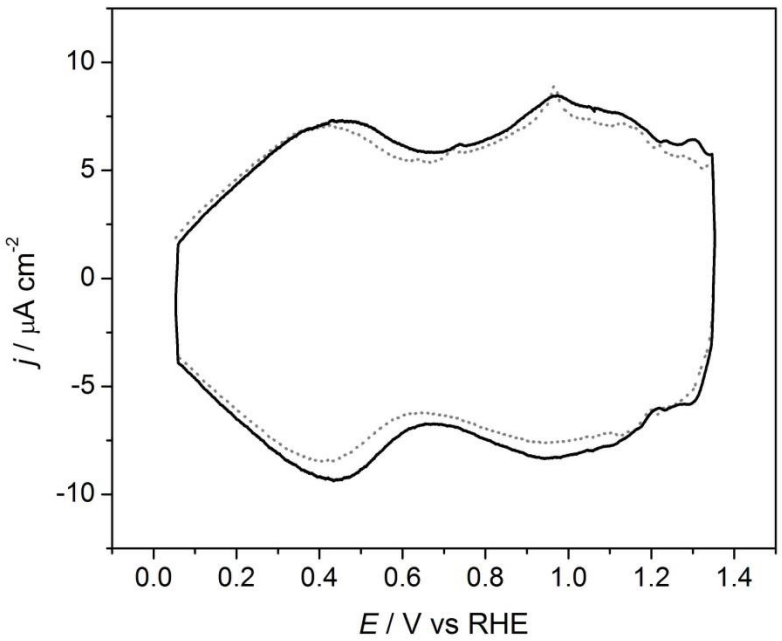

Figure SI4.2. Voltammetric profile of Au polyoriented electrode in DPBS before (dotted line) and after (solid line) potential polarization of the electrode at 1.65 V vs RHE in a solution of 2.6 mg L^{-1} of cisplatin in DPBS. Scan rate υ = 0.05 V s^{-1}

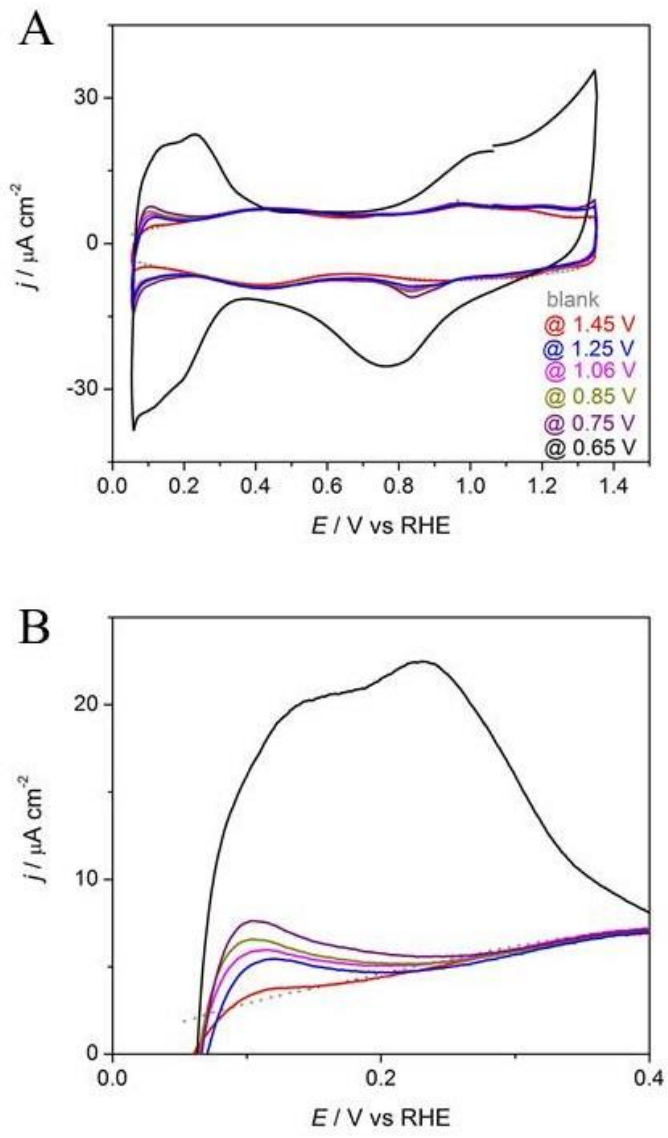

Figure SI4.3. (A) Voltammetric profiles of Pt-modified Au polycrystalline electrode in DPBS. Scan rate υ = 0.05 V s^{-1}. (B) Potential region between 0.0 V vs RHE and 0.4 V vs RHE taken from Figure SI4.3A.

It can be seen on Figure SI4.3, that the charge associated to the hydrogen desorption (0.05 V vs RHE - 0.25 V vs RHE) increases as a function of the adsorption potential from 1.45 V vs RHE to 0.75 V vs RHE. At lower adsorption potentials, the change of the hydrogen adsorption shows a large increase in agreement with the bulk deposition of Pt.

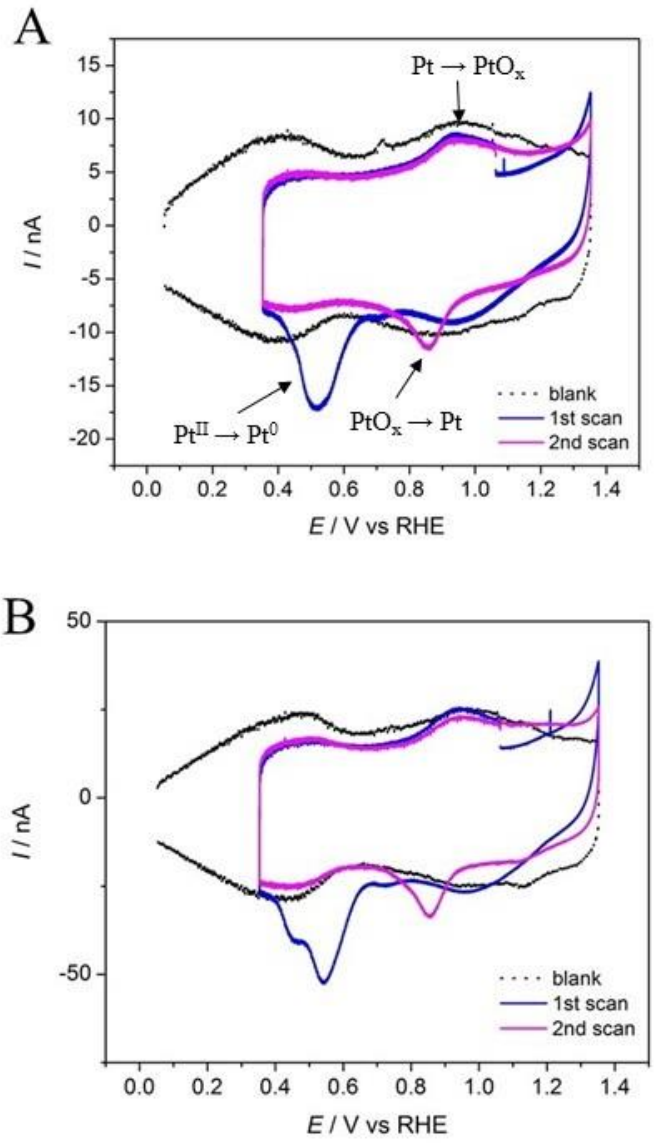

Figure SI4.4. Voltammetric profiles in a cisplatin free phosphate buffer solution of surface-modified Au(poly) electrode. Surface modified electrodes were obtained by polarization of a gold wire in 2.6 mg L^{-1} solution of cisplatin solution during 1 min at 1.06 V. Scan rate υ = 0.05 V s^{-1}. (A) flame-annealed gold wire (B) gold wire after surface roughening using cathodic corrosion method.[1] The cathodic corrosion conditions used for the roughening of the electrode were the following: square wave potential between -4 V and 2 V vs Pt with a frequency of 100 Hz in a 1 M NaOH during 30 s.

The increase of the currents in Figure SI4.4B in comparison with the currents in Figure SI4.4A demonstrates the increase of the surface area of the electrode upon cathodic corrosion polarization. Such increase of the surface area also results in changes in the surface structure and an increase of low coordinated atoms at the surface.

Appendix to Table 4.1

Calculation of the surface concentrations of cisplatin (e.g. the adsorption of cisplatin at 0.85 V vs RHE):

1. The peak corresponding to the reduction of irreversibly adsorbed cisplatin has been integrated using Origin software and Equation 1.

$$s = 2.1 \cdot 10^{-6} \left[\frac{A \times V}{cm^2}\right] \quad \text{(SI4.1)}$$

2. The integrated value was divided by the scan rate resulting in the charge of the electrochemical reduction process (Equation 2).

$$Q = \frac{2.1 \cdot 10^{-6} \left[\frac{A \times V}{cm^2}\right]}{0.05[V \cdot s^{-1}]} = 4.2 \cdot 10^{-5} \left[\frac{A \times s}{cm^2}\right] = 4.2 \cdot 10^{-5} \left[\frac{C}{cm^2}\right] \quad \text{(SI4.2)}$$

3. The number moles of Pt atoms formed during electrochemical reduction can be calculated according to Faraday's Law (Equation 3 and 4).

$$Pt^{2+} + 2e \rightarrow Pt^0 \quad \text{(SI4.3)}$$

Therefore:

$$n_{Pt} = \frac{4.2 \cdot 10^{-5} \left[\frac{C}{cm^2}\right] \cdot 1[mol]}{2 \cdot 96500[C]} = 2.18 \cdot 10^{-10}[mol] \quad \text{(SI4.4)}$$

4.8. References

1. A. I. Yanson, P. Rodriguez, N. Garcia-Araez, R. V. Mom, F. D. Tichelaar and M. T. M. Koper, *Angew. Chem. Int. Ed.*, 2011, **50**, 6346-6350.

Chapter 5: Preface

The aim of Chapter 5 is to determine the electrochemical stability of thiol- and disulfide-modified gold electrodes in a physiological medium.

The electrochemical platform is composed of a monolayer covering the surface of gold electrode. It is important to understand what molecules offer stability in a wide potential range and what factors can affect that. This will imply the potential range that can be used for the adsorption and sensing of Pt-based drugs

Moreover, selected molecules, 3-mercaptopropionic acid, 2-mercaptoethanol, 1,4-dithiothreitol and DL-thioctic acid, have functionalities that offer a range of strategies to be used in order to attach a ligand at the later stages of the project.

Stability of selected molecules was studies using progressive potential-step chronoamperometry. It is of great importance as the electrochemical hemofiltration system, similarly to other commercially viable solution, would work in constant-potential mode.

Additionally, the effect of surface structure on the stability of monolayers was discussed with an intention of using this knowledge in further stages of the project when nanoparticles with preferential orientation could be used as a modification platform.

Chapter 5: Determining the parameters governing the electrochemical stability of thiol and disulfides self-assembled monolayer on gold electrodes in physiological medium

This chapter is a modified version of the research article published as:

A. Kolodziej, F. Fernandez-Trillo, P. Rodriguez, *J. Electroanal. Chem.*, 2018, **819**, 51-57.

Authors contribution

P.R, P.F.T and AK conceived the experiments and contributed to the experimental set-up and discussed the results. AK performed all experimental work. All authors contributed to the analysis of the results, discussion, writing and revision of the manuscript. All authors have given approval to the final version of the manuscript.

Acknowledgements

AK acknowledges the University of Birmingham for the financial support through a PhD scholarship at the School of Chemistry. PR and FFT would like to acknowledge the University of Birmingham for the financial support through the Birmingham fellowship program. FFT also thanks John Evans (John Evans Fellowship) for the financial support.

5.1. Abstract

Herein we study the electrochemical potential-dependent and time-dependent stability of thiols and disulfides as self-assembled monolayers on gold electrodes. The stability of four representative sulfur-containing compounds: 3-mercaptopropionic acid, 2-mercaptoethanol, 1,4-dithiothreitol and DL-thioctic acid, was assessed in simulated physiological conditions (i.e. phosphate buffer saline). The stability of these molecules was evaluated using cyclic voltammetry and step-potential chronoamperometry. Coordination of the thiols and disulfides significantly affects the stability of the self-assembled monolayer. In addition, studies performed using gold single crystal (100) and (111) electrodes show the superior binding strength of the SAM on the Au(100) surface structure.

5.2. Introduction

The functionalization of metal surfaces by self-assembled monolayers (SAMs) of alkanethiols and closely related compounds is a continuously expanding area with enormous impact on corrosion, lubrication, biomimetics, and sensing among others fields.[1-7] Recently, SAMs have also found relevant applications in drug/gene delivery and imaging.[8, 9] The controlled release of drugs and related compounds, is highly relevant in medical applications, for instance to minimize negative side effects, as well as extend the circulation and half-life of these bioactive compounds.[1, 10-12]

Thiol-functionalized molecules have been widely studied by electrochemical means due to their importance in mentioned areas. Understanding the stability of these S-Au SAMs is of paramount importance to benchmark the reliability and reproducibility of the electrochemical devices fabricated with these materials.[13-15] For example, in the development of electrochemical sensors, a robust and stable monolayer would be desirable, in particular one that can operate in a wide potential window. However, SAMs are subject to oxidative and reductive desorption that compromises the integrity of the monolayer. Reductive desorption is more restrictive due to its occurrence at the potentials more likely to be analytically useful.[16,17] For these reasons, reductive desorption of thiols from gold surfaces have been studied by a variety of electrochemical, probe microscopies and spectroelectrochemical techniques.[13-15, 18-34]. While electrochemical and spectroelectrochemical methods provide important information on the coverage, potential window stability and the charge number per molecule adsorbed; in-situ probe microscopy gives information about the packing, unit cell and adsorption symmetry of thiols as a function of the potential.

Previous studies have been mostly conducted using cyclic voltammetry (CV) and chronoamperometry (CA) in alkaline media due to the high solubility of thiolates under these conditions. Important contributions to the understanding of thiols coverage and stability on model systems have been reported by Lipkowski group over the last two decades. Recently, Kunze et al. and Laredo et at. have reported the importance of the methodology implemented to determine the coverage of thiol monolayers on Au(111) single crystal electrodes. In these reports it is highlighted how reductive desorption methods present systematic errors due to the uncertainties associated with the charging current correction. These authors introduced a step potential chronocoulometry as a potentiostatic method to measure the charge density at the electrode at different potentials in 0.1 M NaF, 0.1M $HClO_4$ and 0.1 M NaOH.[13-15] However, the understanding of the stability of adsorbed sulfur-containing molecules on gold electrodes at physiological conditions has enormous implications in sensing and the controlled delivery of drugs in blood (pH=7.2-7.6).[35-37]

Noteworthy, in addition to the pH, the reductive desorption of thiols is influenced by the surface structure of the metal substrate. Such structure-reactivity relationship is attributed to the different coordination of surface atoms[19] and a difference in binding energies to various basal planes.[21, 22, 28, 38-40] In order to provide a rational understanding of the role of the surface structure on the stability of thiols in electrochemical media, spectroelectrochemical methods have been also used.[18, 29, 30] Recently, Bizzotto et al. have used fluorescence microscopy and thiols tagged with fluorescent probes to track the reductive desorption of thiols as a function of the surface structure of polyoriented bead-type gold electrodes.[18, 31] The report by Bizzotto concludes that (111) is more amenable

to desorption of thiol SAMs when compared to the other surface sites of the polycrystalline gold electrode.

The implementation of thiols SAM in controlled delivery of drugs and nano-sensing requires an understanding of the parameters governing the desorption of thiols from polycrystalline surfaces that mimic monocrystalline surfaces and its behaviour in physiological media.

Aware of these needs, here we present a progressive step-potential approach that provides potential and time-dependence insights in the reductive desorption of adsorbed monolayers of thiols from polycrystalline gold electrodes in a physiological media containing phosphate and chloride ions. The protocol was evaluated over 4 representative sulfur-containing molecules: 3-mercaptopropionic acid (**1**), 2-mercaptoethanol (**2**), 1,4-dithiothreitol (**3**) and DL-thioctic acid (**4**) in a phosphate saline buffer solution (DPBS). The progressive step-potential experiments provide relevant information on the stability of the thiols as a function of their nature; at the same time these experiments provide relevant information on the kinetics of the reductive desorption process. We also evaluated the influence of the surface structure of the gold electrode for the desorption of two selected compounds: 3-mercaptopropionic acid (**1**) and DL-thioctic acid (**4**) in a phosphate saline buffer solution.

5.3. Experimental methods

An exhaustive cleaning procedure of the glassware was implemented to ensure reproducible experimental conditions.[41] On a daily basis, the glassware was soaked

overnight in an acidic solution of $KMnO_4$. The glassware was then removed from the $KMnO_4$ solution, and rinsed with a diluted solution of H_2SO_4/H_2O_2 with a ratio of 1:3. The glassware was finally rinsed with boiling Milli-Q water (18.2 MΩ cm, 1 ppb total organic carbon) at least 5 times to ensure the absence of sulfate ions in the working solution. A three-compartment electrochemical cell was employed with a high surface area gold flag counter electrode and a Hg/Hg_2SO_4 reference electrode. All the results were converted to RHE scale as presented in the manuscript. Measurements were performed on μAutoLab III potentiostat. Prior to experiments, Argon (6N, BOC) was used to deoxygenate electrolytic media.

Gold disk electrodes were prepared from high purity (Sigma Aldrich, 99.999%) gold wire. Prior to each experiment, the gold disk electrode was mechanically polished with diamond slurry, rinsed with Milli-Q water, flame-annealed and cooled down under argon atmosphere.

Au(111) and Au(100) bead-type single-crystal electrodes (icryst) were flame annealed and cooled down in Ar atmosphere prior to each experiment. The blank voltammetry of the gold electrode was registered prior to each set of experiments to confirm the cleanness of the system (both electrode and electrolyte). Dulbecco's Phosphate Buffer Saline solution (DPBS pH= 7.4, Lonza) was used as the electrolyte throughout the manuscript. This electrolyte was selected to mimic physiological conditions (i.e. pH and osmolarity) and has been used in a range of scientific reports including examples in drug delivery[42] or cells culture[43]. All the experiments were performed at room temperature which fluctuates between 14°C and 20°C.

Gold electrodes were functionalised with self-assembled layers of the desired compound by immersing the clean gold electrode, following flame-annealing and rinsing with Milli-Q

water, in a solution containing 10 mM of the desired compound. The gold electrode was immersed for 10 min at open circuit potential (OCP). Solutions were prepared as follows: 3-mercaptopropionic acid (**1**) (Sigma Aldrich, ≥ 99%) in 3:1 mixture of Milli-Q water and absolute ethanol; 2-mercaptoethanol (**2**) (Sigma Aldrich, ≥ 99%) and 1,4-dithiothreitol (**3**) (Sigma Aldrich, ≥ 98%) in Milli-Q water; and DL-thioctic acid (**4**) (Alfa Aesar, 98%) in absolute ethanol. The excess of physisorbed molecules was removed by rinsing with a copious amount of Milli-Q water.

5.4. Results and discussion

5.4.1. Assessment of the stability of 3-mercaptopropionic acid, 2-mercaptoethanol, 1,4-dithiothreitol and DL-thioctic acid on Au polycrystalline electrode in phosphate buffer solution

Figure 5.1 shows the voltammetric profiles of the surface-modified Au electrodes with the four different compounds evaluated **1**-**4**. The blank voltammetry of bare gold polycrystalline electrode is included for comparison. In all the cases, a decrease of the double-layer charging current can be observed while the features associated to the lifting of the reconstruction of Au and to the adsorption/desorption of phosphate anions disappear.[44] These changes in the voltammetric profile are a clear evidence of the presence of compounds **1**-**4** on the surface. Differences in the capacitive current for each molecule correspond to different surface defects formed by each monolayer.[45]

In these voltammetric profiles, several features could be identified. At lower potentials (-0.15 to 0.25 V vs RHE) reduction peaks associated to the irreversible desorption of the compounds were observed.[23] The onset potential for the reductive desorption of monothiols (**1**) and (**2**), appeared at more positive values than those for compounds (**3**) and (**4**), where (**3**) and (**4**) have similar desorption kinetics. This difference in potential is associated to the higher stability of those compounds containing two sulfur atoms with respect to the monothiols.[16]

When we compared both monothiols, the desorption of 3-mercaptopropionic acid (**1**) was much faster than the desorption of 2-mercaptoethanol (**2**). We believe that the bulky carboxylic group in (**1**) may affect the order of the monolayer, resulting in a higher number of defects, or pinholes, in the adlayer. The presence of pinholes results in the desorption of thiols,[26] a process that thus happens at more positive potentials.[46, 47] This is in agreement with the larger double layer capacity observed in the case of (**1**), as a consequence of a lower surface coverage.[45] Previous results have also shown that the interaction between the hydroxyl groups of 2-mercaptoethanol (**2**) might play a significant role in the adsorption step of 2-mercaptoethanol on Au(111) resulting in different commensurable and incommensurable structures. The presence of multiple overlapping signals on the desorption of both monothiols (**1**) and (**2**) can be associated to the desorption from different surface structures, the stability of the different incommensurable and commensurable phases of the thiols, or the combination of both (see discussion below).

Finally, from voltammetric profiles we could conclude that the desorption of the thiols was not reversible, as evidenced by the lower charge on the anodic process (re-adsorption of desorbed molecules) observed during the positive scan.

Due to the uncertainties associated to the double layer charging correction and the reconstruction of the gold surface, in particular for polycrystalline electrodes, determining the charge of the desorption of thiols from a cyclic voltammetry results in a large error.

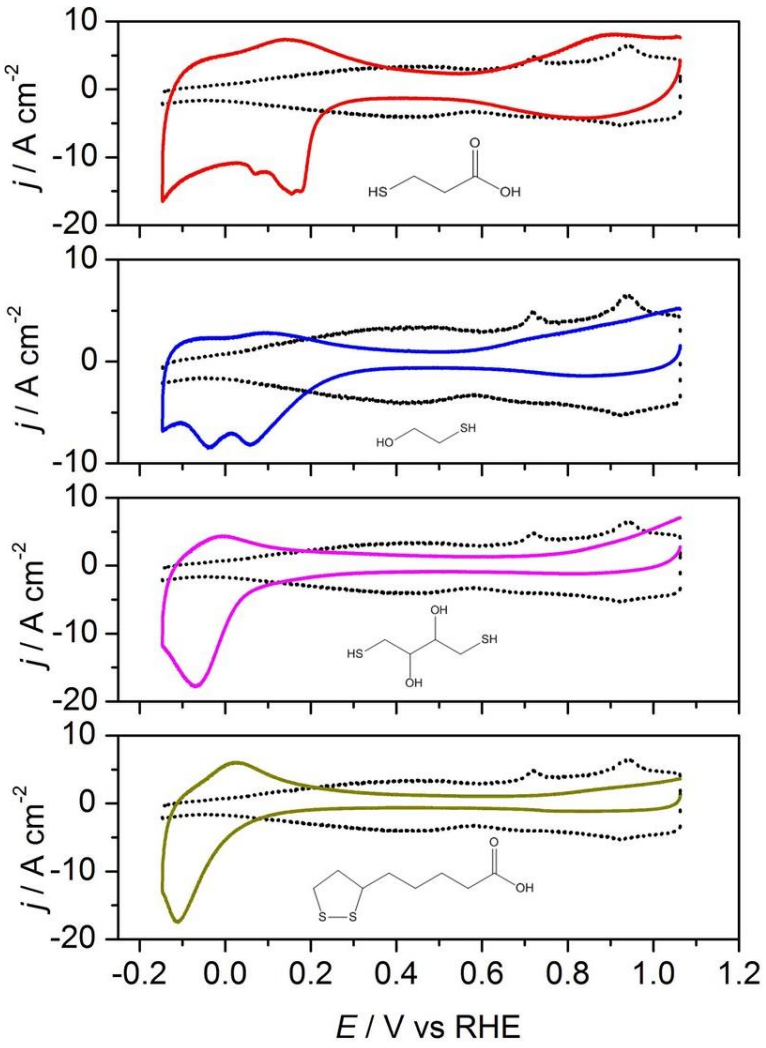

Figure 5.1. Voltammetric profiles of polycrystalline gold electrodes modified with 3-mercaptopropionic acid (**1**), 2-mercaptoethanol (**2**), 1,4-dithiothreitol (**3**) and DL-thioctic acid (**4**) recorded in DPBS. Blank voltammetries of the electrodes in absence of the adsorbed molecules are shown for comparison (dotted line). Scan rate $\upsilon = 0.05\ V\ s^{-1}$.

In order to gain quantitative insights in the stability and desorption kinetics of these sulfur containing molecules from the gold surfaces, a chronoamperometric method was developed (Fig. 5.2A). Previous work by Lipkowski group[13-15] developed and implemented a chronoamperometric method to determine the charge of adsorbed molecules and packing densities of self-assembled monolayers of long chain aliphatic thiols and on single crystal electrodes. Due to the differences in the nature and structure of the molecules (long chain aliphatic thiols vs short chain thiols and disulfides), and the differences of the surface structure of the gold electrodes (single crystal vs polycrystalline electrodes) the implementation of this protocol and the determination of the packing of the molecules was not possible. As an alternative, we modified the protocol: a progressive step-potential strategy was implemented to supress large contributions associated to the charging of the double layer on the current transients. The protocol relies on the application of 10 successive potentials steps (0.05 s each) where only one of the steps is prolonged up to 1 s. This prolonged step provides a distinctive signal of the desorption of the molecules at the given potential. In this way, we were able to minimize contributions of the double layer charging to the transients describing desorption of molecules from the surface by gradually charging double layer before the desorption potential is reached. 1 s step was crucial to fully desorb thiols at a given potential and gain quantitative insight into potential-dependent desorption. The protocol was applied to 5 desorption potentials: 0.25, 0.15, 0.05, -0.05 and -0.15 V vs RHE; for sake of clarity only the results for desorption potentials between 0.15 and -0.15 V vs RHE are shown. Figure 5.2B shows the polarization curves for the progressive step-potential protocol on the 2-mercaptoethanol-modified gold electrode. The polarization curves for the progressive step-potential experiments of (**1**), (**3**) and (**4**) are shown in Figure SI5.1.

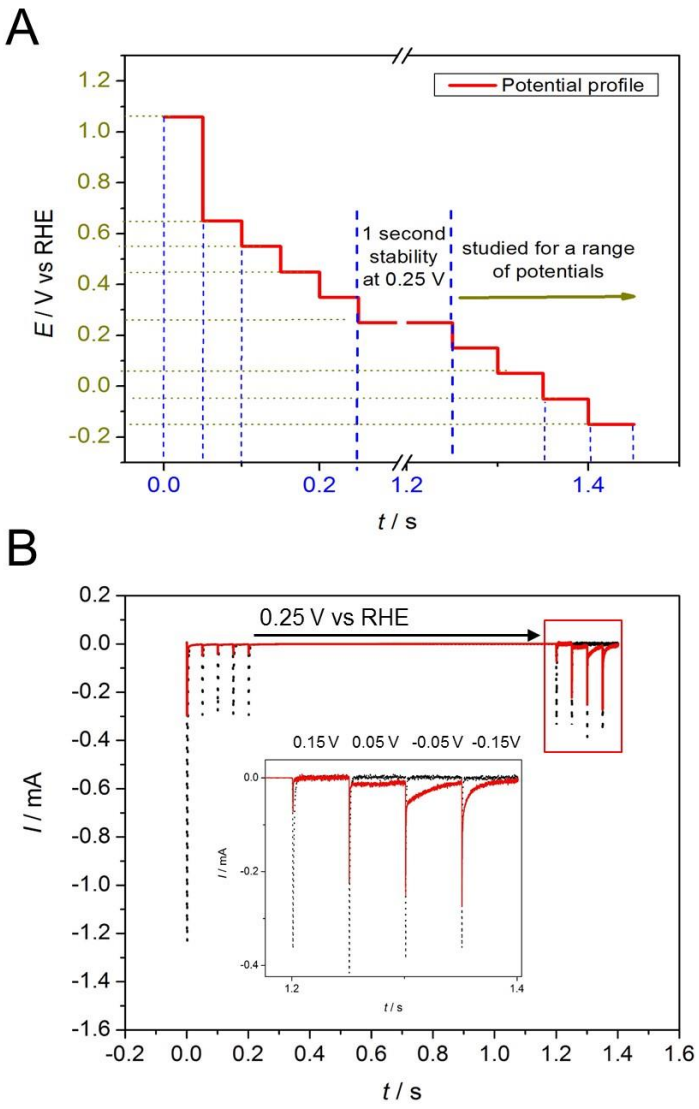

Figure 5.2. (A) Representative experimental procedure for the progressive potential-step chronoamperometry for which each potential step is probed for 0.05 s except one that is probed for 1s (0.25 V vs RHE in the example shown). This prolonged treatment is systematically applied at each potential step. (B) Progressive potential-step chronoamperometry recorded for a bare polycrystalline gold electrode (black dotted line) and for a polycrystalline gold electrode modified with 3-mercaptopropionic acid (**1**) (red solid line) with 1 s step at 0.25 V vs RHE. Inset shows a close up of the desorption at potentials lower than 0.25 V vs RHE.

As can be seen in the inset of Figure 5.2B, the sharp current transient at each potential step associated to the fast double-layer charging is followed by smooth current transient which we assign to the slow desorption of the chemisorbed molecules at the given potential. The selection of the time scale of the steps guarantees the total desorption of the molecule at the given potential, as the current decreases to zero before the next potential is applied. When the modified electrode was probed for a shorter period of time (≤ 0.5s) (Figure SI5.2), the partial desorption of the thiols due to the slow kinetics of desorption affected the quantitative analysis.

Quantitative information on the desorption process of these molecules as a function of the potential was obtained by integrating the charge under each step potential. An example of the potential limits and baseline taken for the integration is shown in Figure SI5.3. The resulting values of the integrated charge as a function of applied potential, -0.05 and -0.15 V, are shown in Figure 5.3, The comparison of the desorption charges for the potentials between 0.25 and -0.15V are presented in Figure SI5.4.

The step potential experiments confirm the low stability of the monothiols (**1)** and (**2**) in comparison with the stability of (**3**) and (**4**) adsorbed on gold. The desorption of each of the compounds was potential dependent and only a partial desorption of the compounds took place at every single potential. The onset potential for desorption of (**1**) and (**2**) appeared at 0.1 V vs RHE in both cases. The onset potential determined using step-potential chronoamperometries is slightly less positive to the onset potential estimated from cyclic voltammetries (0.2 V vs RHE). This is related to the uncertainty of the value of the cyclic voltammetry due to the overlapping of the desorption process of the thiol and the adsorption/desorption of anions. The desorption process of the thiol was favoured when a longer step potential of 1s was applied at -0.05 V and

-0.15 V. However, additional charge, but of lower magnitude, was measured at more negative potentials indicating the need for a more negative potential to trigger the desorption of the remaining strongly adsorbed molecules. This trend can be associated to the formation of different phases at the different surface sites present on the polycrystalline electrode. It is expected that the surface is dominated by (111) adsorption sites while (100) adsorption sites and step sites appear in smaller proportions. As it will be discussed in the second part of this manuscript, the desorption of these compounds is favoured at early potentials on the (111) surface structure.

The onset potential for desorption of the molecules containing two sulfur atoms (**3**) and (**4**) appeared at more negative potentials (-0.05 V vs RHE), suggesting a stronger interaction between these molecules and the gold surface. In both cases, the charge associated to the desorption process increased at more negative potentials and just in the case 1,4-dithiothreitol (**3**), the charge associated to the desorption slightly decreased at -0.15 V.

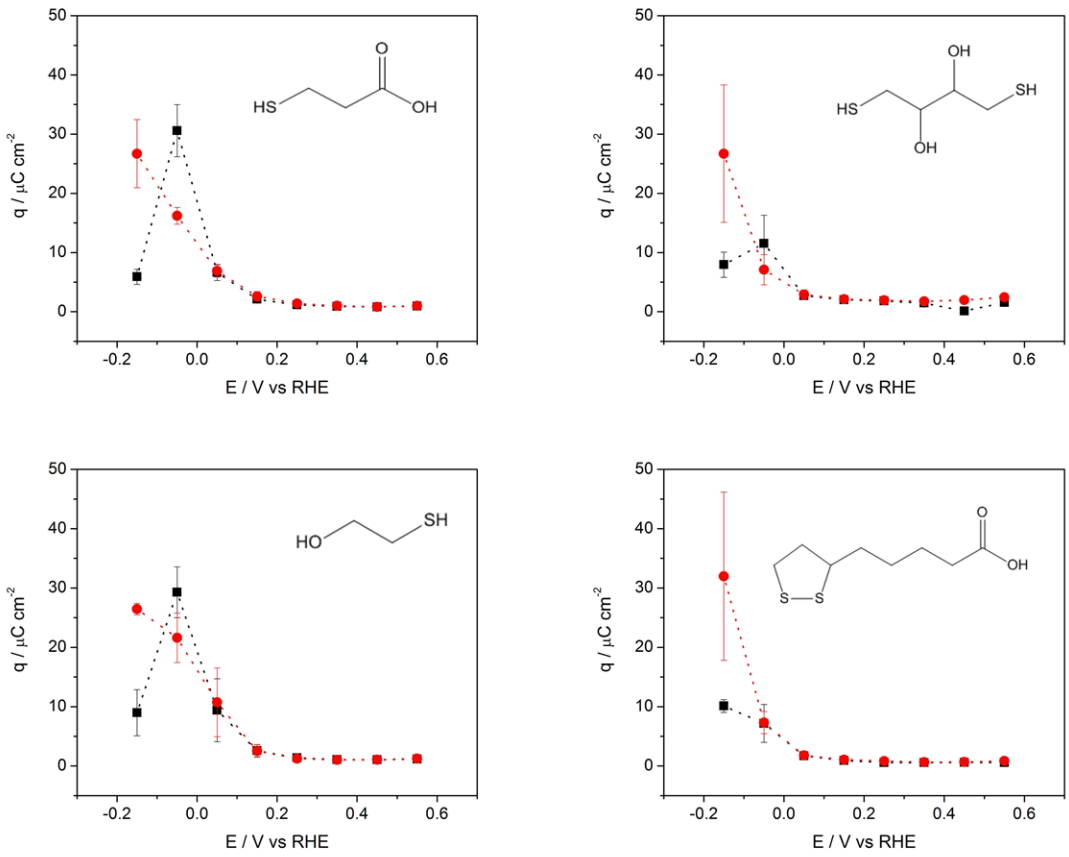

Figure 5.3. Charge of the reductive desorption from polycrystalline gold electrodes of the sulfur-containing compounds **1-4** obtained from step-potential chronoamperometries recorded with 1 s step at-0-05 (■) and -0.15 (●) V vs RHE.

Using the step-potential chronoamperometries we have determined the charge density curves for the thiol covered and thiol free electrodes in NaF and DPBS (Fig. SI5.5). The charge corresponding to adsorbed thiol was determined by the difference between the charge measured for a thiol covered electrode and the charge measured in the nonadsorbing electrolyte (NaF).

The total charge of desorption of monothiols (**1**) and (**2**) were 66 ± 11 µC cm^{-2} and 57 ± 10 µC cm^{-2} respectively. Unfortunately, due to the overlapping of the desorption

of (**3**) and (**4**) with the hydrogen evolution reaction, it was not possible to determine the total charge of desorption of these molecules. The charge for the desorption of (**3**) and (**4**) in the potential region under study were 47± 16 μC cm^{-2} and 45 ± 15 μC cm^{-2}, respectively.

Since the utilization of the sulfur-containing self-assembled monolayers in electrochemical sensors requires long term stability, we increased the duration of the probed potentials to 1 min. When the step potential was increased from 1 s (Fig. 5.3) to 1 min (Fig. SI5.6) the desorption kinetics were identical. These results show that the thiol desorption at a given potential is completed after 1 s.

5.4.2. Effect of the surface structure on the stability of the SAMs: 3-mercaptopropionic acid vs DL-thioctic acid

As mentioned above, one of the parameters that governs the adsorption/desorption of these molecules from the gold surface is the surface structure. To investigate the surface structure dependent stability, layers of 3-mercaptopropionic acid (**1**) and DL-thioctic acid (**4**) adsorbed onto Au(100) and Au(111) electrodes in phosphate buffer saline solution were prepared, and their stability against the applied potential evaluated using cyclic voltammetry as described before. Anionic compounds (**1**) and (**4**) were selected because of the similarities in their chemical functionality, but presented significant differences in their stability on the polycrystalline gold surface (Fig. 5.1 and Fig. 5.3)

Fig. 5.4 shows voltammetric profiles of the Au(100) and Au(111) surface modified electrodes with 3-mercaptopropionic acid. Blank voltammetry of the bare gold electrodes in DPBS are included to demonstrate the quality of the single-crystal electrodes and the

cleanness of the electrochemical cell and electrolyte. The voltammetry of the surfaces modified single-crystal electrodes showed a suppression of the features present on the blank voltammetry between 0.2 and 1 V which are associated to the lifting of the reconstruction and the adsorption/desorption of the anions.[44] This confirms the presence of (**1**) adsorbed onto the surface of single crystal electrodes. In the negative scan, at potentials lower than 0.2 V, the voltammetric profiles of the modified electrodes displayed the reductive peak corresponding to desorption of 3-mercaptopropionic acid. When both single crystals were compared (Fig. 5.4C) it could be noticed that desorption of 3-mercaptopropionic acid from (111) sites was favoured. While the onset potential of the desorption of 3-mercaptopropionic acid on both electrodes takes place at similar potentials, desorption of (**1**) on the Au(111) takes place in a narrow potential window (0.2 and 0.05 V), while the desorption of 3-mercaptopropionic acid on Au (100) electrodes occurred over a broader potential window. These differences in the desorption potential (E_{des}) of thiols have been associated to a combination of the potential of zero charge (pzc) - provided for no specific adsorption of ions- and the strength of the intermolecular interaction -which it will depends on the number of Au-S bonds.[48]

The potential of zero charge is a fundamental property of the interface and its understanding is critical for a detailed description of the double layer phenomenon. However, the adsorption of thiols on the electrode surface may lead to a large shift of the potential of zero charge. When the electrode is covered by a thiol monolayer, the charge density (σ_M) of the Au electrode is a function of the electrode potential (E) and the surface Gibbs excess (Γ) of the monolayer. The charge measured during the reductive desorption process is called the total charge and includes both the charge flowing from the electrode to change the oxidation state of thiol molecules and the charging of the electrical double

layer. The potential at which the total charge is equal to zero is referred as potential of the zero total charge (pztc) and depends on the number of Au-S bonds formed and the adsorption/desorption of anions[49, 50].

It is also important to notice that the coverage and packing of these compounds on the (111) and (100) crystal structure may differ. As was mentioned before, the desorption of thiols from gold surfaces is delayed to more negative potentials on closely packed self-assembled monolayers, which may justify the significantly larger value of charge (85.3 ± 5.2 μC cm^{-2}) associated to the desorption of 3-mercaptopropionic acid from the Au(111) electrode in comparison with the desorption from the Au(100) electrode (70.7 ± 5.1 μC cm^{-2}).

It has been reported that the SAMs of 3-mercaptopropionic acid (**1**) on Au(111) surfaces in a pH 7 phosphate buffer pack into several phases.[51] The most predominant phase is an incommensurate p×√3 structure, but several commensurate (px√3) phases are also present. Due to the different phases of the thiols and inconmesurable nature of the structures it is not possible to accurately determine the number of molecules in the surface and thus the maximum coverage of 3-mercaptopropionic acid on the Au(111) electrode. No information has been previously reported on the adsorption of this compound on Au(100) surfaces, however the higher stability observed for its absorption on the Au(100) electrode might be associated to the conformation and packing of the 3-mercaptopropionic acid molecules on the Au(100) surface.

In the reverse scan, a broad peak between -0.15 V and 0.4 V vs RHE was observed, that was associated to the re-adsorption of desorbed molecules from the electrolyte. Such process is also remarkably kinetically-favoured by the presence of (111) sites giving a defined peak when compared to broad voltametric signal of re-adsorption on Au(100). The

integrated charge for this process indicated that over 60% of the desorbed molecules are re-adsorbed on both (111) and (100) sites.

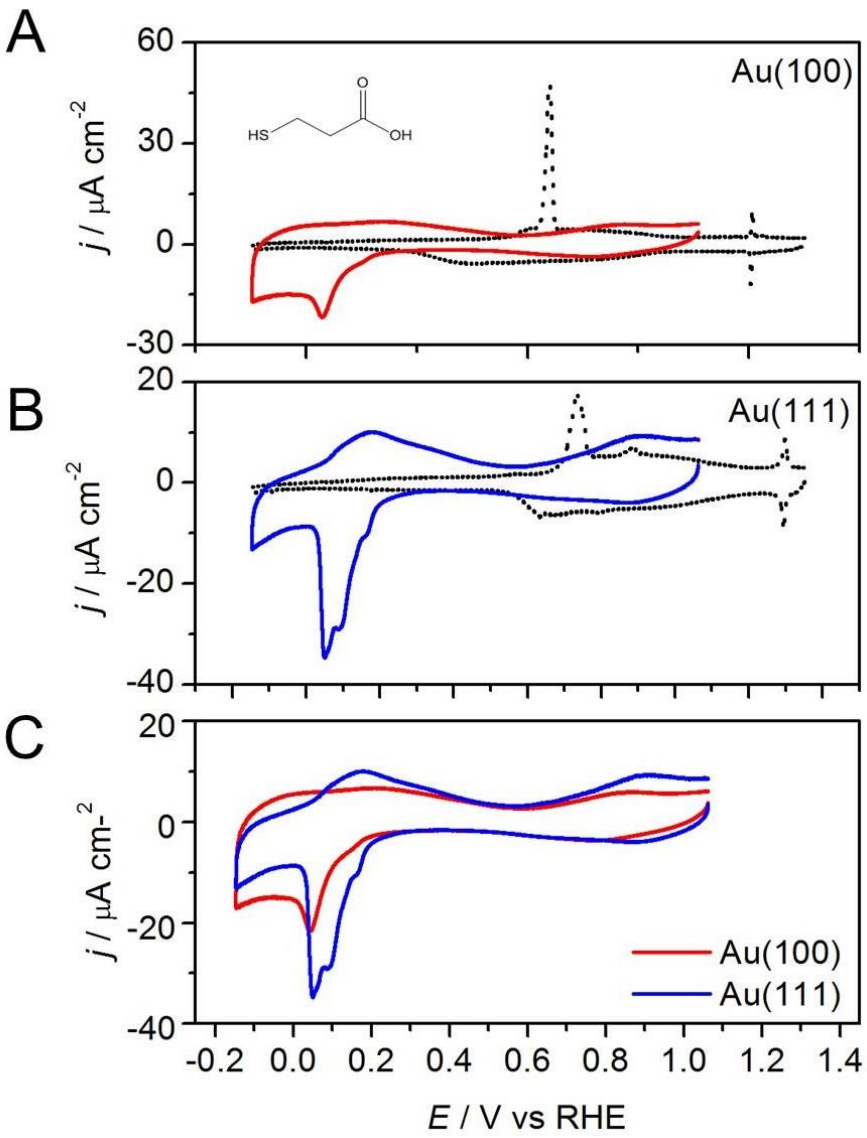

Figure 5.4. Voltammetric profiles of (A) Au(100), and (B) Au(111) modified with 3-mercaptopropionic acid (**1**) recorded in DPBS. Voltammetries of the single-crystal electrodes in absence of the adsorbed 3-mercaptopropionic acid are shown for comparison (dotted line). C) Comparison of Au(100) and Au(111) single crystal electrodes modified with (**1**). Scan rate υ = 0.05 V s^{-1}.

Similar to the results presented above for (**1**), the voltametric profiles of the Au(100) and Au(111) electrodes modified with DL-thioctic acid (**4**) showed a suppression of the features associated to the adsorption of anions onto the gold electrode in the region between 1 and 0 V followed by the reductive desorption of the compound at potentials lower than 0 V (Fig. 5.5). This potential was ~0.2 V lower than the desorption potential of 3-mercaptopropionic acid (**1**), a clear indication of the higher stability of the DL-thioctic acid (**4**) monolayers in comparison with those made with **1**, as shown previously for the polycrystalline electrode (Fig. 5.1 and Fig 5.3). Moreover, the comparison between the reductive desorption of DL-thioctic acid (**4**) between both basal planes (Fig. 5.5C), clear indicates a higher stability of the DL-thioctic acid on the Au(100) electrode. While a rapid desorption takes place on the Au(111) electrode between 0 and -0.15 V, just a small fraction of compound (**4**) is desorbed from the Au(100) electrode in the same potential window. The desorption of DL-thiotic acid (**4**) from this electrode takes place at more negative potentials (Fig. SI5.7) where the hydrogen evolution reaction (HER) on gold also takes place. This overlap prevents quantification of the charge associated to the desorption of the this disulphide from Au(100) surfaces. To our knowledge, this is the first time the stability of DL-thioctic acid (**4**) monolayers on single crystal gold electrodes has been evaluated.

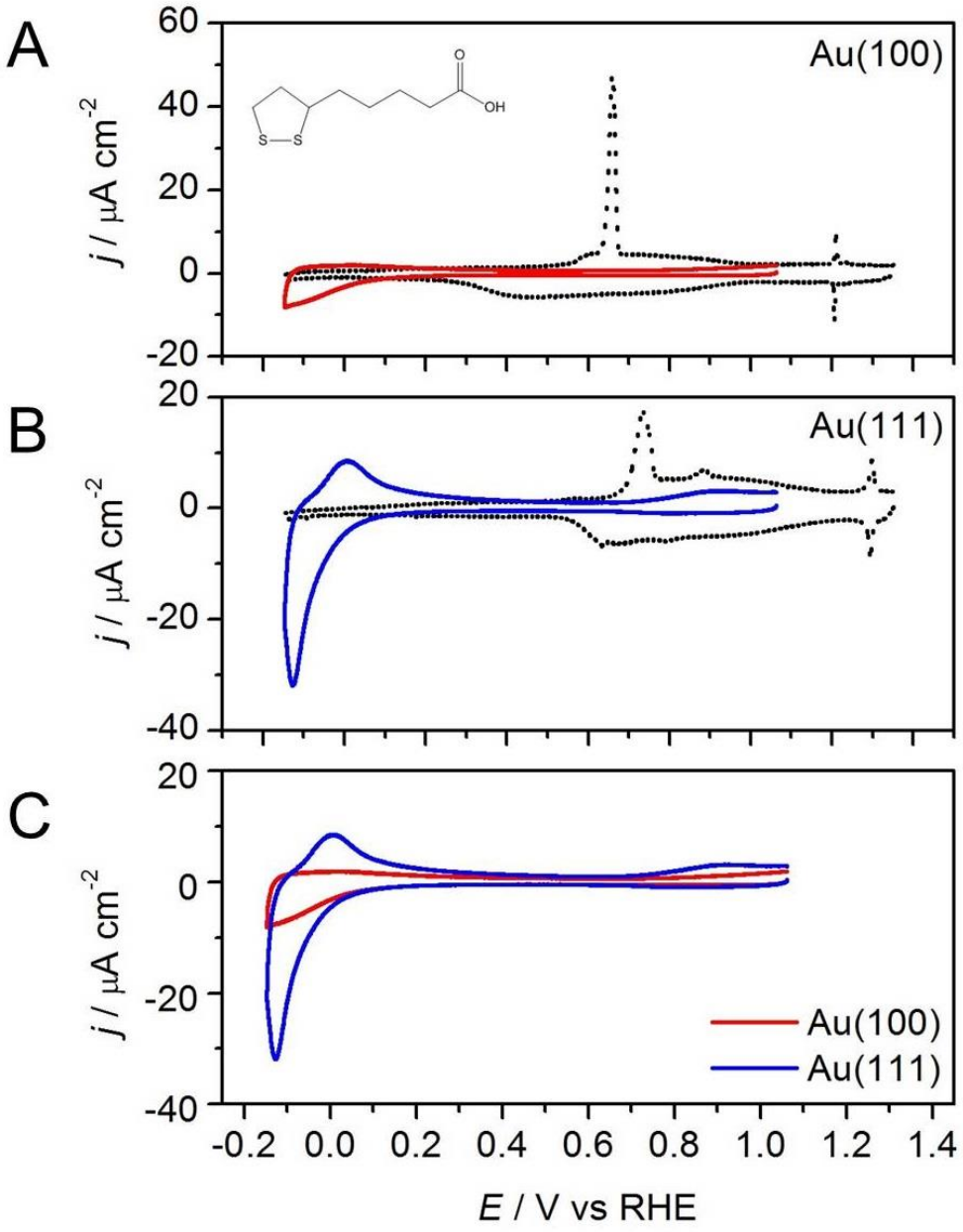

Figure 5.5. Voltammetric profiles of (A) Au(100), and (B) Au(111) modified with DL-thioctic acid (**4**) in DPBS solution. Voltammetries of the single-crystal electrodes in absence of the adsorbed (**4**) are shown for comparison (dotted line). C) Comparison of Au(100) and Au(111) single crystal electrodes modified with (**4**). Scan rate $\upsilon = 0.05\ V\ s^{-1}$.

The superior stability of these compounds on the Au(100) electrode with respect to the Au(111) is in agreement with previous results for other thiols,[18] and has been attributed to the potential of zero charge. However, when comparing the adsorption of monothiols vs disulfides, due to the difference in electron transfer, 1 vs 2 electron, one must consider the potential of zero total charge (pztc) instead of the potential of zero charge (pzc). Previous reports have shown significant differences between numerical values of pzc and pztc of SAM on Au(111) electrodes.[15] Unfortunately, common strategies to determine the pztc such as charge displacement using carbon monoxide[52, 53] cannot be applied to determine the pztc of the SAMs of thiols and disulfides.

5.5. Conclusions

This manuscript provides important information regarding the parameters governing the stability of self-assembled monolayers of sulfur-containing molecules on Au electrodes in physiological media. In particular, we have implemented cyclic voltammetry and progressive step potential chronoamperometry to determine the stability of four representative sulfur-containing compounds, 3-mercaptopropionic acid (**1**), 2-mercaptoethanol (**2**), 1,4-dithiothreitol (**3**) and DL-thioctic acid (**4**), in physiological media as a function of the potential and the surface structure. The differences in desorption potential between these molecules can be attributed to the adsorption energy of the S-single and S-double coordination to the surface, to the strength of the lateral intermolecular interaction (resulting in different packing and coverage) and to the changes of the potential of zero total charge (pztc) of the surface.

Our results also show that the desorption of self-assembled monolayers of monothiols (**1**) and (**2**) on polycrystalline gold takes place at approximately 0.15 V vs RHE. In addition,

we show that compounds (**3**) and (**4**), that carry two coordinating sulfur atoms in their structure, have an improved stability so that more negative potentials are required for the reductive desorption. Among these two, electrodes modified with DL-thioctic acid showed the highest potential-dependent and time-dependent stability, presumably due to stabilization through Van der Waals lateral interactions between hydrophobic aliphatic chains.[27] The possible application of Anson's monolayer model[54-56], as suggested by one reviewer of this manuscript, is limited in this case due to the complexity of the surface structure and adsorption sites on polycrystalline electrodes, the specific adsorption and replacement by anions during the thiol and disulphide desorption, and the overlapping of the hydrogen evolution signal with the desorption for 1,4-dithiothreitol (**3**) and DL-thioctic acid (**4**). Finally, we report for the first time a higher stability on (100) sites when compared to (111) sites, for SAMs of compounds (**1**) and (**4**).

We believe our results contribute to the development and understating of more robust electrochemical systems such as electrochemical sensors. In addition, the reported methodology can be implemented for the study of the desorption kinetics of self-assembly monolayers relevant in the development of drug-released devices using electrochemical control.

5.6. References

1. X. Jiang, R. Ferrigno, M. Mrksich and G. M. Whitesides, *J. Am. Chem. Soc.*, 2003, **125**, 2366-2367.
2. R. S. Kane, S. Takayama, E. Ostuni, D. E. Ingber and G. M. Whitesides, *Biomaterials*, 1999, **20**, 2363-2376.

3. T. Wink, S. J. van Zuilen, A. Bult and W. P. van Bennekom, *Analyst*, 1997, **122**, 43R-50R.

4. J. C. Love, L. A. Estroff, J. K. Kriebel, R. G. Nuzzo and G. M. Whitesides, *Chem. Rev.*, 2005, **105**, 1103-1170.

5. C. Vericat, M. E. Vela, G. Benitez, P. Carro and R. C. Salvarezza, *Chem. Soc. Rev.*, 2010, **39**, 1805-1834.

6. F. P. Zamborini and R. M. Crooks, *Langmuir*, 1998, **14**, 3279-3286.

7. P. E. Laibinis and G. M. Whitesides, *J. Am. Chem. Soc.*, 1992, **114**, 9022-9028.

8. D. Pissuwan, T. Niidome and M. B. Cortie, *J. Controlled Release*, 2011, **149**, 65-71.

9. J. Gao, X. Huang, H. Liu, F. Zan and J. Ren, *Langmuir*, 2012, **28**, 4464-4471.

10. C. D. Hodneland and M. Mrksich, *Langmuir*, 1997, **13**, 6001-6003.

11. S. S. Agasti, A. Chompoosor, C.-C. You, P. Ghosh, C. K. Kim and V. M. Rotello, *J. Am. Chem. Soc.*, 2009, **131**, 5728-5729.

12. C. D. Hodneland and M. Mrksich, *J. Am. Chem. Soc.*, 2000, **122**, 4235-4236.

13. J. Kunze, J. Leitch, A. L. Schwan, R. J. Faragher, R. Naumann, S. Schiller, W. Knoll, J. R. Dutcher and J. Lipkowski, *Langmuir*, 2006, **22**, 5509-5519.

14. T. Laredo, J. Leitch, M. Chen, I. J. Burgess, J. R. Dutcher and J. Lipkowski, *Langmuir*, 2007, **23**, 6205-6211.

15. Z. Su, J. Leitch and J. Lipkowski, *Z. Phys. Chem.*, 2012, **226**, 995-1009.

16. E. Chow, D. B. Hibbert and J. J. Gooding, *Anal. Chim. Acta*, 2005, **543**, 167-176.

17. E. Chow, D. B. Hibbert and J. J. Gooding, *Analyst*, 2005, **130**, 831-837.

18. Z. L. Yu, J. Casanova-Moreno, I. Guryanov, F. Maran and D. Bizzotto, *J. Am. Chem. Soc.*, 2015, **137**, 276-288.

19. C.-J. Zhong, J. Zak and M. D. Porter, *J. Electroanal. Chem.*, 1997, **421**, 9-13.

20. M. M. Walczak, D. D. Popenoe, R. S. Deinhammer, B. D. Lamp, C. Chung and M. D. Porter, *Langmuir*, 1991, **7**, 2687-2693.

21. D. F. Yang, C. P. Wilde and M. Morin, *Langmuir*, 1996, **12**, 6570-6577.

22. M. M. Walczak, C. A. Alves, B. D. Lamp and M. D. Porter, *J. Electroanal. Chem.*, 1995, **396**, 103-114.

23. F. Loglio, M. Schweizer and D. M. Kolb, *Langmuir*, 2003, **19**, 830-834.

24. N. S. Pesika, K. J. Stebe and P. C. Searson, *Langmuir*, 2006, **22**, 3474-3476.

25. D. F. Yang and M. Morin, *J. Electroanal. Chem.*, 1998, **441**, 173-181.

26. W. H. Mulder, J. J. Calvente and R. Andreu, *Langmuir*, 2001, **17**, 3273-3280.

27. M. D. Porter, T. B. Bright, D. L. Allara and C. E. D. Chidsey, *J. Am. Chem. Soc.*, 1987, **109**, 3559-3568.

28. S.-S. Wong and M. D. Porter, *J. Electroanal. Chem.*, 2000, **485**, 135-143.

29. J. D. C. Jacob, T. R. Lee and S. Baldelli, *J. Phys. Chem. C*, 2014, **118**, 29126-29134.

30. D. F. Yang, H. Al-Maznai and M. Morin, *J. Phys. Chem. B*, 1997, **101**, 1158-1166.

31. J. L. Shepherd, A. Kell, E. Chung, C. W. Sinclar, M. S. Workentin and D. Bizzotto, *J. Am. Chem. Soc.*, 2004, **126**, 8329-8335.

32. B. Cui, T. Chen, D. Wang and L.-J. Wan, *Langmuir*, 2011, **27**, 7614-7619.

33. W. T.Liu and Y. R. Shena, *PNAS*, 2014, **111**, 1293-1297.

34. M. J. Esplandiu, M. L. Carot, F. P. Cometto, V. A. Macagno and E. M. Patrito, *Surf. Sci.*, 2006, **600**, 155-172.

35. P. Mali, N. Bhattacharjee and P. C. Searson, *Nano Lett.*, 2006, **6**, 1250-1253.

36. D. Svirskis, J. Travas-Sejdic, A. Rodgers and S. Garg, *J. Controlled Release*, 2010, **146**, 6-15.

37. M. B. Fritzen-Garcia, V. C. Zoldan, I. R. W. Z. Oliveira, V. Soldi, A. A. Pasa and T. B. Creczynski-Pasa, *Biotechnol. Bioeng.*, 2013, **110**, 374-382.

38. A. Cossaro, R. Mazzarello, R. Rousseau, L. Casalis, A. Verdini, A. Kohlmeyer, L. Floreano, S. Scandolo, A. Morgante, M. L. Klein and G. Scoles, *Science*, 2008, **321**, 943-946.

39. M. Byloos, H. Al-Maznai and M. Morin, *J. Phys. Chem. B*, 1999, **103**, 6554-6561.

40. N. C. III, C. E. D. Chidsey, G. Y. Liu and G. Scoles, *J. Chem. Phys.*, 1993, **98**, 4234-4245.

41. J. Souza-Garcia, A. Berná, E. A. Ticianelli, V. Climent and J. M. Feliu, *J. Electroanal. Chem.*, 2011, **660**, 276-284.

42. J. Cui, Y. Yan, Y. Wang and F. Caruso, *Adv. Funct. Mater.*, 2012, **22**, 4718-4723.

43. Y. A. Romanov, A. N. Darevskaya, N. V. Merzlikina and L. B. Buravkova, *Bull. Exp. Biol. Med.*, 2005, **140**, 138-143.

44. A. Cuesta, M. Kleinert and D. M. Kolb, *Phys. Chem. Chem. Phys.*, 2000, **2**, 5684-5690.

45. E. Pensa, C. Vericat, D. Grumelli, R. C. Salvarezza, S. H. Park, G. S. Longo, I. Szleifer and L. P. Mendez De Leo, *Phys. Chem. Chem. Phys.*, 2012, **14**, 12355-12367.

46. C. A. Widrig, C. Chung and M. D. Porter, *J. Electroanal. Chem.*, 1991, **310**, 335-359.

47. L. Y. S. Lee and R. B. Lennox, *Langmuir*, 2007, **23**, 292-296.

48. T. Doneux, M. Steichen, A. De Rache and C. Buess-Herman, *J. Electroanal. Chem.*, 2010, **649**, 164-170.

49. W. Schmickler and E. Santos, *Interfacial electrochemistry*, Springer Science & Business Media, 2010.

50. V. Climent, R. Gomez, J. Orts, A. Aldaz and J. Feliu, *Electrochemical Double Layer*, 1997, **97**, 17.

51. M. J. Giz, B. Duong and N. J. Tao, *J. Electroanal. Chem.*, 1999, **465**, 72-79.

52. J. Clavilier, R. Albalat, R. Gomez, J. M. Orts, J. M. Feliu and A. Aldaz, *J. Electroanal. Chem.*, 1992, **330**, 489-497.

53. B. Alvarez, V. Climent, A. Rodes and J. M. Feliu, *Phys. Chem. Chem. Phys.*, 2001, **3**, 3269-3276.

54. Y. Xie and F. C. Anson, *J. Electroanal. Chem.*, 1995, **384**, 145-153.

55. Y. Xie and F. C. Anson, *J. Electroanal. Chem.*, 1995, **396**, 441-449.

56. Y. Xie and F. C. Anson, *J.Electroanal. Chem.*, 1996, **404**, 209-213.

Chapter 5: Supporting Information

5.7. Supporting figures

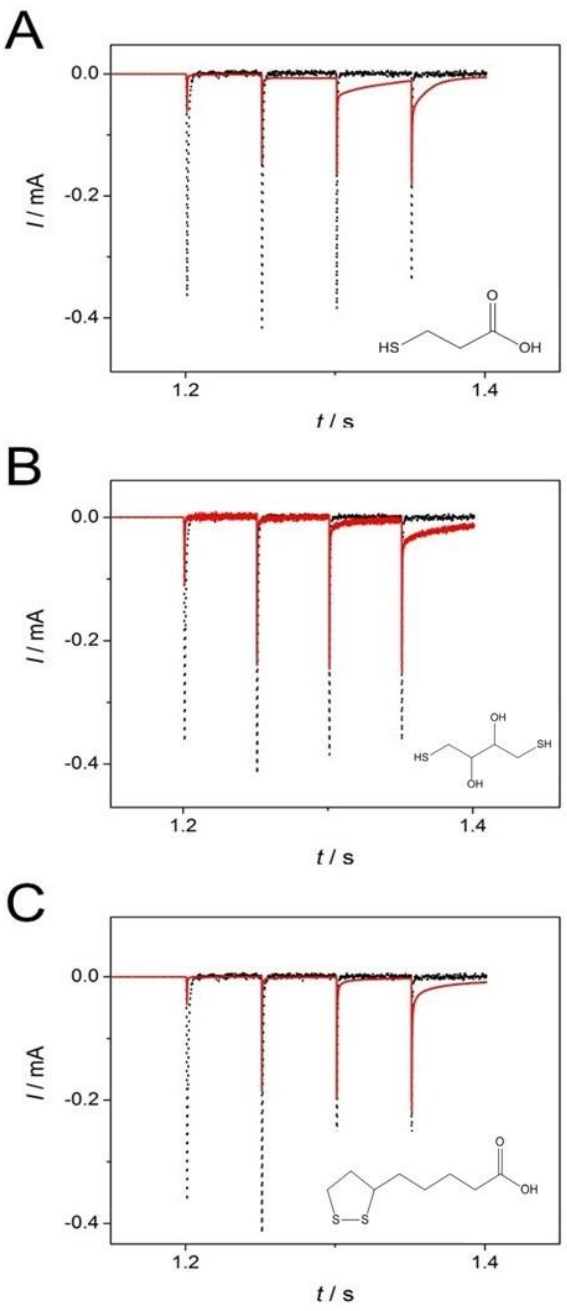

Figure SI5.1. Progressive potential-step chronoamperometry (at potentials lower than 0.25 V vs RHE) recorded for a bare polycrystalline gold electrode (black dotted line) and for a thiol-modified polycrytalline gold electrode (red solid line) with 1 s step at 0.25 V vs RHE. (A) 3-mercaptopropionic acid (**1**) (B) 1,4-dithiothreitol (**3**) (C) DL-thioctic acid (**4**).

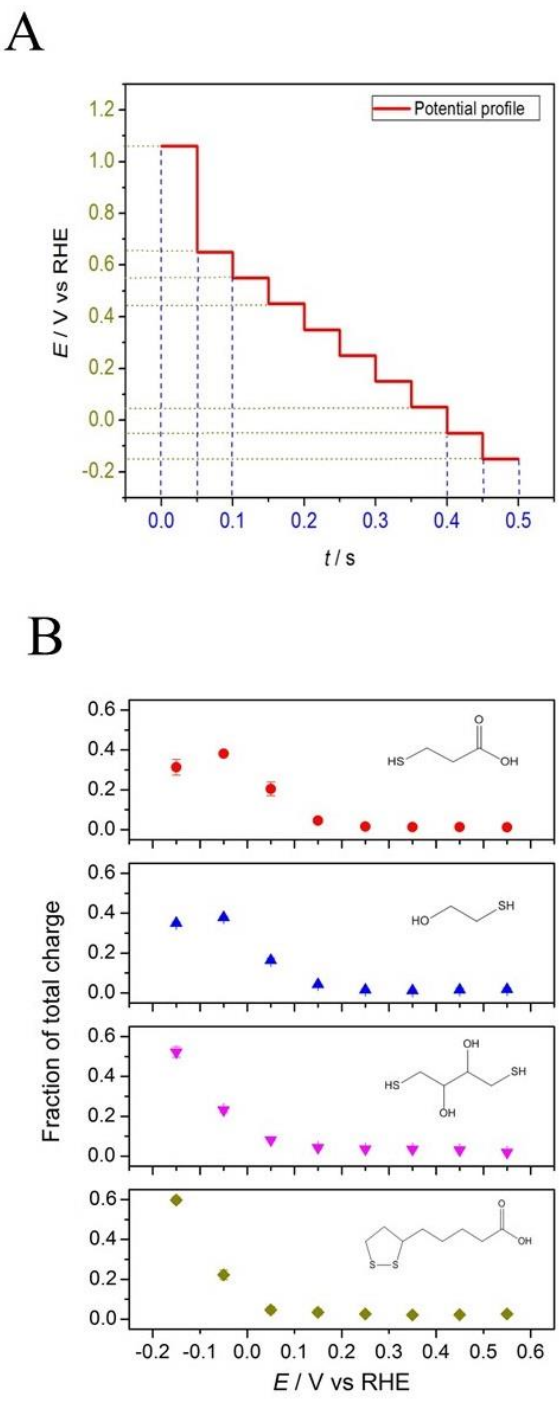

Figure SI5.2. (A) Experimental procedure for the progressive potential-step chronoamperometry for which each potential step is probed for 0.05 s. (B) Quantitative data obtained from the integration of current spikes (value of charge) after each potential change for all studied sulfur-containing molecules. Values are represented as a fraction of total charge measured throughout the experiment.

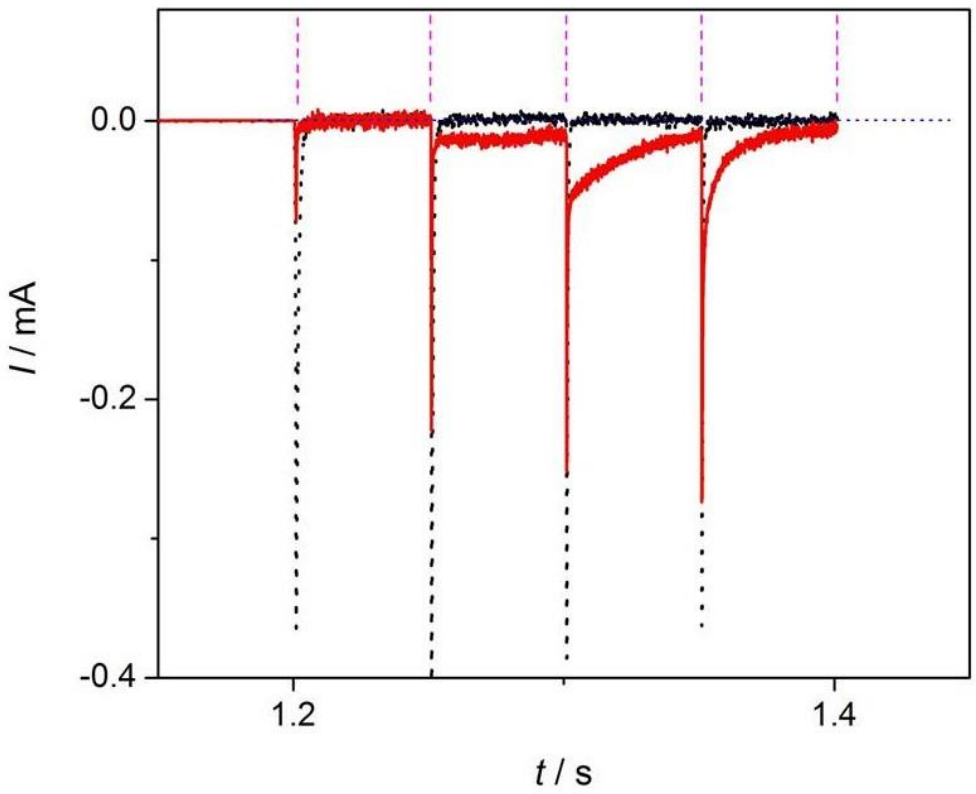

Figure SI5.3. Representative example of the potential limits (vertical dashed lines) and base line (horizontal dotted line) used for the quantitative analysis of the progressive potential-step chronoamperometry. The figure corresponds to the progresive –step chronoamperometry with 1s step at 0.25 V vs RHE for the case of bare and ME-modified electrode.

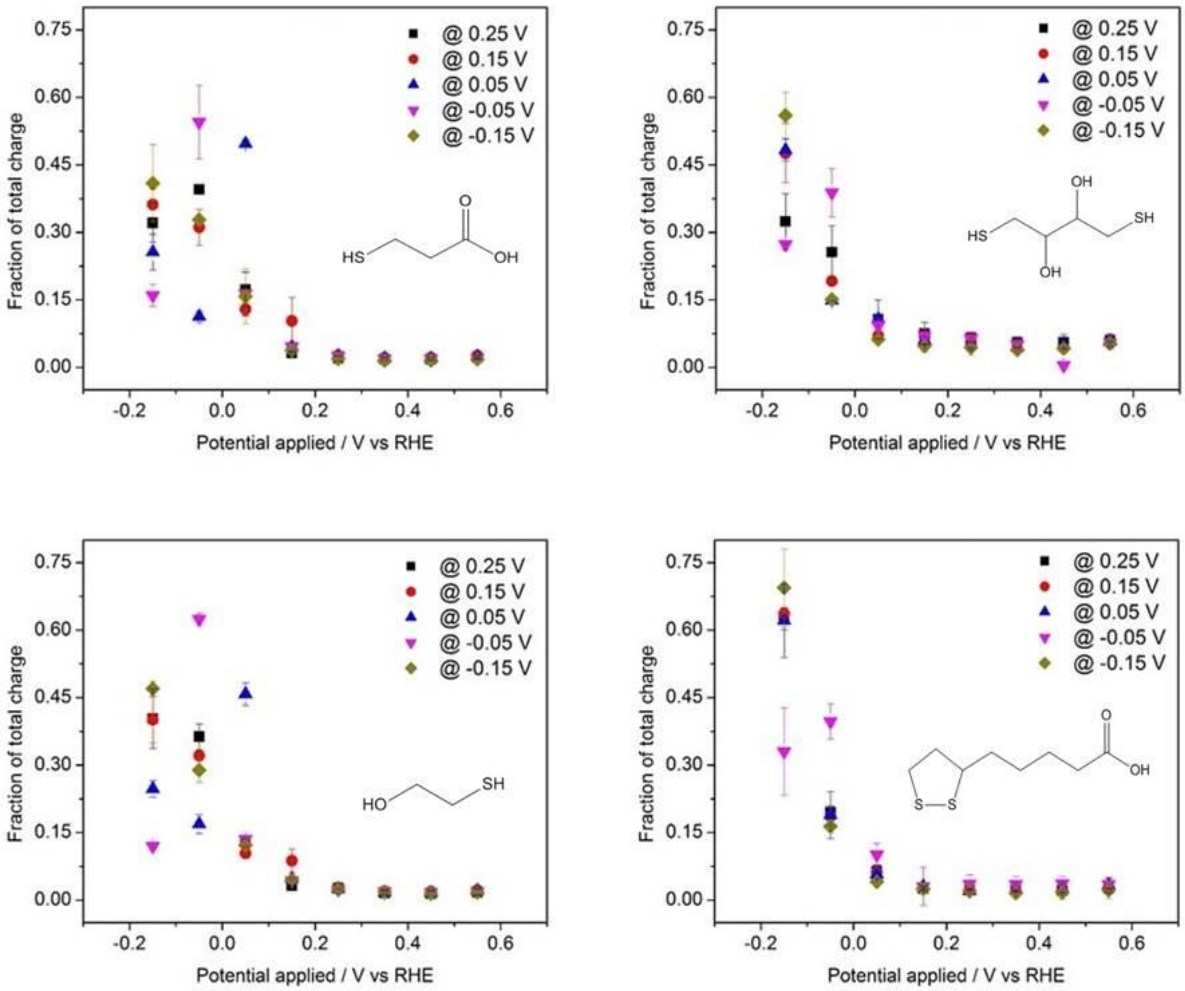

Figure SI5.4. Charge of the reductive desorption from polycrystalline gold electrodes of the sulfur-containing compounds **1**-**4** obtained from step-potential chronoamperometries recorded with 1 s step at 0.25 (■), 0.15 (●), 0.05 (▲), -0-05 (▼) and -0.15 (◆) V vs RHE.

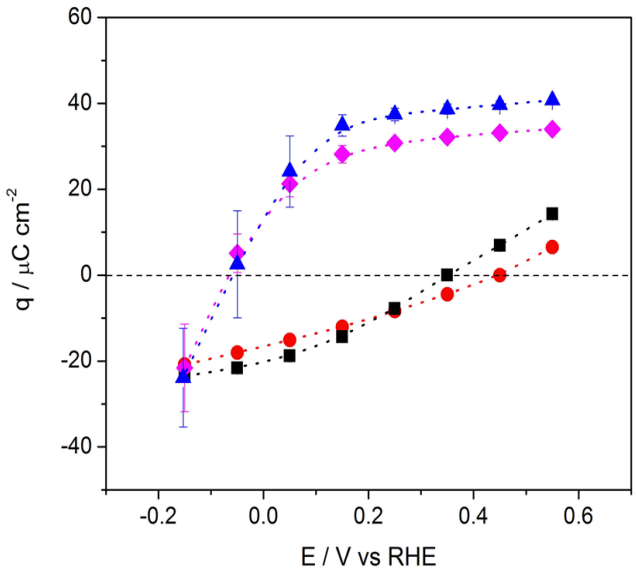

Figure SI5.5. Total charge density curves of bare Au polycrystalline electrode in NaF(●) and DPBS(■) and modified with MPA (▼) and ME(◆).

The figure shows the charges density of the metal obtained from the progressive potential-step chronoamperometry for a bare gold polycrystalline electrode in NaF and DPBS and in DPBS in presence of adsorbed MPA and ME. The results in NaF and DPBS are comparable to those reported in the literature[1]and the trend in the charge density associated to the desorption of MPA and ME is similar to the desorption of the thiols in the references above.

This figure could not be obtained in the case of the molecules (**3**) and (**4**) due to the overlapping of the desorption signal with the hydrogen evolution reaction at low potentials.

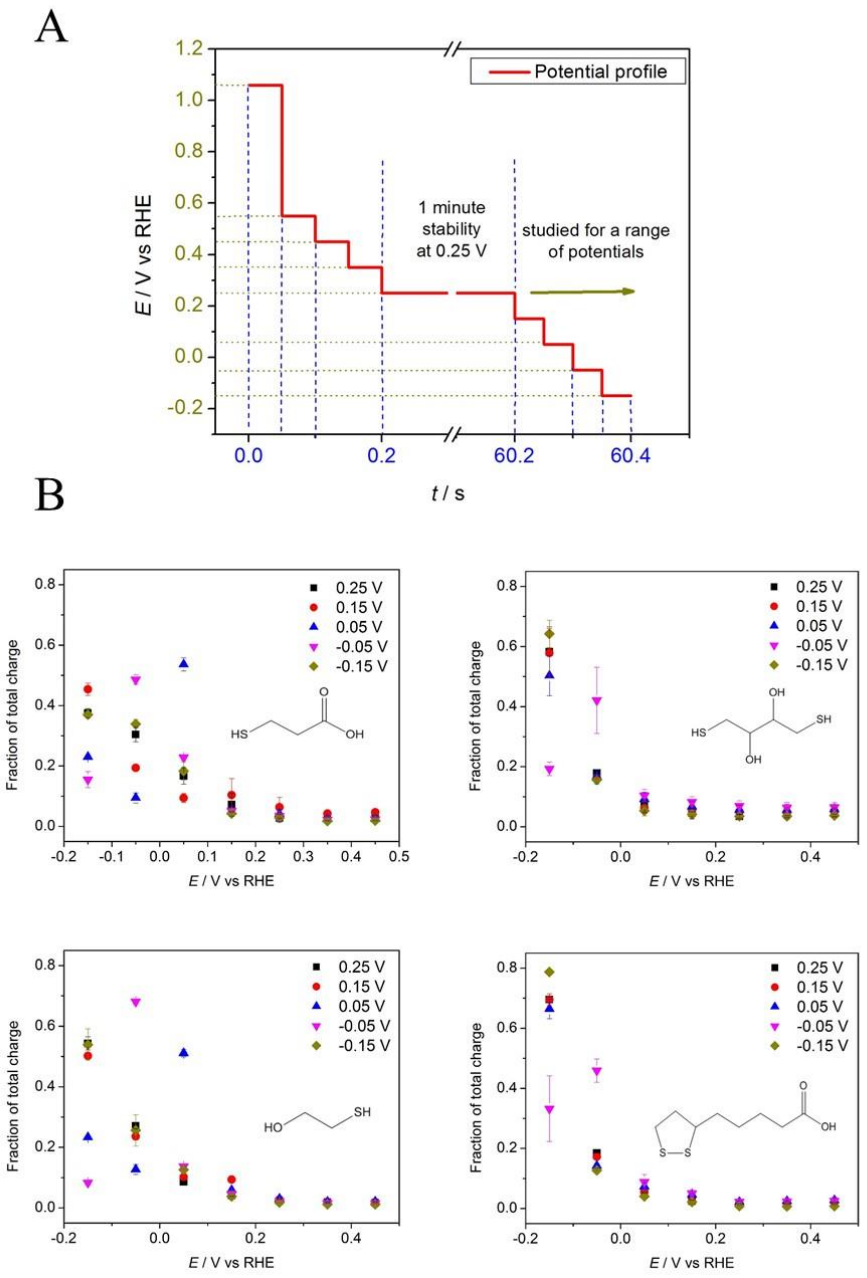

Figure SI5.6. (A) Experimental procedure for the progressive potential-step chronoamperometry for which each potential step is probed for 0.05 s except one that is probed for 1 min. (B) Quantitative data obtained from the integration of current spikes (value of charge) after each potential change for all studied compounds. Values are represented as a fraction of total charge measured throughout the experiment.

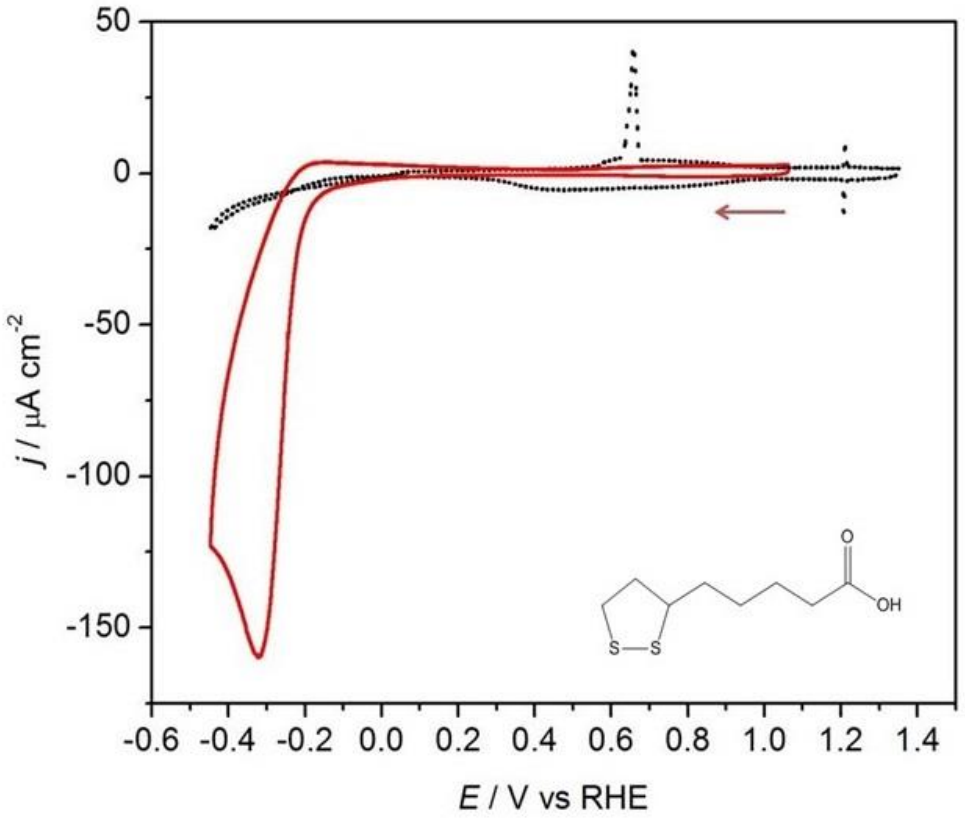

Figure SI5.7. Voltammetric profiles of Au(100) modified with DL-thioctic acid in DPBS solution recorded over an extended potential window. Voltametriy of the single-crystal electrode in absence of the adsorbed compound are shown for comparison (dotted line). Scan rate υ = 0.05 V s^{-1}.

5.8. References

1. T. Laredo, J. Leitch, M. Chen, I. J. Burgess, J. R. Dutcher and J. Lipkowski, *Langmuir*, 2007, **23**, 6205-6211.

Chapter 6: Preface

Chapter 6 describes the work that led to formation of the molecular architecture as described in Chapter 2. The first part of this work was devoted to identifying the most suitable ligand for the coordination of cisplatin. These interactions were studied in great details using UV-Vis and NMR spectroscopies. Once a suitable ligand was found, it was immobilised on the thiol-modified gold electrode through EDC coupling chemistry.

Gold surfaces modified with selected molecules were exposed to the source of Pt species and studied using cyclic voltammetry and electrochemical impedance spectroscopy in order to provide a proof-of-concept experiments for this approach. Additional techniques, such as XPS and contact angle measurements complemented the analysis of the system.

Chapter 6: Design of surface-modified electrodes for the electrochemical adsorption of Pt-based anticancer drugs

This chapter is a modified version of the research article published as:

A. Kolodziej, C. S. Le Duff, J. Bergueiro, M. Walker, A. Keeler, A. E. Russell, P. Fernandez-Trillo, P. Rodriguez, *Chem. Mater.*, 2019, **31**, 8012-8018.

Authors contribution

P.R, P.F.T and AK conceived the experiments and contributed to the experimental set-up and discussed the results. AK performed all experimental work. CSLD contributed in the NMR experiments and analysis. The XPS experiments and analysis of the data were performed by MW. AJK and AER contributed in the EIS and contact angle experiments. The ICP experiments and analysis was performed by JB. AER provided supervision and advice to AK whilst on secondment to the University of Southampton. All authors contributed to the analysis of the results, discussion, writing and revision of the manuscript. All authors have given approval to the final version of the manuscript.

Acknowledgments

This work was supported by the University of Birmingham through PhD studentship (AK) and fellowships (PFT and PR), Wellcome Trust ISSF Grant 184ISSFPP (PFT) and John Evans Fellowship (PFT).

6.1. Abstract

The design of a hemofiltration method that minimizes the side effects produced by accumulation of Pt-based drugs such as cisplatin represents an important technology for cancer treatment. This work establishes the foundation for the development of an efficient platform for the electrochemical hemofiltration and simultaneous sensing of anti-tumour drugs, such as cisplatin and carboplatin, from a medium that mimics physiological conditions (later denoted as physiological). The electrochemical filtration system is based on a gold surface-modified electrode using tris(carboxyethyl)phosphine (TCEP) ligands that coordinate to Pt-based drugs. The platinum-phosphine interaction is shown to be more time efficient, as compared to naturally occurring formation of a glutathione-platinum adduct and displayed a highly cooperative nature of binding. Altogether, we demonstrate that the presence of ligands capable of binding to Pt results in a differential spectroscopic and electrochemical response, and the potential to adsorb and monitor the concentration of Pt salts in complex aqueous media.

6.2. Introduction

Since its discovery, cisplatin and its analogues have become important drugs in the treatment of several solid tumours.[1-4] Even though the use of Pt-based drugs in chemotherapy has brought cure rates above 90%, patients who undergo cisplatin-based chemotherapy are affected by several side-effects. These side-effects are caused by the poor selectivity of the drugs for cancer tissues and the accumulation of Pt-based drugs in non-cancer tissues.[5] In particular, a high systemic accumulation of platinum[6] results in nephrotoxicity, gastrointestinal toxicity or neuropathy.[7, 8] In light of these side effects, the maximum dose of cisplatin to be administered has been reduced and consequently the chance of complete apoptosis of cancerous cells and full cancer remission have also been reduced. To overcome these disadvantages, number of methods to neutralise and remove cisplatin from blood have been investigated. For example, Florea *et al.* found that sodium thiosulfate can be used as a chelating agent to neutralize cisplatin in blood. However, thiosulfate also decreases the anticancer properties of the drug.[8] An alternative approach, which has had positive results to a certain extent, is the filtration of Pt-based drugs using localized extracorporeal circuits or drug perfusion. These methods are advantageous as they enable a localized increase of drug levels in tumour tissues, up to ten-times higher than with systemic treatments, while minimizing at the same time long-term toxicities and side effects. Unfortunately, the haemoperfusion and hemofiltration methods reported so far are non-selective and suffer from low extraction efficiencies.[9-13] Moreover, they do not provide a way of monitoring drug levels in blood.

Here, we report the use of surface-modified electrodes and electrochemical methods as a platform for the adsorption and monitoring of Pt-based drugs in physiological medium.

The design of the reported surface-modified electrodes was underpinned by the identification of ligands capable of binding to platinum ions in complex aqueous media. Tris(carboxyethyl)phosphine (TCEP), the ligand with the highest affinity for Pt, was immobilized on the gold electrodes via coupling onto a self-assembled layer of cysteamine. The performance of the resulting surface-modified electrodes was assessed using cyclic voltammetry, impedance spectroscopy, X-ray photoelectron spectroscopy (XPS) and contact angle. Altogether, we demonstrate that the presence of ligands capable of binding to Pt results in a differential spectroscopic and electrochemical response, and the potential to absorb and monitor the concentration of Pt salts in complex aqueous media.

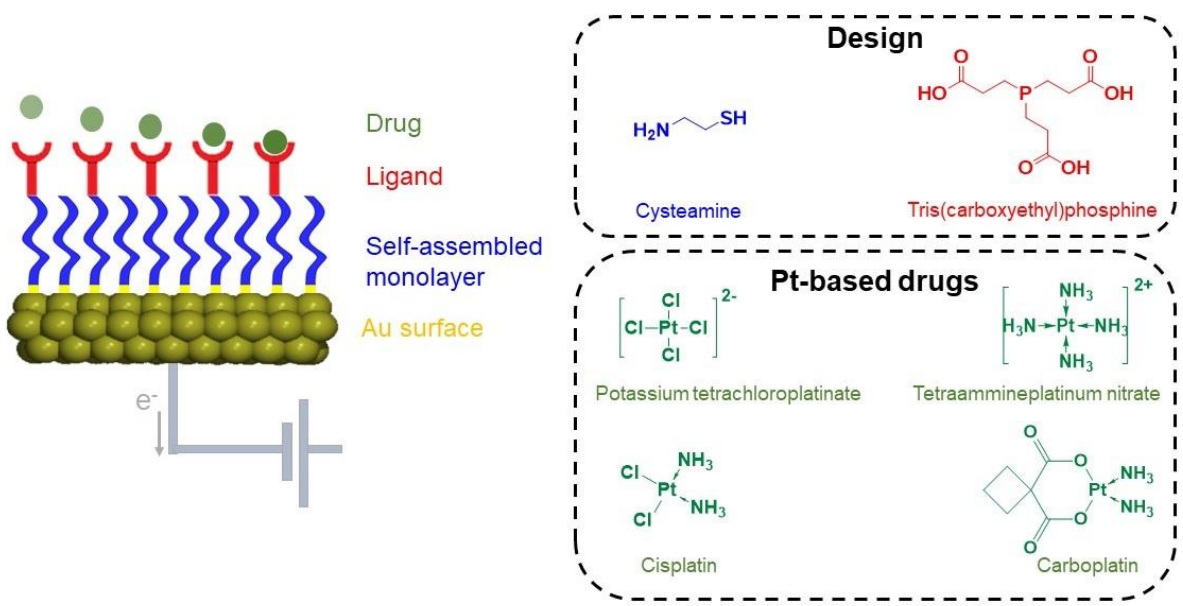

Figure 6.1. Schematic representation of the surface design of the working electrode for the adsorption and monitoring of Pt-based drugs along with molecules used to build the electrode and a scope of Pt-based compounds used throughout the study.

6.3. Experimental methods

Electrode preparation

Prior to any modification a gold electrode was flame-annealed and rinsed with ultrapure water (Elga, 18.2 MΩ cm, 1 ppb total organic carbon). Subsequently, the electrode was immersed in a freshly prepared 100 mM solution of cysteamine (Sigma Aldrich, ≥98%) in water for 30 minutes. Afterwards, the cysteamine-modified electrode was rinsed with ultrapure water and immersed in a freshly prepared mixture (1:1 by volume) of solutions of 20 mM TCEP·HCl and 80 mM EDC·HCl for 60 minutes.

Stock solutions of TCEP·HCl (Alfa Aesar, 98%) and EDC·HCl (Fluorochem, >98%) were made in 100 mM MES monohydrate (Alfa Aesar, 98%) buffer and kept at 4 °C before its use. All the modification steps were performed at room temperature.

In the case of the high surface area gold electrodes used in XPS experiments, the gold electrodes were immersed in 250 mM solution of cysteamine for 60 minutes in order to avoid the depletion of the reactants and ensure the ideal formation of the SAM.

The detailed description of the electrochemical measurements and the characterization by UV, XPS, NMR, EIS and contact angle are presented in the Supporting Information.

6.4. Results and discussion

In nature, Pt-based drugs form stable adducts with the nitrogen in position N-7 of guanine in nucleic acids.[14] Additionally, glutathione (GSH) is known to scavenge the administered drug, due to the high affinity of thiols for Pt centres.[15] To evaluate whether either of these two molecules had the potential to bind quickly to Pt-based drugs in complex aqueous

media, they were mixed with 1 equivalent of cisplatin in a phosphate buffer saline solution, and the binding monitored via UV-Vis spectroscopy. The complexation of Pt in this physiological media is not trivial due to the affinity and competitive reaction with phosphate anions to metal centres.[16, 17] While no changes could be observed when guanine was used as the ligand (Fig. SI6.1), the interaction between cisplatin and GSH resulted in the appearance of a Pt-ligand band at ~295 nm (Fig. SI6.2A). This band kept increasing even after 8 h of incubation, suggesting that Pt-S binding for GSH was slow and the saturation was not achieved. In search for a suitable chelating agent for Pt-based drugs, we evaluated the affinity of other thiol-containing molecules searching for a faster kinetics of chelation of the Pt complex. To this end commercially available $_{DL}$-thioctic acid (TOA) and 1,4-dithiothreitol (DTT) were investigated because both molecules have two thiols that could result in a higher affinity for the Pt centre in cisplatin (Fig. SI6.2B-C). The appearance of a ligand-to-metal band could be clearly observed after incubation of cisplatin with 1 equiv. of these thiol-containing molecules but, as before, no saturation could be observed even after 8 h of incubation.

Since Pt is a class (b) metal[18] and preferentially binds to “heavier” atoms, we investigated then the ability of phosphorous containing molecules to scavenge Pt-based drugs from aqueous solution. To this end, 1 equiv. of water-soluble phosphine TCEP was incubated in the presence of cisplatin and the resulting UV-Vis spectrum recorded as a function of time (Fig. SI6.2D). As before, a ligand to Pt band could be observed in this case at ~305 nm. More importantly, saturation of this band could be observed even after only 1 h of incubation, suggesting that Pt-P binding was much faster than for any of the other molecules investigated. One of the parameters that define a good ligand for the capture of the Pt-drugs is the reaction time. A fast reaction between the Pt-based drug and the

electrode, will avoid the distribution and recirculation of the drug in the body through the blood, thus reducing the side effects. In addition, will enable fast detection times.

To further investigate the binding of TCEP to Pt, samples were prepared again, and the kinetics of the binding now monitored using a quartz cuvette that allowed us to identify any bands resulting from Pt-P binding in the 210-300 nm window (Fig. 6.2A). An absorption band at 230 nm could now be observed that we attributed to the formation of the complex TCEP-cisplatin, in agreement to what has been reported in the literature.[19] The intensity of this band quickly increased until it reached a plateau indicating that the reaction was completed within 1h (Fig. 6.2B). Addition of 2 and 4 equiv. of TCEP had very little effect on the rate of the coordination but resulted in higher overall intensities, suggesting that more of the UV-responsive bonds could be formed under these conditions. A similar effect was observed for the reaction between TCEP and carboplatin, although reaction rates were now slower, as anticipated due to the presence of a bulky bidentate ligand in this Pt-based drug.

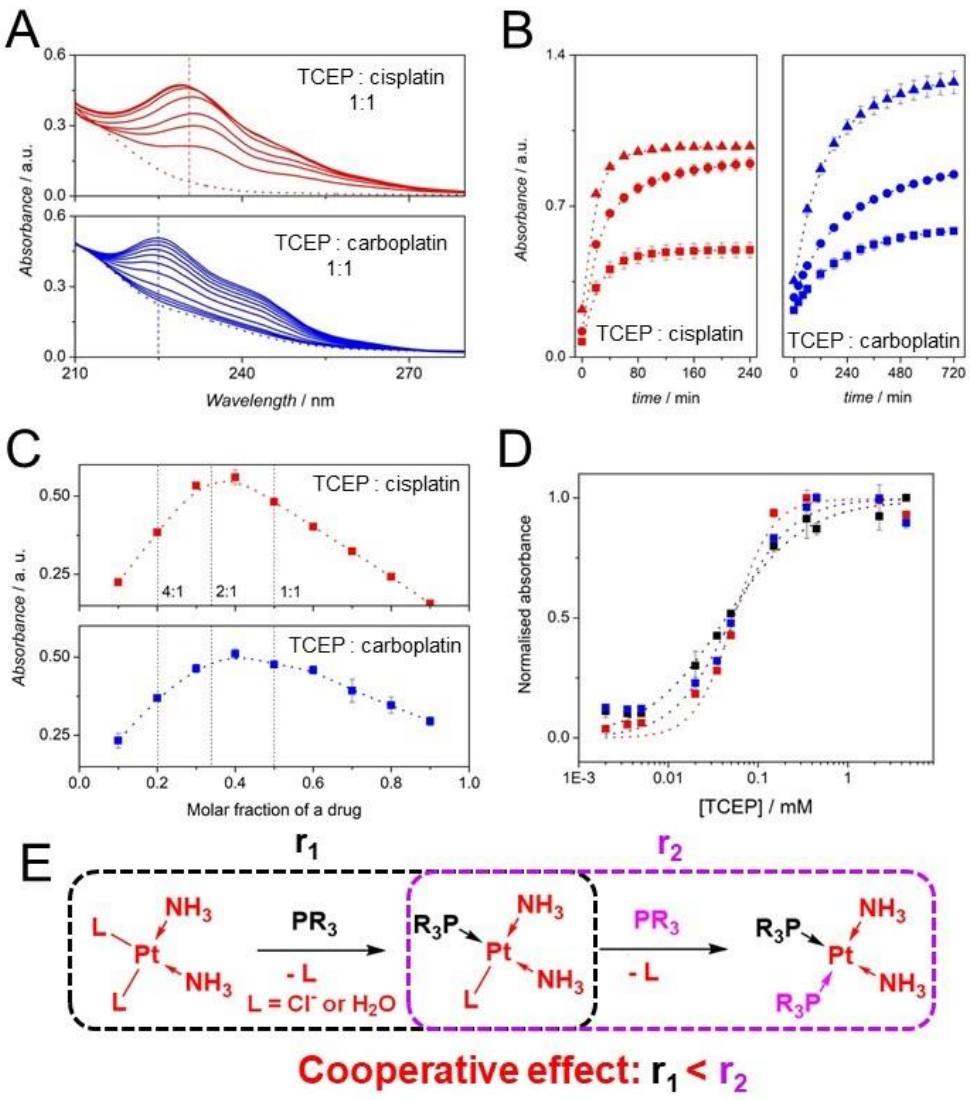

Figure 6.2. (A) UV-Visible spectroscopy monitoring of the reaction progress for the coordination of TCEP to cisplatin and carboplatin at 1:1 molar ratio. Dotted lines correspond to as mixed samples whereas solid lines indicate consecutive spectra. (B) Time-dependence intensity of the signal at 230 nm and 225 nm for the TCEP coordination to cisplatin and carboplatin, respectively at molar ratios of 1:1 (■, ■), 2:1 (●, ●), 4:1 (▲, ▲). (C) Job plots for the complexation process between TCEP and cisplatin/carboplatin suggesting a 2:1 binding ratio. (D) Hill plots for binding between TCEP and potassium tetrachloroplatinate (■), cisplatin (■), and carboplatin (■). It suggests a cooperative binding in the case of cisplatin (n = 2.04 ± 0.35) and carboplatin (n = 1.33 ± 0.29) as compared to a non-cooperative binding of K_2PtCl_4 (n = 0.97 ± 0.09) with a consistent value of dissociation constant. (E) A schematic representation of the ligand exchange on cisplatin substitution by two TCEP molecules with apparent cooperative effect.

Job plots revealed that the coordination between TCEP and both Pt-based drugs was mainly via a 2:1 binding ratio, with a clear maximum of absorbance observed when that stoichiometry was employed (Fig. 6.2C). While the presence of more labile ligands, as in the case of chlorides for potassium tetrachloroplatinate (K_2PtCl_4), had a beneficial effect on the rate of the complexation (Fig. SI6.3A-B), it did not affect the stoichiometry of the binding ratio between TCEP and Pt (Fig. SI6.3C). Therefore, under the studied reaction conditions, each Pt centre could be only coordinated by a maximum of two TCEP molecules. Alternatively, replacing the first coordination sphere ligands for NH_3, which are not good leaving groups[20],resulted in no apparent coordination of TCEP to Pt (Fig. SI6.4), suggesting that TCEP mainly coordinates to the Pt-centre by replacing chloride or water ligands. It should be noted that in aqueous media, Pt-based drugs undergo ligand substitution where chlorides can be substituted by water molecules.[21] The binding of one molecule to the metal centre can induce changes to the electronic properties and configuration of the complex, resulting in different complexation kinetics for a second ligand.[22] To investigate whether binding of a TCEP molecule to Pt could result in a positive cooperative effect, where the binding of a second ligand would be favoured, Pt-based drugs were incubated with increasing amounts of TCEP and the changes in absorbance monitored. Fitting the normalised increase in absorbance observed to a Hill model[23] (Fig. 6.2D) indicated that the coordination of TCEP to cisplatin exhibited a cooperative effect, with a Hill constant (n) of 2.04 ± 0.35. This value suggests that upon the coordination of a TCEP molecule to the Pt-centre, the coordination of a second molecule to the Pt-centre is facilitated. On the other hand, the Hill constant for carboplatin was 1.33 ± 0.29, indicating a lower level of cooperativity, possibly as a result of the poorer leaving group character of the large organic ligand as compared to chlorides. Interestingly,

increasing the number of good leaving groups results in the counter-intuitive loss of cooperativity, as indicated by the Hill constant for K_2PtCl_4 = 0.97 ± 0.10. We propose that the absence of cooperativity for the binding of TCEP and K_2PtCl_4 could be associated to the electronic screening or buffering across the remaining chloride ligands. In line with these observations, affinity constants were determined to be 0.0533 ± 0.0047, 0.0508 ± 0.0090 and 0.0431 ± 0.0051 for cisplatin, carboplatin and potassium tetrachloroplatinate, respectively.

Further insight into the coordination of cisplatin or potassium tetrachloroplatinate with TCEP was achieved by monitoring the complexation via ^{31}P NMR (Fig. SI6.5 and Fig. SI6.6). In addition to the 2:1 TCEP:Pt stoichiometry described above, complex scenarios for the coordination should be considered, including the formation of different isomers. In our case, incubation of the Pt-containing molecules with TCEP (Fig SI6.5 and SI6.6, B and C spectra) resulted in the formation of two distinctive sets of signals. Two singlets at approximately 12-13 ppm were attributed to the *cis*- and *trans*-oriented di-substituted products assuming possible inversion of the configuration through a pentacoordinate state.[24, 25] An additional singlet at 7-8 ppm could be attributed to the second-sphere coordination of a TCEP molecule. In the case of K_2PtCl_4 (Fig. SI6.6), another singlet at ~6.5 ppm was also observed. We attribute this signal to the mono-substituted product which should be present due to the lack of cooperativity observed for this Pt salt.

The nature of the second-sphere coordination signal at 7-8 ppm was confirmed when $Pt(NH_3)_4(NO_3)_2$ was used instead of the Pt-based drugs. As discussed before, this Pt salt does not undergo ligand displacement in the first-sphere of coordination and only the

signal at ~7 ppm was observed (Fig. SI6.7). This second-sphere coordination in $Pt(NH_3)_4^{2+}$ salts had been previously described.[26, 27] Increasing the ratio of TCEP did not result in the appearance of any new signal, beyond the presence of uncoordinated TCEP at ~ -16 ppm (Fig. SI6.7). Finally, performing the experiments in the absence of NaCl facilitated the Cl/H_2O-to-TCEP exchange and as a result no second sphere coordination band was observed for both K_2PtCl_4 and cisplatin (Fig. SI6.8A-B). As expected, this was not the case for $Pt(NH_3)_4(NO_3)_2$, for which only second-sphere coordination could be observed in any of the buffers investigated (Fig SI6.8C).

Once it was determined that the TCEP was the most suitable ligand for the coordination of cisplatin or carboplatin and understanding of the nature of the Pt-P interaction was achieved, the surface of a gold electrode was functionalized to introduce this Pt scavenger. Figure 6.3A shows the schematic representation of the step-by-step immobilization of TCEP. Cysteamine (CA) was selected as a linker based on the presence of a terminal amine group and the electrochemical stability of its Au-layers in physiological medium.[28] Immobilization of cysteamine and TCEP was monitored by cyclic voltammetry of the surface-modified gold electrodes at different stages of the modification (Fig. 6.3B). The self-assembled monolayer of cysteamine on gold was stable in a broad potential region down to 0.1 V vs RHE with the signal below 0.1 V vs RHE associated to the reductive desorption of cysteamine.[28] Following modification with cysteamine, TCEP was immobilized on the cysteamine layer through EDC coupling.[29, 30] No significant changes in the voltammetry profiles were observed confirming that the step-by-step surface modification did not affect the stability of the layer in the potential window under investigation and only a small shift of 25 mV in the desorption peak towards less positive

potential was observed. This shift can be attributed to the larger size of the CA-TCEP adlayer which results in higher energy needed to desorb the adlayer from the gold surface as compared to the cysteamine layer.[31] This shift was not observed when the Au-CA electrode was exposed to the solution of EDC, confirming the TCEP coupling (Fig. SI6.9). The step-by-step surface modification and integrity of the layer was also confirmed by electrochemical impedance spectroscopy. As shown in Fig. 6.3C, phase shift plots showed a clear difference between the pristine gold electrode and the surface-modified electrodes. In these plots, a phase angle (-φ) of 90° in the frequency domain at 1 Hz to 1 kHz indicates the presence of an ideal capacitor, while lower angles are related to current leakage on defect sites of the layer.[32] In our case, the phase angles for the surface modified electrodes at 1 Hz were φ=78° which indicated a pseudocapacitive behaviour. This response could be associated to the presence of some defects in the layer or to the formation of a less compact film that would allow the permeation of ions such as K^+, HPO_4^{2-}, and $H_2PO_4^-$ through the layer.[32, 33] The presence of inhomogeneities in the layer or the presence of a less compact layer could also be the cause of the local minimum at 10 Hz. While the formation of SAMs of long-chain alkane thiols gives compact layers due to Van der Waals interactions, the presence of functional groups in the CA-TCEP layer architecture could lead to the presence of less compact layers. At high frequencies (>10 kHz), the total impedance is dominated by the solution resistance. Finally, evidence of the functionalization of the gold electrodes with CA-TCEP was obtained using contact-angle measurements. As expected, the contact angle decreased upon functionalization with TCEP (Fig 6.3D), indicating that the surface had become more hydrophilic when compared to the pristine gold electrode.

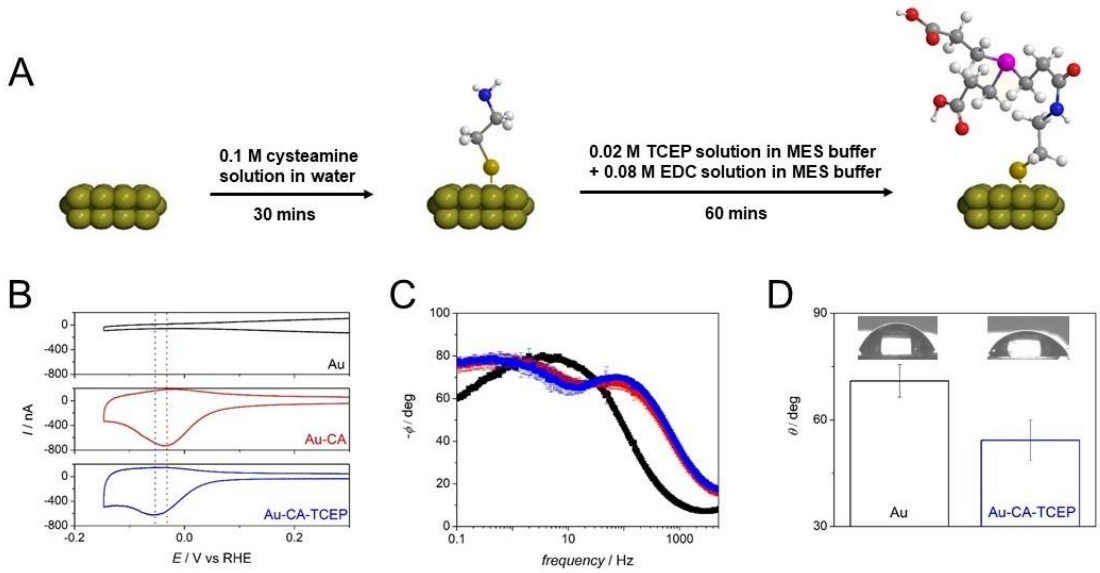

Figure 6.3. (A) Schematic representation of the strategy for the surface modification of the gold electrodes. (B) Voltammetric profiles of electrode at different stages of modification. Self-assembly of cysteamine (—) results in the presence of reductive desorption peak at low potential value. This peak shifts by 30 mV once TCEP is coupled to self-assembled cysteamine (—), (C) Bode plots of phase shift vs. frequency showing Au (■), Au-CA (■), Au-CA-TCEP (■). Au-CA-TCEP shows a clear difference between unmodified and modified electrodes, but no change between Au-CA and Au-CA-TCEP, suggesting that the integrity of the initial CA SAM is not affected by coupling of TCEP. (D) Contact angles for the wetting of Au and Au-CA-TCEP with deionised water.

Once the stability of electrodes modified with CA-TCEP was confirmed, the adsorption of Pt-based drugs and the electrochemical response were examined by cyclic voltammetry, electrochemical impedance spectroscopy, X-ray photoelectron spectroscopy and contact angle measurements. Upon adsorption of cisplatin on the TCEP-modified electrode, the oxidation state of the Pt was analysed by *ex-situ* XPS, where bands at 72 eV and 75.3 eV corresponding to the Pt $4f_{7/2}$ and Pt $4f_{5/2}$ components arising from Pt(II)-Cl confirmed the presence of unreduced cisplatin adsorbed on the TCEP-modified gold electrode(Fig. 6.4A, bottom). On the other hand, cyclic voltammetry of the TCEP-modified electrode after

exposure to cisplatin indicated that the capacitive current slightly increased in the region between 0.8 and 0.3 V but no obvious Faradic process was observed (Fig. 6.4B). In the second cycle, no relevant changes in the voltammetric profile were observed. These results suggested that cisplatin was adsorbed on the TCEP-modified electrode but it was not reduced to Pt(0) in the given potential window. The adsorption without reduction to Pt(0) is an important parameter to consider for future applications as the formation of Pt(0) species might result in the electrochemical oxidation/reduction of other species present in the blood. To confirm this observation, this electrode was also analysed by XPS after cycling (Fig. 6.4A, top). In this case, the signal of Pt(II)-Cl slightly reduced, with only a small fraction (<15 %) at 74 eV and 71 eV associated to reduced Pt(0). We believe reduction of the adsorbed cisplatin on the TCEP-modified electrode to Pt(0) would be achievable only at much lower potentials, potentials at which the reductive desorption of the self-assembled layer would also be observed (Fig. SI6.11).[28] These results were in contrast with those obtained for the adsorption and electrochemical reduction of cisplatin on a bare Au electrode, where the reduction of cisplatin occurred at 0.48 V vs RHE (Fig. SI6.10). XPS analysis of this bare gold electrode after exposure to cisplatin confirmed that different behaviours were observed when depositing cisplatin on functionalised and unmodified gold electrodes with a significantly larger amount of reduced Pt being observed in the latter case (Fig. SI6.12). However, this effect can be associated to the photoreduction of the platinum complex on gold induced by the X-rays, although sample exposure was minimized in an effort to negate these effects.[34, 35]

The interaction of TCEP-modified electrodes with cisplatin was also monitored via EIS and the results obtained compared to those of the bare gold electrode. On the bare gold electrode, as the potential decreased the resistive response appeared at a lower

frequency (Fig. SI6.13A, top) as the reduction of platinum took place on the surface of the gold electrode. On the other hand, the phase angle profiles for the TCEP-modified electrodes (Fig. SI6.13A, bottom) with cisplatin did not show any differences as the potential was stepped more negative suggesting that the binding on Au-CA-TCEP and the reduction of cisplatin did not take place on the pinholes of the layer where Au remains uncovered. Similar observations were made using K_2PtCl_4 as a source of Pt (Fig. SI6.13B).

In order to gain more information on the interaction of the surfaces and the different Pt-based drugs electrochemical impedance spectroscopy measurements were performed. The Nyquist plot and the corresponding analysis can be found in Fig. SI6.14. Finally, contact angle measurements showed that upon adsorption of cisplatin on the CA-TCEP-modified electrode, its surface becomes more hydrophobic (Fig. SI6.15).

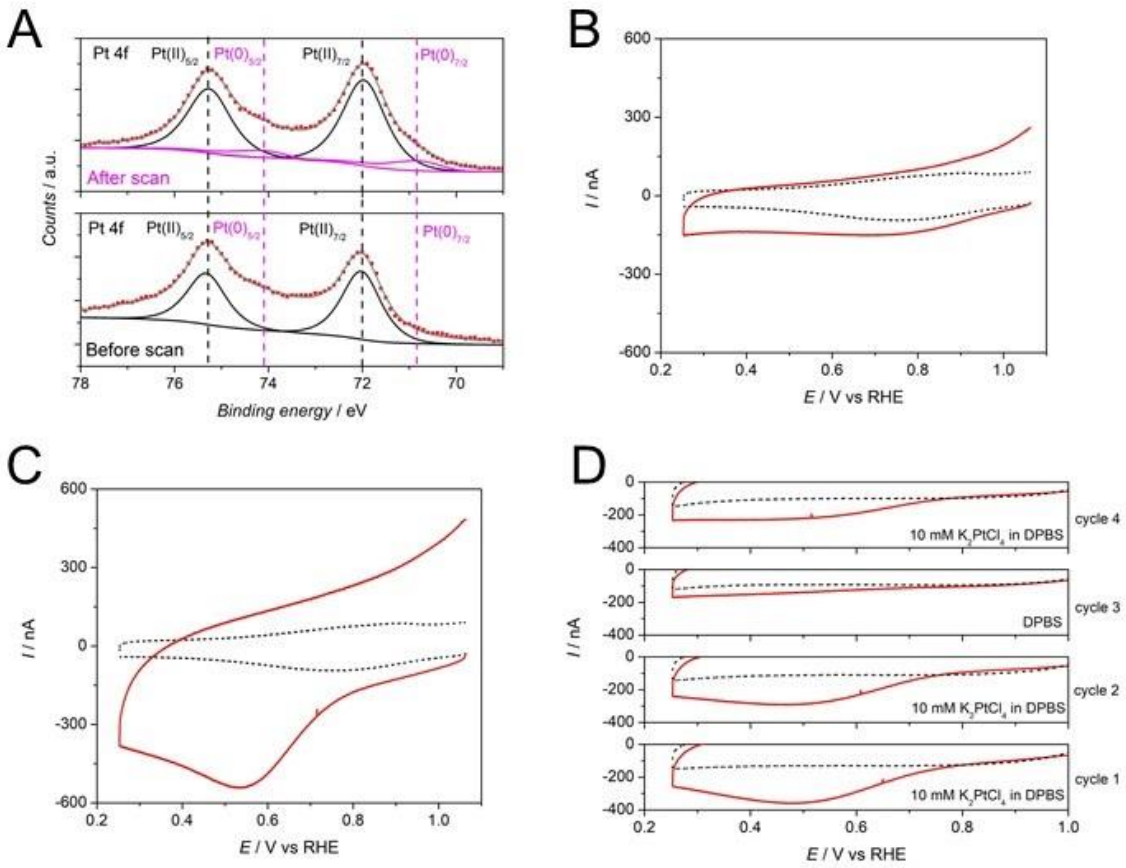

Figure 6.4. (A) XPS spectra of Au-CA-TCEP exposed to 1 mM solution of cisplatin for 30 mins before and after electrochemical conditioning (a scan in the potential range as the one in the Fig. 4B). (■) full spectra and the corresponding fitting (—), (—) and (—) peak convolution of the Pt(II) and Pt(0) species, respectively. Vertical dashed lines (¦) and (¦) are shown for the sake of comparison. Voltammetric profiles of Au-CA-TCEP before and after exposure to (B) 1 mM solution of cisplatin in DPBS for 30 mins, (C) 10 mM solution of K_2PtCl_4 in DPBS for 15 mins. (—) correspond to experiments after exposure, whereas (···) stand for blanks. (D) Adsorption experiment where Au-CA-TCEP was immersed in 10 mM solution of K_2PtCl_4 and electrochemically reduced multiple times (cycle 1, 2 and 4). A control experiment where the electrode was immersed in Pt-free DPBS (cycle 3) shows no reductive feature. (—) corresponds to experiments after exposure, whereas (···) are blanks voltammograms.

The adsorption and electrochemical assessment were also performed on the CA-TCEP-modified electrode after adsorption of $PtCl_4^{2-}$. In contrast to the results obtained with cisplatin on CA-TCEP-modified electrodes, the voltammetric profile in Fig. 6.4C shows a reductive current contribution in the region between 0.7 and 0.3 V vs RHE corresponding to the reduction of Pt(II) to Pt(0). Interestingly, this signal was clearly different from that observed for the reduction of $PtCl_4^{2-}$ to Pt(0) on a bare gold electrode (Fig. SI6.16A). In order to gain further insight into the process taking place on the Au-CA-TCEP electrode, and discard the possibility that the reduction of $PtCl_4^{2-}$ to Pt(0) was occurring on the underlying gold electrode, experiments of consecutive cycles of adsorptions of $PtCl_4^{2-}$ and reduction experiments were performed. According to the nucleation and growth process, the formation of a nucleation centre – Pt(0) cluster – during the first cycle of $PtCl_4^{2-}$ absorption, will favour the growth of such clusters in the following adsorption/reduction cycles. As a result, the signal of the reduction of the adsorbed $PtCl_4^{2-}$ should shift towards more positive potentials.[36, 37]

On the other hand, if the $PtCl_4^{2-}$ is adsorbing on the available TCEP sites, the signal associated to the adsorption of $PtCl_4^{2-}$ should decrease as number of available sites decreases in each cycle. As can be seen in Figure 6.4D, consecutive adsorption/reduction cycles of the $PtCl_4^{2-}$ lead to reduction signals appearing in all voltammograms (except a control experiment with DPBS only – cycle 3) with no changes to the onset potential for the reduction process being observed. These results confirm that the growth of the nucleus was not taking place but that consecutive cycles lead to the adsorption of lower amount of $PtCl_4^{2-}$ on TCEP sites. More importantly, the presence of this reductive current provides a means to monitor the adsorption of $PtCl_4^{2-}$ and this ability to monitor the adsorption process makes the concept of electrochemical hemofiltration even more

versatile, ultimately providing a way to follow the amount of a drug in the blood stream. Our preliminary results have shown that adsorption can be qualitatively measured by the integration of charge involved in the irreversible electrochemical reduction of Pt^{2+} to Pt^{0} with a reasonable signal-to-concentration correlation (Fig. SI6.17-18).

6.5. Conclusions

In conclusion, we have demonstrated here the feasibility of employing surface modified electrodes for the electrochemical adsorption and monitoring of Pt-based drugs from complex aqueous media. Our strategy is underpinned by the identification of commercially available TCEP as an efficient scavenger of Pt. Using UV-Vis and 1D ^{31}P-NMR we have demonstrated that TCEP has a higher affinity for Pt than chelators found in nature, such as guanine or glutathione, or than representative thiol containing molecules. Moreover, these homogeneous-phase studies have allowed us to identify the nature, affinity and stoichiometry of the binding of TCEP to common Pt-based drugs such as cisplatin and carboplatin, a knowledge that should inform the future design of improved surfaces with high-capacity for the adsorption of Pt-based drugs. Immobilization of TCEP onto flat electrodes could be achieved through a simple EDC-mediated coupling onto a cysteamine-modified gold electrode. The interaction of Pt-based drugs with these TCEP-modified electrodes was evaluated using cyclic-voltammetry, impedance spectroscopy, X-ray photoelectron spectroscopy and contact angle, to demonstrate that a differential response could be observed for the TCEP-modified electrodes suggesting that Pt is preferentially absorbed on the TCEP sites and not on the pinholes at the gold surface. Appearance of a reductive current for the immobilization of K_2PtCl_4 on these TCEP-modified electrodes highlights the feasibility of using electrochemical filtration to monitor

the concentration of Pt-based drugs in complex aqueous environments such as the blood stream. Altogether, these results demonstrate the potential of electrochemical devices for the development of new systems for the filtration and monitoring of Pt-based anticancer drugs. Our efforts to translate these results from flat surfaces into more applicable high-surface area systems with improved Pt adsorption, as well as the evaluation of other electrochemical techniques for the monitoring of Pt-based drugs in solution, will be reported in due course.

This article represents the first insight into the concept of the electrochemical hemofiltration of anti-cancer drugs. The implementation of this electrochemical platform in a real system will need however further studies including the effects of proteins and haemoglobin, as well the presence of other possible interference such as sugars.

6.6. References

1. B. Rosenberg, L. Van Camp and T. Krigas, *Nature*, 1965, **205**, 698-699.
2. B. Rosenberg, L. Vancamp, J. E. Trosko and V. H. Mansour, *Nature*, 1969, **222**, 385-386.
3. E. Wong and C. M. Giandomenico, *Chem. Rev.*, 1999, **99**, 2451-2466.
4. R. B. Weiss and M. C. Christian, *Drugs*, 1993, **46**, 360-377.
5. L. Kelland, *Nat. Rev. Cancer*, 2007, **7**, 573-584.
6. D. P. Gately and S. B. Howell, *Br. J. Cancer*, 1993, **67**, 1171-1176.
7. D. Von Hoff, R. Schilsky, C. Reichert, R. Reddick, M. Rozencweig, R. Young and F. Muggia, *Cancer Treat. Rep.*, 1979, **63**, 1527-1531.
8. A.-M. Florea and D. Büsselberg, *Cancers*, 2011, **3**, 1351-1371.
9. J. F. Pingpank, S. K. Libutti, R. Chang, B. J. Wood, Z. Neeman, A. W. Kam, W. D. Figg, S. Zhai, T. Beresneva and G. D. Seidel, *J. Clin. Oncol.*, 2005, **23**, 3465-3474.
10. H. Yatzidis, *Proc. Eur. Dial. Transplat. Assoc.*,1964, **1**, 83-87.

11. K. E. Hagstam, L. E. Larsson and H. Thysell, *Acta Med. Scand.*, 1966, **180**, 593-603.
12. D. Webb, *Br. J. Hosp. Med.*, 1993, **49**, 493-496.
13. R. A. Graham, Z. H. Siddik and D. C. Hohn, *Cancer Chemother. Pharmacol.*, 1990, **26**, 210-214.
14. B. Chiavarino, M. E. Crestoni, S. Fornarini, D. Scuderi and J.-Y. Salpin, *J. Am. Chem. Soc.*, 2013, **135**, 1445-1455.
15. Y. Kasherman, S. Sturup and D. Gibson, *J. Med. Chem.*, 2009, **52**, 4319-4328.
16. T. G. Appleton, J. R. Hall, S. F. Ralph and C. S. M. Thompson, *Inorg. Chem.*, 1984, **23**, 3521-3525.
17. A. Kolodziej, M. C. Figueiredo, M. T. M. Koper, F. Fernandez-Trillo and P. Rodriguez, *Electrochim. Acta*, 2017, **248**, 409-415.
18. E. Nieboer and D. H. S. Richardson, *Environ. Pollut. B*, 1980, **1**, 3-26.
19. S. Chen, H. Jiang, K. Wei and Y. Liu, *Chem. Commun.*, 2013, **49**, 1226-1228.
20. A. J. Gregory, W. Levason, R. E. Noftle, R. Le Penven and D. Pletcher, *J. Electroanal. Chem.*, 1995, **399**, 105-113.
21. Y. Zhang, Z. Guo and X.-Z. You, *J. Am. Chem. Soc.*, 2001, **123**, 9378-9387.
22. J. Chatt, L. A. Duncanson and L. M. Venanzi, *J. Chem.Soc.*, 1955, 4456-4460.
23. A. V. Hill, *J. Physiol.*, 1910, **40**, 4-7.
24. M. S. Holt and J. H. Nelson, *Inorg. Chem.*, 1986, **25**, 1316-1320.
25. J. J. Macdougall, J. H. Nelson and F. Mathey, *Inorg, Chem.*, 1982, **21**, 2145-2153.
26. D. R. Alston, A. M. Z. Slawin, J. F. Stoddart, D. J. Williams and R. Zarzycki, *Angew. Chem. Int. Ed.*, 1987, **26**, 693-696.
27. F. M. Raymo and J. F. Stoddart, *Chem. Ber.*, 1996, **129**, 981-990.
28. A. Kolodziej, F. Fernandez-Trillo and P. Rodriguez, *J. Electroanal. Chem.*, 2018, **819**, 51-57.
29. E. Chow, D. B. Hibbert and J. J. Gooding, *Analyst*, 2005, **130**, 831-837.
30. K. Seo, I. C. Jeon and D. J. Yoo, *Langmuir*, 2004, **20**, 4147-4154.
31. I. Shin-ichiro, I. Minehiko, H. Daisuke, F. Zhi Qiang, N. Katsumi and K. Takashi, *J. Electroanal. Chem.*, 1997, **428**, 33-38.
32. E. Boubour and R. B. Lennox, *Langmuir*, 2000, **16**, 4222-4228.
33. E. Boubour and R. B. Lennox, *J. Phys. Chem. B*, 2000, **104**, 9004-9010.

34. E. Ozkaraoglu, I. Tunc and S. Suzer, *Surf. Coat. Tech.*, 2007, **201**, 8202-8204.
35. F. Karadas, G. Ertas, E. Ozkaraoglu and S. Suzer, *Langmuir*, 2005, **21**, 437-442.
36. B. Scharifker and G. Hills, *Electrochim. Acta*, 1983, **28**, 879-889.
37. B. R. Scharifker, J. Mostany, M. Palomar-Pardave and I. Gonzalez, *J. Electrochem. Soc.*, 1999, **146**, 1005-1112.

Chapter 6: Supporting Information

6.7. Experimental details

Electrochemical experiments

General electrochemical methods

An exhaustive cleaning procedure of the glassware was implemented to ensure reproducible experimental conditions. Daily, the glassware was soaked overnight in an acidic solution of $KMnO_4$. The glassware was then removed from the $KMnO_4$ solution and rinsed with a diluted solution of H_2SO_4/H_2O_2 with a ratio of 1:3. The glassware was finally rinsed with boiling Milli-Q water (18.2 MΩ cm, 1 ppb total organic carbon) at least 5 times to ensure the absence of sulfate ions in the working solution. A three-compartment electrochemical cell was employed with a high surface area gold flag counter electrode and a Hg/Hg_2SO_4 reference electrode. All the results were converted to RHE scale as presented in the manuscript. Measurements were performed on μAutoLab III potentiostat. Prior to experiments, Argon (6N, BOC) was used to deoxygenate electrolytic media. Gold disk electrodes were prepared from high purity gold wire (Sigma Aldrich, 99.999%). Prior each experiment, the gold disk electrode was mechanically polished with diamond slurry, rinsed with Milli-Q water, flame-annealed and cooled down under argon atmosphere. A blank voltammetry of the gold electrode was registered prior each set of experiments to confirm the cleanness of the system (both electrode and electrolyte). Dulbecco's phosphate-buffered saline solution (DPBS, Lonza, pH = 7.4) was used as the electrolyte throughout the manuscript to mimic physiological conditions. All the experiments were performed at room temperature.

Potentiostatic Electrochemical Impedance Spectroscopy

Prior to Potentiostatic Electrochemical Impedance Spectroscopy experiments the general cleaning procedure was followed (as described above) with the exception of N_2 (Oxygen-free, BOC) being used as the inert gas. Experiments were performed using a Biologic SP-150 potentiostat by applying 10 mV of potential amplitude over the range of frequencies from 500 kHz to 100 mHz.

UV-Vis Spectroscopy

UV-Vis spectra were recorded on a Cary 50 UV-Visible Spectrophotometer using a quartz cuvette (16.100/F/Q/10, Starna Scientific). Fresh stock solutions of reagents were prepared in commercially available DPBS prior each experiment.

For kinetic assays: After addition of a ligand solution to Pt-rich solution, the mixture was conditioned for 1 minute at room temperature before measuring the corresponding spectrum in a blank-subtracted mode.

'Pt' : TCEP ratio	**Concentration of 'Pt' solution (mM)**	**Volume of 'Pt' solution (mL)**	**Concentration of TCEP solution (mM)**	**Volume of TCEP solution (mL)**
1:1	0.1	0.75	0.1	0.75
1:2	0.1	0.75	0.2	0.75
1:4	0.1	0.75	0.4	0.75

Table SI6.1. Experimental conditions for the UV-Vis experimental analysis.

Coordination of cisplatin by guanine was studied at 1:1 ratio with accordance to table above. Note: Guanine is poorly soluble in DPBS and preparation of 0.1 mM solution resulted in cloudy but stable dispersion.

For Job's/Hill's plots: After addition of a ligand solution to Pt-rich solution, the mixture was conditioned at room temperature in accordance to the kinetic data to ensure reactions completion before measuring the corresponding spectra in a blank-subtracted mode.

'Pt' : TCEP ratio	**Concentration of 'Pt' solution (mM)**	**Volume of 'Pt' solution (mL)**	**Concentration of TCEP solution (mM)**	**Volume of TCEP solution (mL)**
1:9	0.1	0.1	0.1	0.9
2:8	0.1	0.2	0.1	0.8
3:7	0.1	0.3	0.1	0.7
4:6	0.1	0.4	0.1	0.6
5:5	0.1	0.5	0.1	0.5
6:4	0.1	0.6	0.1	0.4
7:3	0.1	0.7	0.1	0.3
8:2	0.1	0.8	0.1	0.2
9:1	0.1	0.9	0.1	0.1

Table SI6.2. Experimental conditions for the Job's plots experimental analysis.

Final concentration of TCEP (mM)	Concentration of 'Pt' solution (mM)	Volume of 'Pt' solution (mL)	Concentration of TCEP solution (mM)	Volume of TCEP solution (mL)	Volume of DPBS added (mL)	Final volume (mL)
4.5	0.5	0.1	5	0.9	0	1
2.25	0.5	0.1	2.5	0.9	0	1
0.45	0.5	0.1	0.5	0.9	0	1
0.35	0.5	0.1	0.5	0.7	0.2	1
0.15	0.5	0.1	0.5	0.3	0.6	1
0.05	0.5	0.1	0.5	0.1	0.8	1
0.035	0.5	0.1	0.5	0.07	0.83	1
0.02	0.5	0.1	0.5	0.04	0.86	1
0.005	0.5	0.1	0.5	0.01	0.89	1
0.0035	0.5	0.1	0.5	0.007	0.893	1
0.002	0.5	0.1	0.5	0.004	0.896	1

Table SI6.3. Experimental conditions for the Hill's plots experimental analysis.

Initial screening of ligands was performed on a BMG Labtech Microplate Reader using Greiner 96 F-bottom plates as described below.

Ligand	Concentration of 'Pt' solution (mM)	Volume of 'Pt' solution (mL)	Concentration of ligand solution (mM)	Volume of ligand solution (mL)
Glutathione	1	0.1	1	0.1
1,4-dithiothreitol	1	0.1	1	0.1
DL-thioctic acid	1	0.1	1	0.1
TCEP	1	0.1	1	0.1

Table SI6.4. Experimental conditions for the UV-Vis experimental analysis using the microplate reader

Guanine was not initially screened using the Microplate Reader due to its low solubility in aqueous media and no possibility of preparing a solution to give a clear and comparable result.

NMR Spectroscopy

Nuclear Magnetic Resonance spectra were recorded on a Bruker Avance III 300 MHz. Stock solutions of reagents were prepared in 1 M phosphate buffer (pH=8.1 ± 0.1) in the presence or absence of 150 mM NaCl, to study the chloride anion effect. Final samples were prepared by collecting 540 µL of a reaction mixture and adding 60 µL of D_2O for lock purposes. All ^{31}P NMR experiments were performed in a proton-decoupled mode with relaxation time = 1s and number of scans = 400.

After addition of a ligand solution to Pt-rich solution, the mixture was conditioned at room temperature in accordance to the kinetic data to ensure reaction completion before measuring corresponding spectra.

TCEP : 'Pt' ratio	Concentration of 'Pt' solution (mM)	Volume of 'Pt' solution (mL)	Concentration of TCEP solution (mM)	Volume of TCEP solution (mL)	Volume of buffer added (mL)
1:1	10	0.5	10	0.5	0
2:1	10	0.25	10	0.5	0.25
4:1	10	0.125	10	0.5	0.375
10:1	10	0.050	10	0.5	0.45
TCEP only	10	0	10	0.5	0.50

Table SI6.5. Experimental conditions for the NMR analysis of the coordination of K_2PtCl_4 and $Pt(NH_3)_4(NO_3)_2$ with TCEP.

TCEP : 'Pt' ratio	Concentration of 'Pt' solution (mM)	Volume of 'Pt' solution (mL)	Concentration of TCEP solution (mM)	Volume of TCEP solution (mL)	Volume of buffer added (mL)
1:1	2	0.5	10	0.1	0.4
2:1	2	0.25	10	0.1	0.65
4:1	2	0.125	10	0.1	0.775
10:1	2	0.05	10	0.1	0.85
TCEP only	2	0	10	0.1	0.9 `

Table SI6.6. Experimental conditions for the NMR analysis of the coordination of $Pt(NH_3)_2Cl_2$ and with TCEP.

.X-ray Photoelectron Spectroscopy

XPS measurements were conducted in the main analysis chamber of a Kratos Axis Ultra DLD spectrometer (Kratos Analytical) with a base pressure of 2×10^{-10} mbar. Samples were mounted to a metallic sample bar using conductive carbon tape in order to prevent surface charging during the experiment. The samples, at room temperature, were illuminated using a monochromatic Al Kα X-ray source, with photoelectrons collected at take off angle of 90° with respect to the sample surface. Survey spectra were acquired using a pass energy of 160 eV, with core level spectra recorded using a pass energy of 20 eV (resolution of approximately 0.4 eV). The data were analyzed using the CasaXPS package, using Shirley backgrounds, mixed Gaussian–Lorentzian (Voigt) line shapes, and asymmetry parameters where appropriate. All binding energies were calibrated using the Fermi edge of a polycrystalline Ag sample, measured immediately prior to commencing the measurements.

Contact Angle Measurements

Contact Angle Measurements were performed on appropriately modified gold-coated glass slides using 1 µL of deionised water on a Drop Shape Analyzer – DSA100 by KRÜSS.

6.8. Supporting figures

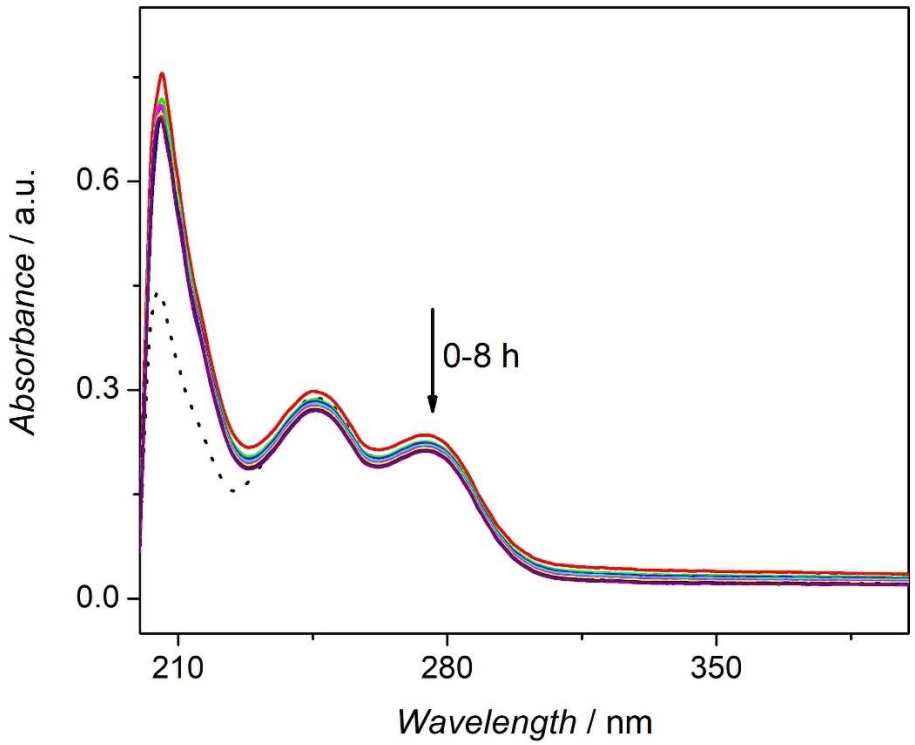

Figure SI6.1. UV-Visible profiles for the coordination of cisplatin with guanine over the period of 8h with 1h intervals. (⋯) corresponds to the spectrum recorded for the solution of guanine for the sake of comparison. The reaction was performed at 1:1 molar ratio using 100 µM solutions. Of note: this spectrum was recorded using a quartz cuvette, analysis of this reaction using Microplate Reader was not possible due to low solubility of guanine.

The reaction between guanine and cisplatin followed by UV-Vis spectroscopy has shown no measurable progress over the period of 8 hours. A slight decrease in the absorbance values in the region of 230 – 300 nm is related to the lack of long-term stability of guanine dispersion in water which is formed due to low solubility of this nucleobase. The spectra

recorded over time show the same behaviour as the one corresponding to the spectrum of guanine.

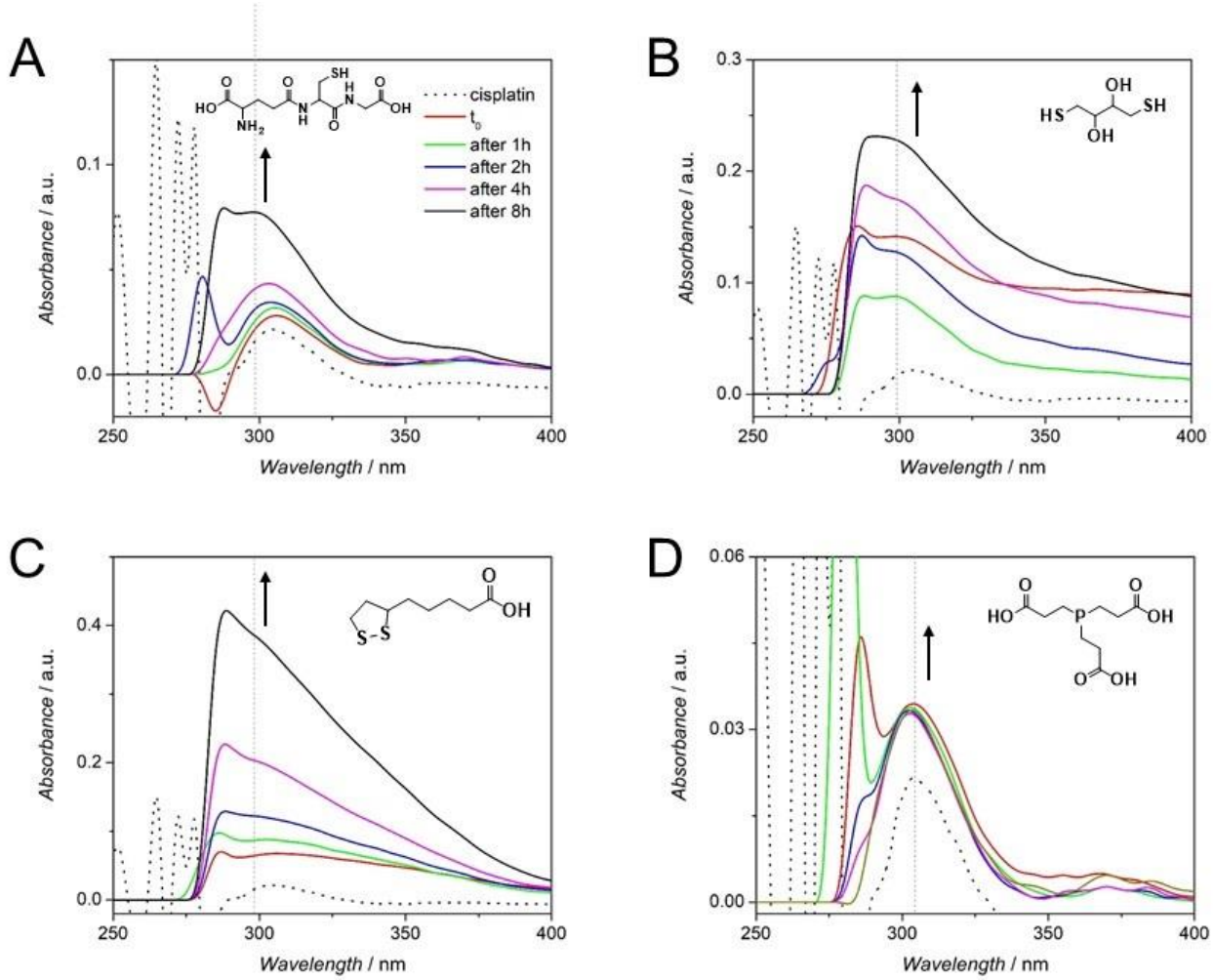

Figure SI6.2. Preliminary screening of ligands using microplate reader. Evolution of UV-Vis spectrum for the reaction of cisplatin with (A) glutathione, (B) 1,4-dithiothreitol, (C) DL-thioctic acid, (D) tris(carboxyethyl)phosphine. Spectra recorded right after preparing a well plate (—), after 1h (—), after 2h (—), after 4h (—), after 8h (—). Spectrum of cisplatin (⋯) included for the sake of comparison. All reactions were performed in 1:1 molar ratio by mixing 1 mM solutions prepared in DPBS.

Reactions in (A), (B), (C) progress over the studied period (8h), whereas the one in (D) was quickly completed. Due to low quality of spectra caused by the light absorption of well plate material, we decided to take the most promising ligand, TCEP (D), and perform more detailed study using a quartz cuvette on a Cary 50 UV-Visible Spectrophotometer.

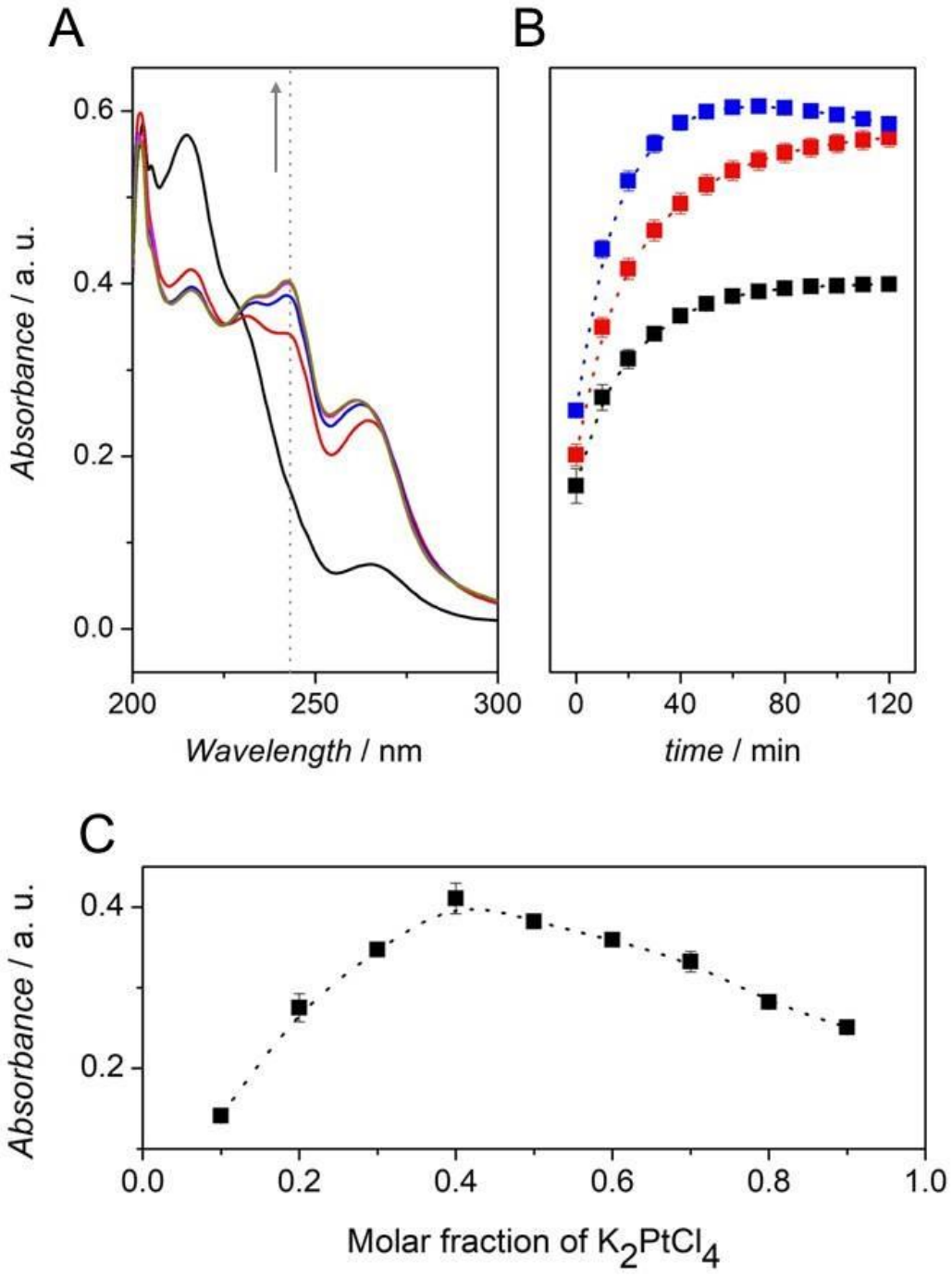

Figure SI6.3. (A) UV-Vis spectra of an equimolar mixture of K_2PtCl_4 and TCEP in DPBS over the period of 2 hours with 30 minutes intervals. Grey vertical line stands for the wavelength of 243 nm that has been used to collect quantitative data. (B) Kinetic profiles of the coordination of K_2PtCl_4 by TCEP in the molar ratio of 1:1 (■), 1:2 (■), 1:4 (■). (C) Corresponding Job's plot.

The reaction between K_2PtCl_4 and TCEP can be monitored by the evolution of a band at 243 nm (Fig. SI6.3A). As can be see in Fig. SI6.3B, the reaction is completed within 40 minutes. Moreover, band intensities recorded for the reactions performed at different ratios suggest that one Pt centre can be coordinated by two TCEP moieties.This was further confirmed by the Job's plot(Fig. SI6.3C)

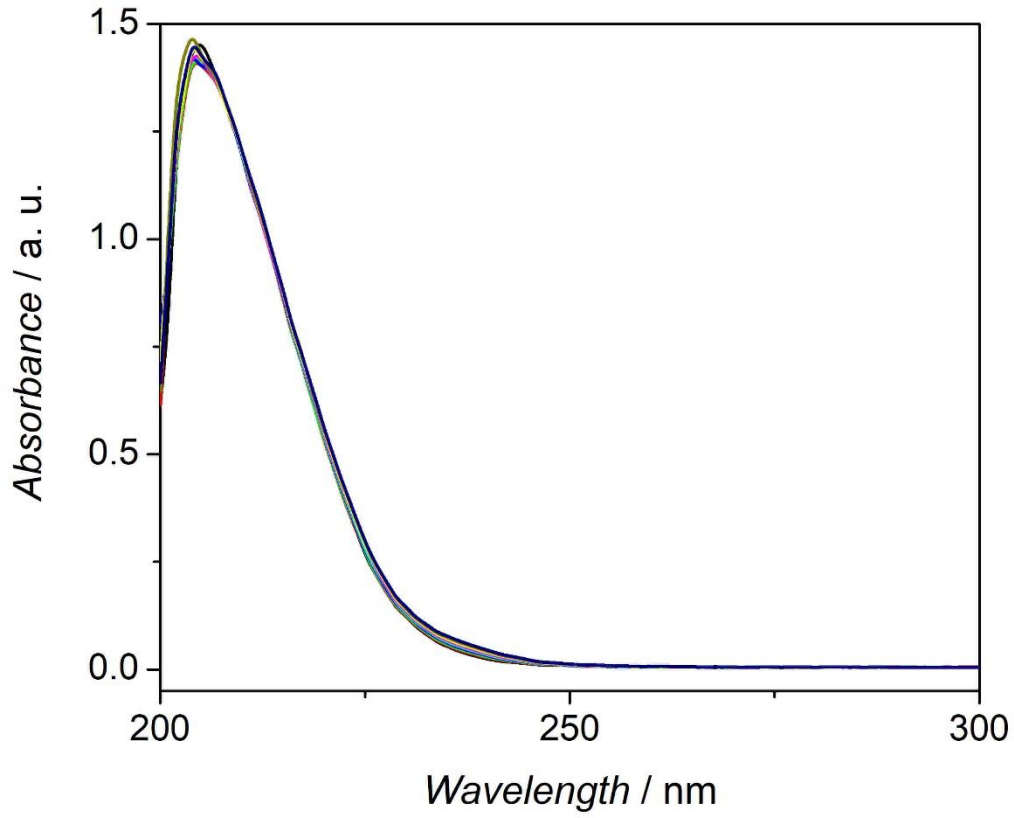

Figure SI6.4. UV-Vis spectra of an equimolar mixture of TCEP and $Pt(NH_3)_4(NO_3)_2$ in DPBS over the period of 4 hours with a 30 minutes interval in between.

As can be seen in the Figure SI6.4, there is no reaction that would give an increase in the UV-Vis signal over time, therefore, we concluded no process changing the nature of metal-ligand charge transfer to take place in this system.

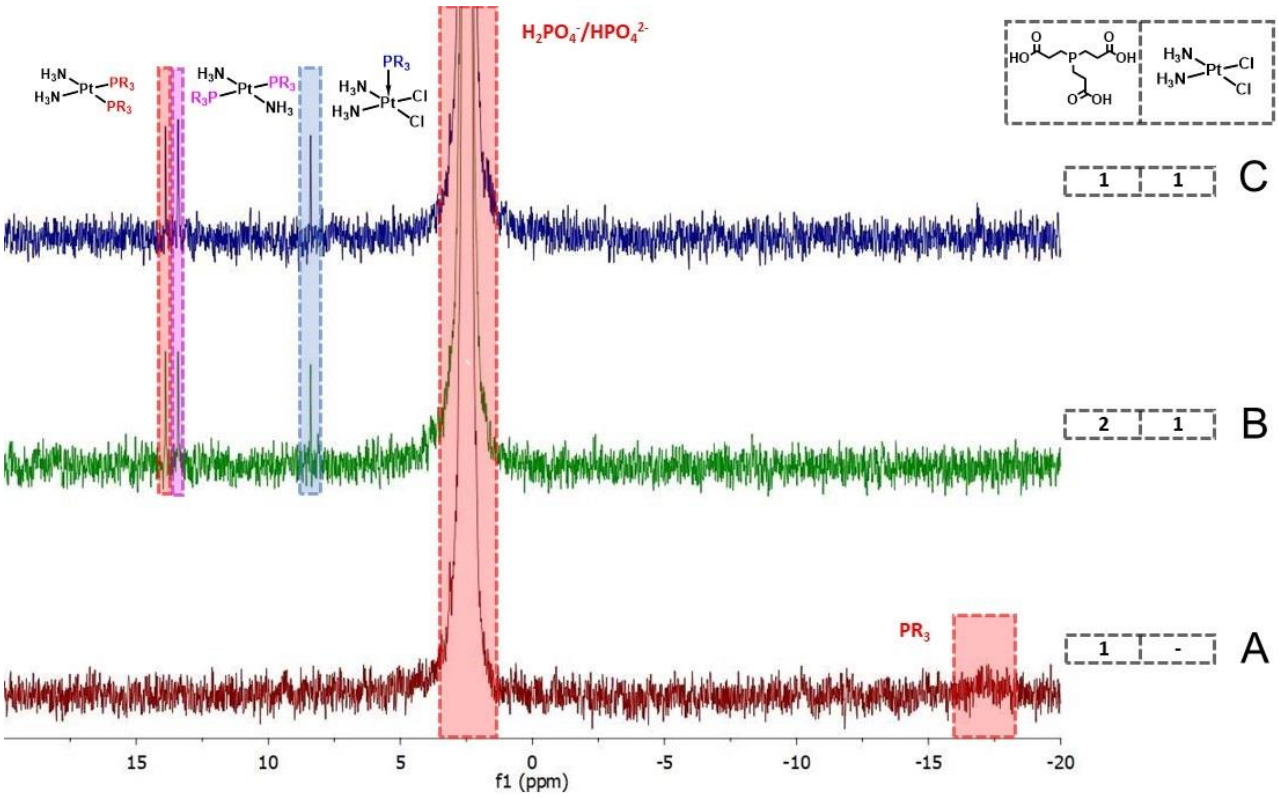

Figure SI6.5. 1D ^{31}P NMR spectra for the reaction of TCEP with cisplatin (ratios indicated in the side panel) in 1 M phosphate buffer with 150 mM of NaCl (pH = 8.1 ± 0.1). The spectra were measured at the operating frequency of 300MHz for ^{1}H.

The sharp peak at +2.5 ppm corresponds to the inorganic phosphate peak from the phosphate buffer solution in all studied samples (Fig. SI6.5-7).

The free phosphine ligand appears at -17 ppm (Fig. SI6.5-7, panels A).[1] Once cisplatin is added (Fig. SI6.5B-C), two singlet peaks are observed around +13 ppm, probably corresponding to two chemically non-equivalent phosphorus atoms and suggesting the presence of both *cis*- and *trans*- oriented di-substituted cisplatin species considering literature reports.[2] However, these spectra represent a relatively complex scenario when comparing to the recently published data on the same reaction run in acidic medium.[3] Additionally, a singlet peak at +7 ppm is observed. We believe this peak can be attributed to the second sphere coordination of Pt centre by TCEP that is further explained

in Fig. SI6.7. Since cisplatin has a low solubility, the concentrations used in this experiment are too weak to obtain a strong signal-to-noise ratio in these spectra and the small peaks due to the ^{195}Pt splitting of the ^{31}P resonances are not visible. This would have allowed definitive assignment of both the cis- and trans- cisplatin species, as the coupling constant is very different in these two compounds. To address it, we run analogous experiment using highly soluble K_2PtCl_4 (Fig. SI6.6).

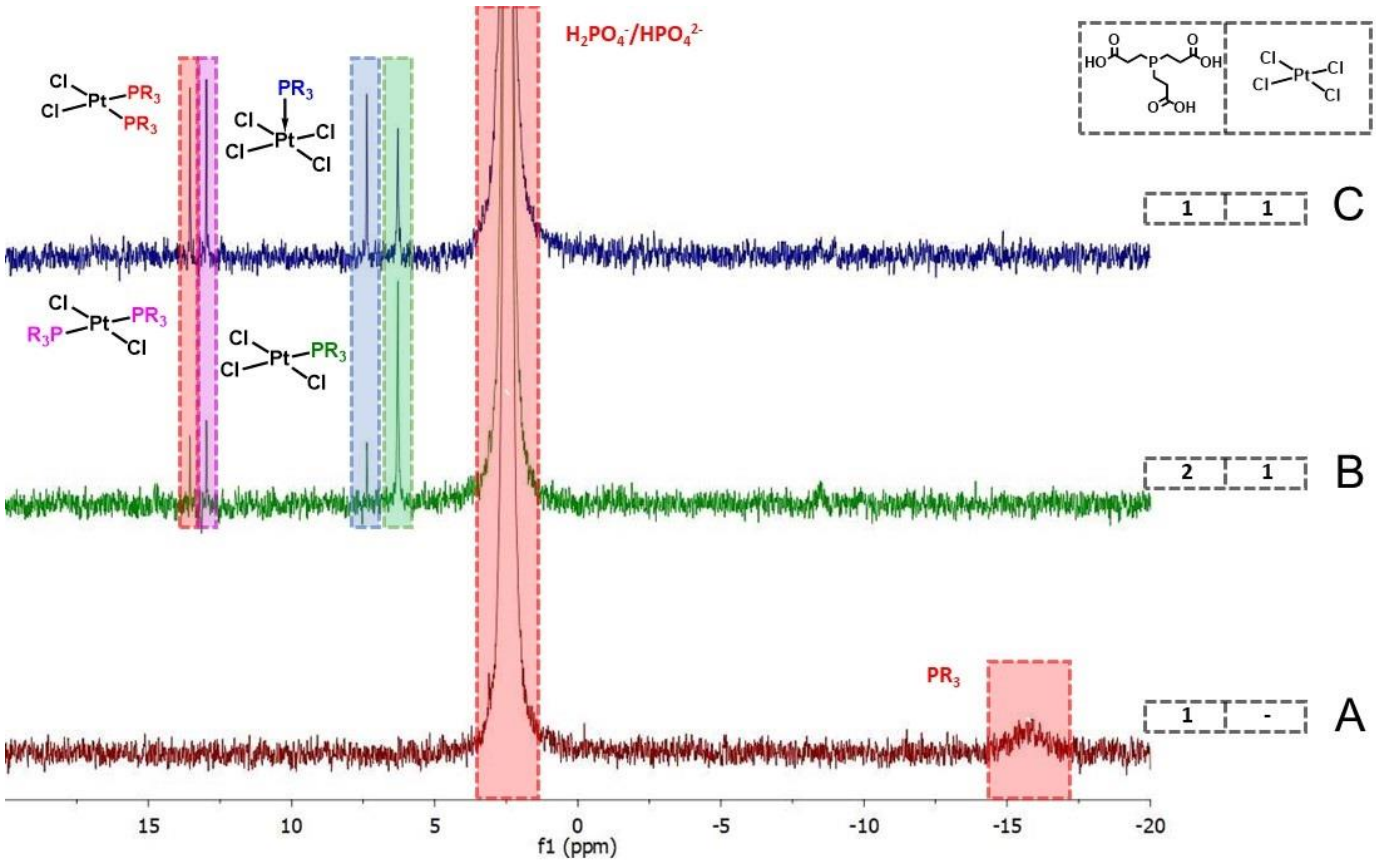

Figure SI6.6. 1D ^{31}P NMR spectra for the reaction of TCEP with K_2PtCl_4 (ratios indicated in the side panel) in 1 M phosphate buffer with 150 mM of NaCl (pH = 8.1 ± 0.1). The spectra were measured at the operating frequency of 300MHz for ^{1}H.

Similarly to Fig. SI6.5, addition of K_2PtCl_4 results in a decrease of the TCEP peak at -17 ppm along with the formation of new ones. Once TCEP molecules coordinate to the K_2PtCl_4 we observe two singlet peaks at + 13 ppm (likely *cis*- and *trans*-oriented products) and two singlet peaks at +6 ppm and + 7 ppm. The latter can be attributed to the second-sphere coordination. As K_2PtCl_4 is more soluble than cisplatin, two small satellite peaks at +22 ppm (not shown) and -8 ppm with a coupling constant of J = 3580 Hz around the peak at +6 ppm are visible resulting from the ^{195}Pt splitting the ^{31}P signal This suggests formation of mono-substituted Pt-centre[4] as a result of the lack of cooperativity when compared to cisplatin.

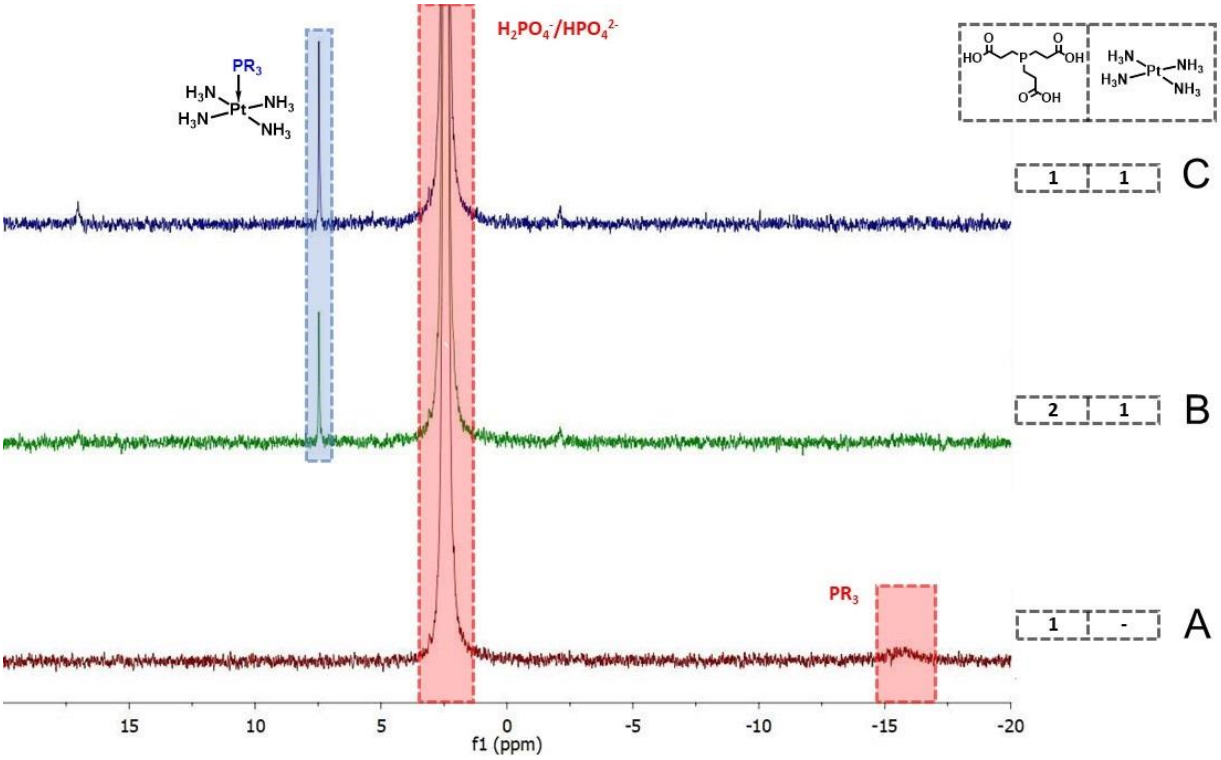

Figure SI6.7. 1D ^{31}P NMR spectra for the reaction of TCEP with $PT(NH_3)_4(NO_3)_2$ (ratios indicated in the side panel) in 1 M phosphate buffer with 150 mM of NaCl (pH = 8.1 ± 0.1). The spectra were measured at the operating frequency of 300MHz for ^{1}H.

Addition of $Pt(NH_3)_4(NO_3)_2$ results in a decrease of that signal along with an increase of a new signal at +7 ppm that we attribute to the second sphere coordination of Pt centre by TCEP ligands. Small peaks at +17 ppm and -2 ppm are suspected to be the resonances resulting from the coupling of ^{31}P with the NMR active nucleus ^{195}Pt, with a 33.7% natural abundance. It was not possible to measure their intensities given the weak signal-to-noise ratio in these spectra. However, the coupling constant J can be estimated to be 2320 Hz.

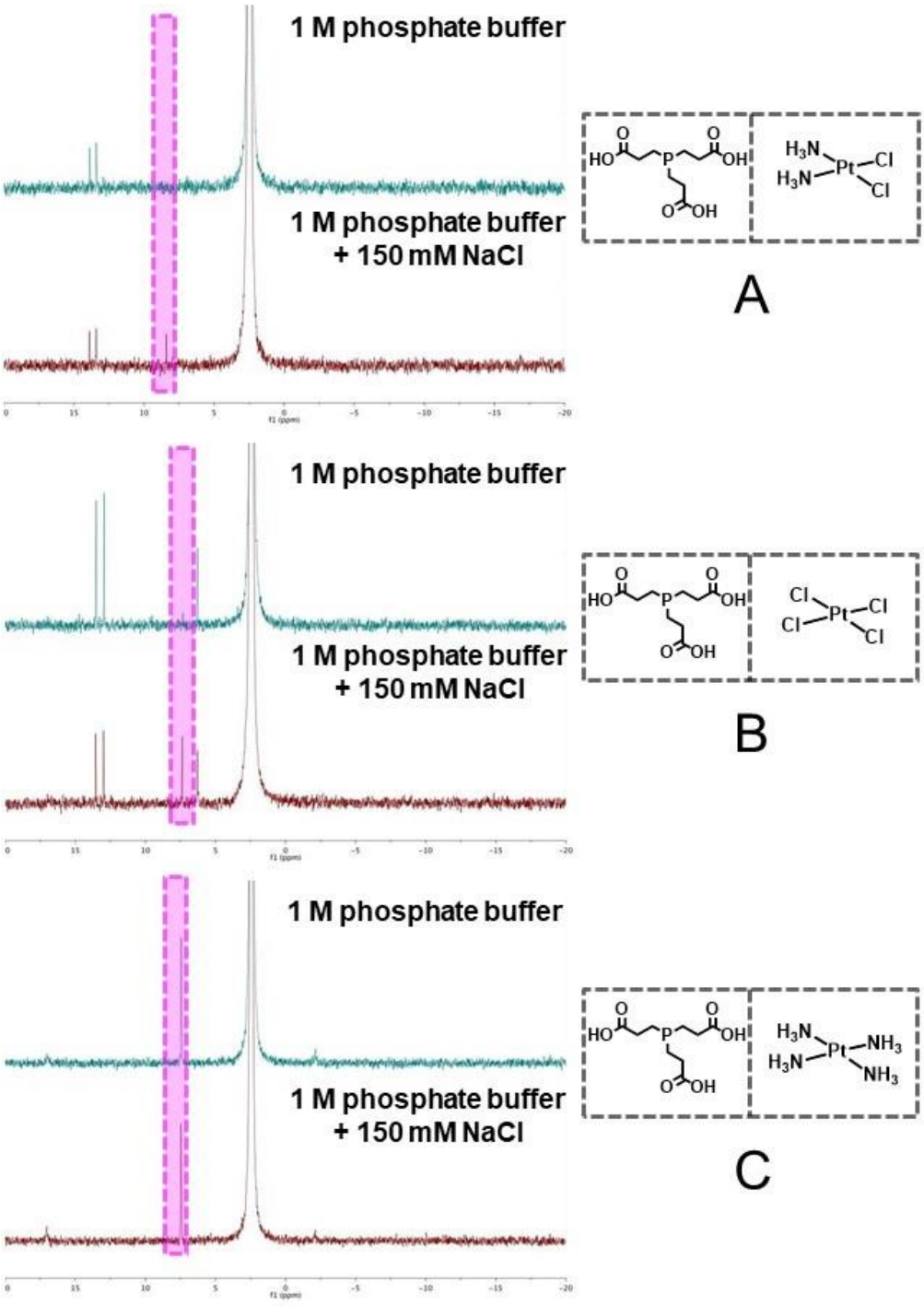

Figure SI6.8. ^{31}P spectra for the reaction of TCEP with (A) 1 equivalent of cisplatin (B) 1 equivalent of K_2PtCl_4 (C) 1 equivalent of $Pt(NH_3)_4(NO_3)_2$ in 1M phosphate buffer (pH = 8.1 ± 0.1) in the presence (i) and absence (ii) of 150 mM NaCl.

In the case of cisplatin (A) coordination by TCEP ligands, the absence of NaCl results in no formation of the peak corresponding to the second-sphere coordination. The second-sphere coordination peak is not present due to the facilitated Pt-Cl dissociation and TCEP being involved only in a direct metal coordination. These results are confirmed by the case of K_2PtCl_4 (B) and clearly suggest the impact of Pt-Cl dissociation equilibria on the reaction progress. Similar experiment performed for the coordination of $Pt(NH_3)_4(NO_3)_2$ (C) shows no effect of NaCl addition.

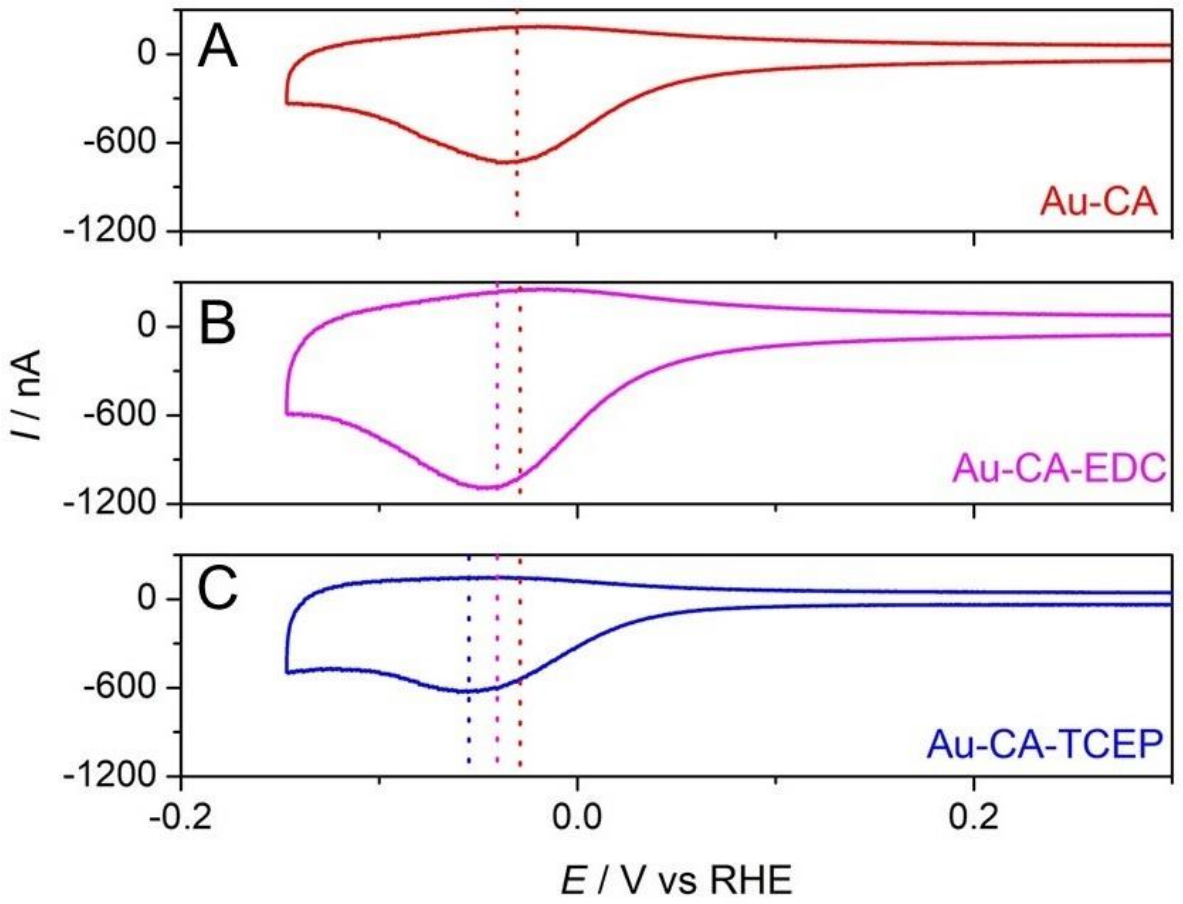

Figure SI6.9. Voltammetric profiles of Au electrodes at different stages of modification, namely (A) for Au-CA, (B) for Au-CA and exposed to the solution of EDC (with no TCEP intentionally added), (C) for Au-CA-TCEP. Vertical dotted lines are shown for the clearer indication of the peak potential shift. All recorded in DPBS medium at a scan rate of $\upsilon = 0.05\ V\ s^{-1}$.

As discussed in the manuscript, coupling of TCEP to the CA-assembled on gold electrode results in the shift of the thiol desorption peak towards more negative values. Here we confirm that this shift cannot be attributed to the exposure to EDC (B) as it gives only slight change in the peak value. Moreover, exposure to EDC with no TCEP being present results in the overall increase in the double-layer currents what may be attributed to interactions between Au-CA and EDC.

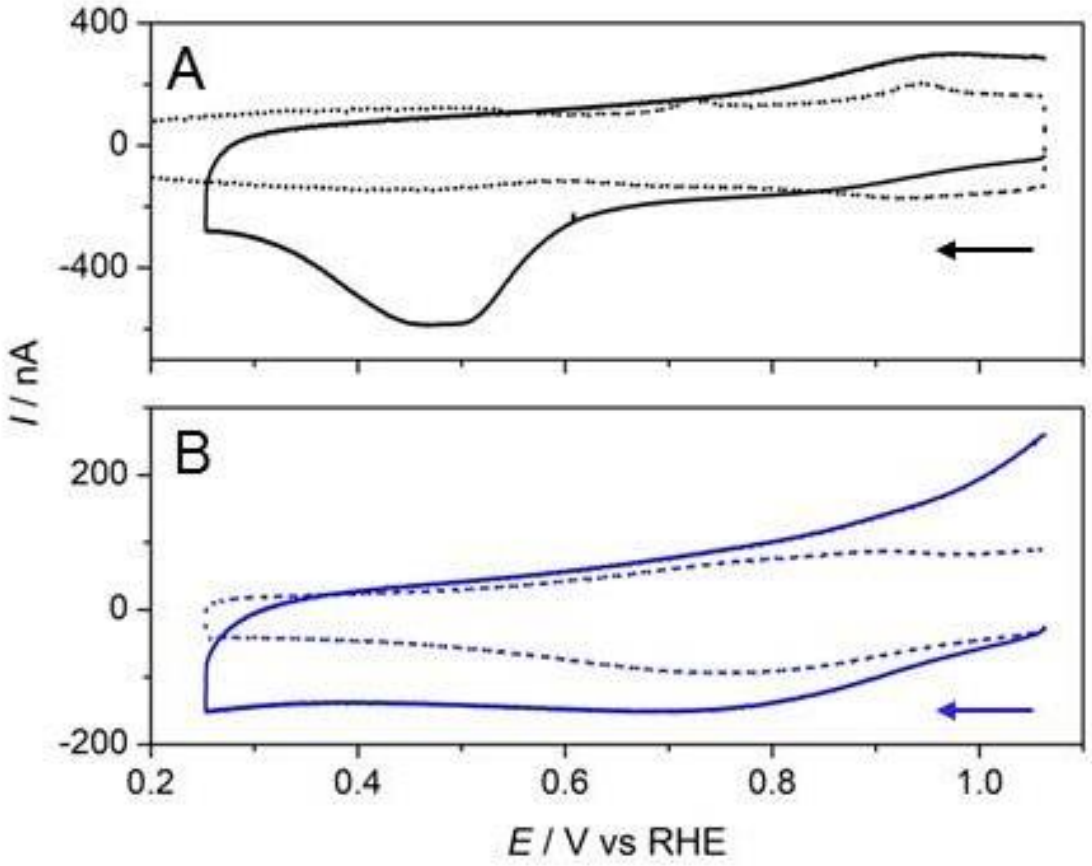

Figure SI6.10. Voltammetric profiles of Au (A), Au-CA-TCEP (B) before (⋯) and after (—) exposure to 1 mM solution of cisplatin in DPBS over 30 minutes. Scan rate υ = 0.05 V s^{-1}.

Cisplatin irreversibly adsorbs on the surface of bare gold (A) and gets reduced in the first scan, as reported in the literature.[5] In case of Au-CA-TCEP, we observe a not well-defined cathodic wave that cannot be unambiguously assigned to the reduction of Pt^{2+} to Pt^{0}. More prominent features suggesting the presence of cisplatin are observable in voltammetric profiles recorded in a broader potential range (Fig. SI6.11).

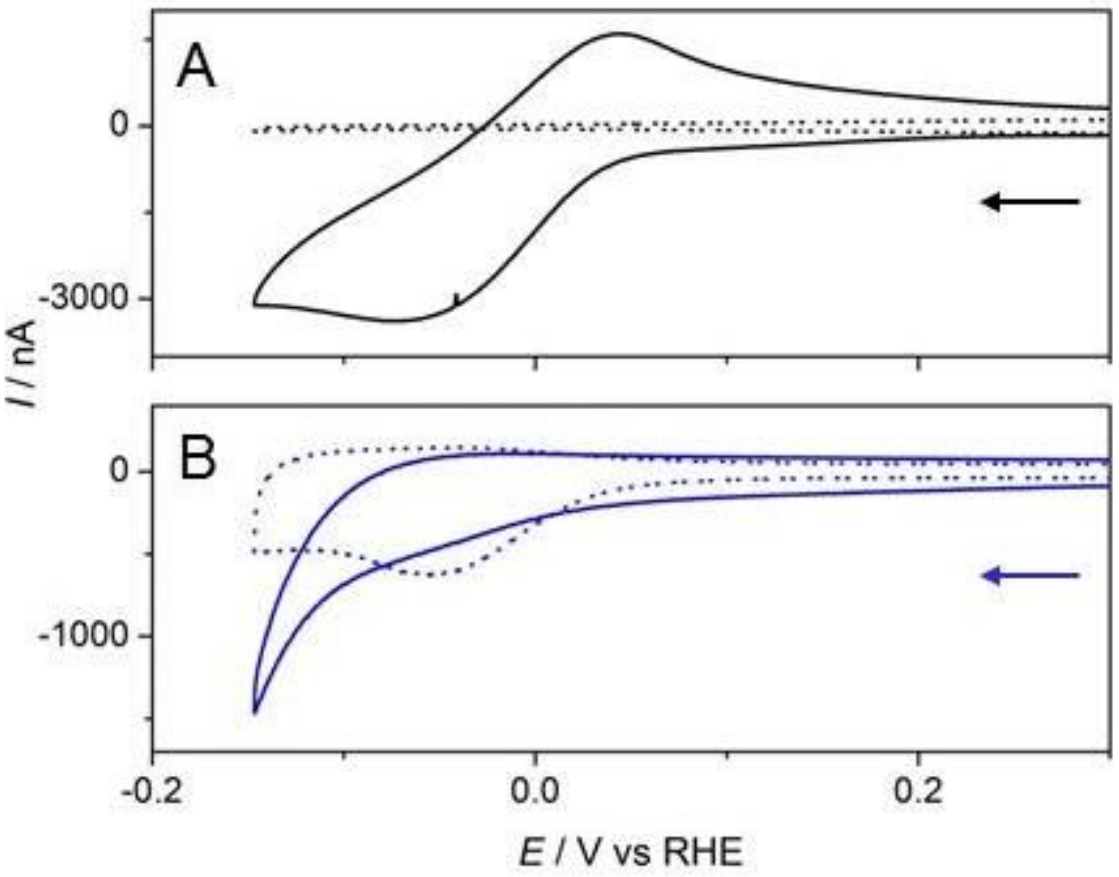

Figure SI6.11. Voltammetric profiles of Au (A), Au-CA-TCEP (B) before (⋯) and after (—) exposure to 1 mM solution of cisplatin in DPBS over 30 minutes. These profiles were recorded in a potential region of high electrochemical activity of Pt. Scan rate υ = 0.05 V s^{-1}.

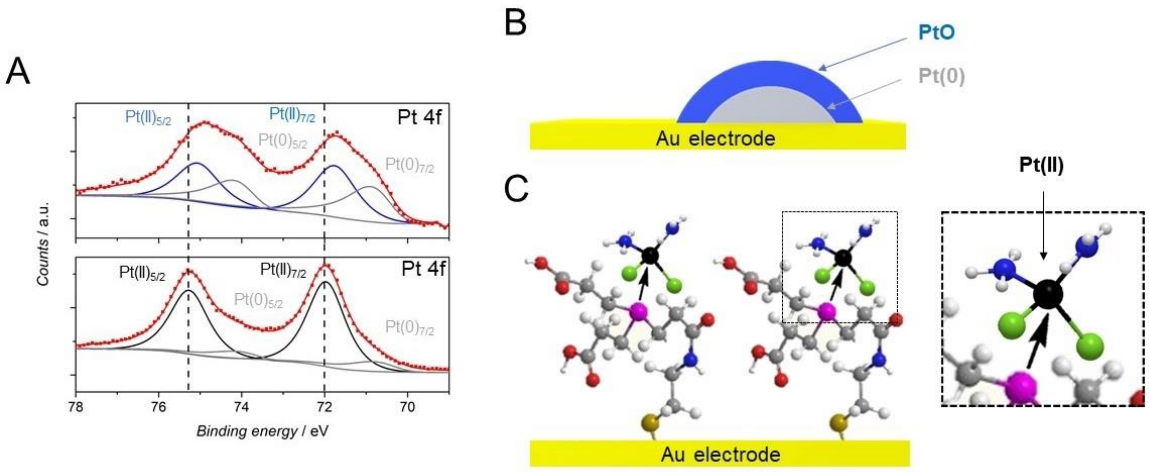

Figure SI6.12. (A) XPS spectra corresponding to Au (top), Au-CA-TCEP (bottom) after exposure to cisplatin solution in DPBS and electrochemical cycle in a studied potential range along with the corresponding models (B, C). (■) and (—) correspond to experimental data and the fitting, respectively. (—), (—), (—) correspond to deconvoluted peaks assigned to be Pt(II) (origining from cisplatin), Pt(II) (origining from re-oxidized Pt(0)) and Pt (0), respectively . Vertical dashed line (¦) is shown for the sake of comparison.

A clear shift in the position of a peak corresponding to Pt(II) species can be observed. We believe this shift reflects on different scenarios taking place at two electrodes. Electrochemical reduction of cisplatin adsorbed on bare gold (B) leads to the formation of Pt(0) particles that undergo partial oxidation to the corresponding oxide due to being exposed to air. Cisplatin adsorbed on Au-CA-TCEP (C) does not undergo complete reduction during electrochemical cycle (Fig. SI6.10B) in the studied potential range, most of it remains in its initial form Pt(II).

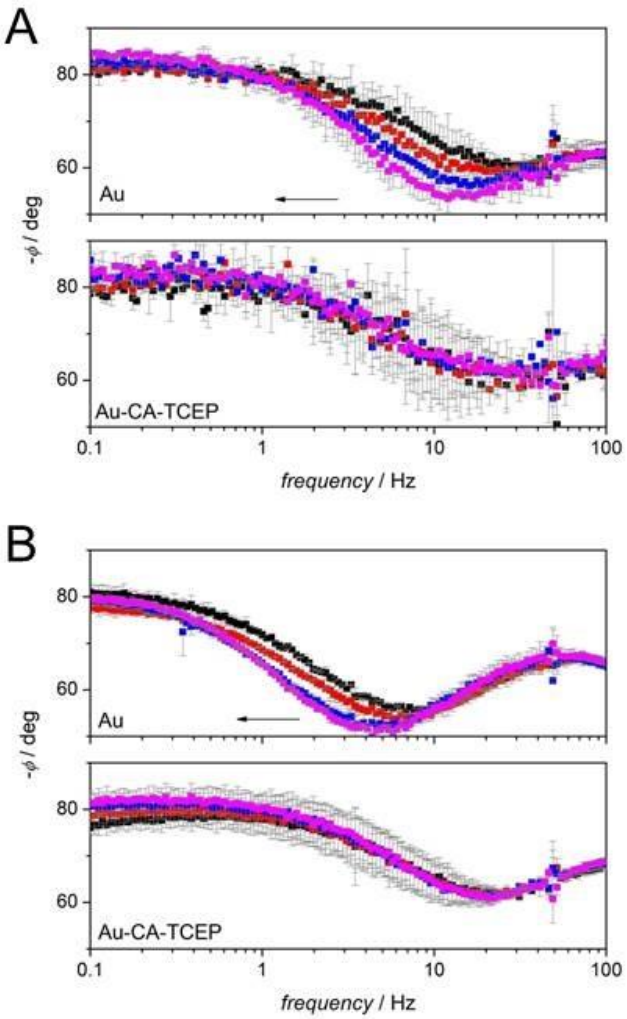

Figure SI6.13. Phase angle profiles for the interactions of Au and Au-CA-TCEP with cisplatin (A) and K_2PtCl_4 (B) at 0.95 V (■), 0.85 V (■), 0.75 V (■), 0.65 V (■) vs RHE. Error bars are presented in grey for the sake of clarity.

As can be seen, gold electrodes exposed to solutions of cisplatin and K_2PtCl_4 display similar behaviour, where the phase angle minimum shifts towards lower frequency values as the potential applied to the electrode is lower. This behaviour is not observed when Au-CA- TCEP electrodes are exposed to the same solutions – phase angles profiles overlap across studied potential range. Although both, Au and Au-CA-TCEP adsorb Pt-based species, their potential-dependent behaviour upon binding to Pt is different,

suggesting that binding on Au-CA-TCEP does not take place in the pinholes of the monolayer where Au remains uncovered.

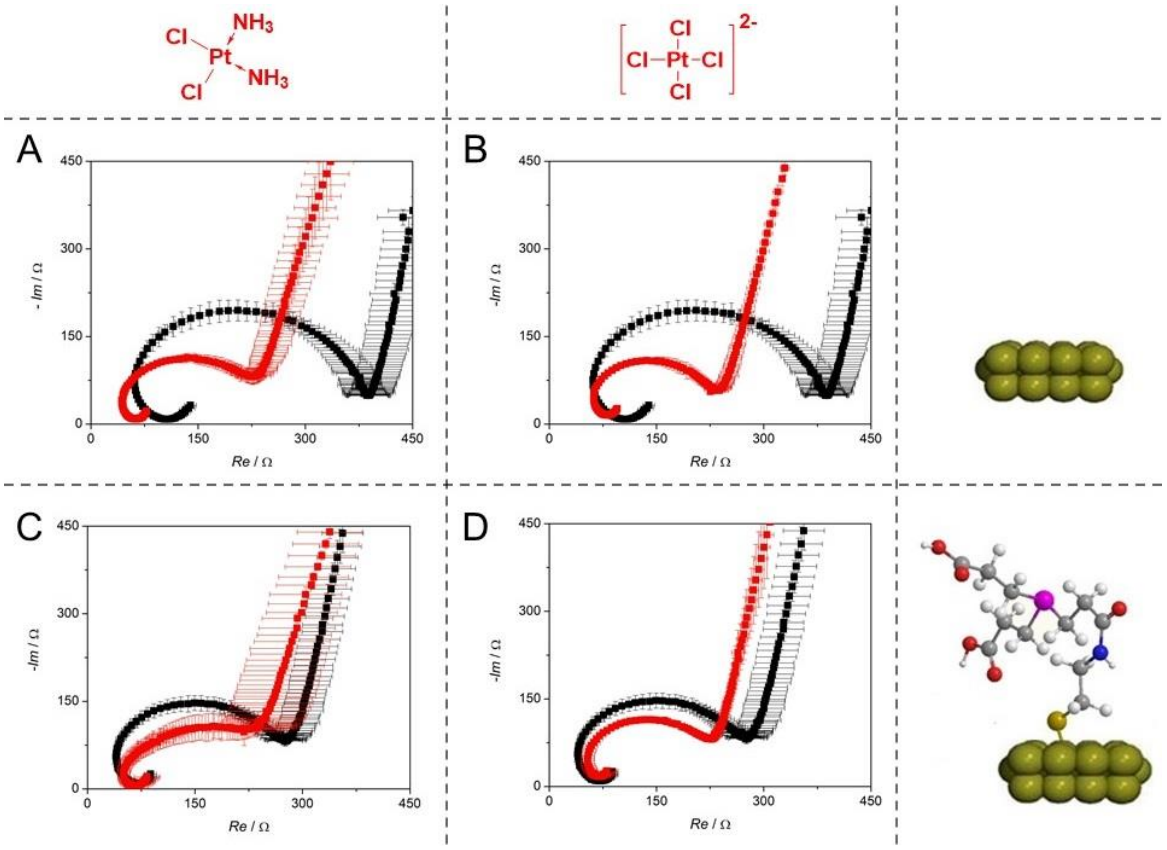

Figure SI6.14. Nyquist plots recorded after exposure of Au (A,B) and Au-CA-TCEP (C,D) to solutions of cisplatin (A,C) and K_2PtCl_4 (B,D) (10 mM and 1 mM in DPBS, respectively) recorded at 0.95 V vs RHE in DPBS. (■) correspond to blank spectra, (■) correspond to spectra after adsorption step.

Figure SI6.14 shows Nyquist plots of Au and the Au-CA-TCEP electrodes. Spectra of both surfaces show a series combination of the interfacial capacity and the solution resistance. These data imply that ion transport in the SAM was occurring over the timescale of the experiment. The real part of the impedance, which is associated to the charge-transfer resistance, decreased in the case of CA-TCEP-modified electrodes when compared to bare gold electrodes. This is an indication that the ion diffusion through the CA-TCEP layer is impeded. When the electrodes were exposed to cisplatin, the impedance spectrum of Au bare electrode showed a significant decrease of real component of the resistance.

This change is due to the adsorption of charged Pt- ionic species on the surface of gold. The CA-TCEP-modified electrodes exposed to the cisplatin also showed a decrease on the resistance associated to the adsorption of charged Pt- ionic species. The decrease of the resistance was smaller probably associated to electron tunnelling through the CA-TCEP.[6] Nevertheless, this system requires more experimental work to be fully understood.

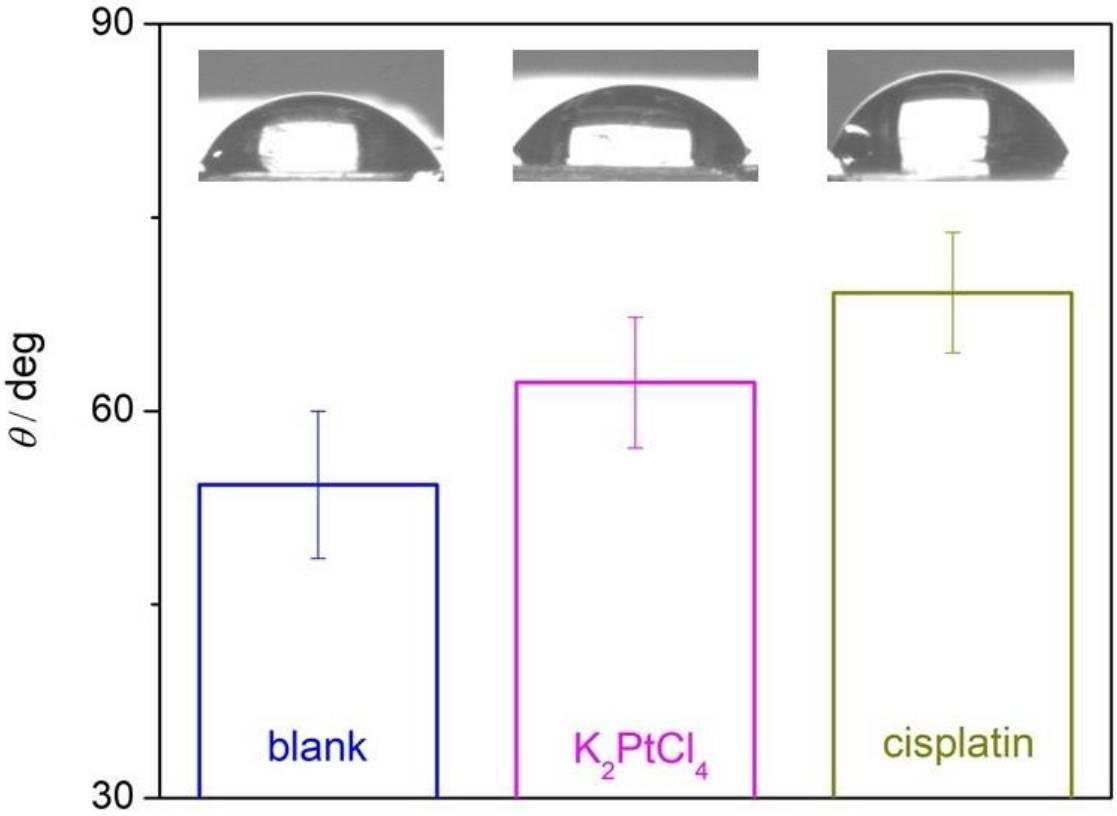

Figure SI6.15. Contact angle measurements using deionised water of Au-CA-TCEP before and after exposure to the solution of K_2PtCl_4 or cisplatin.

Au-CA-TCEP (blank) provides highly hydrophilic carboxylic acid groups that increase the wettability. Exposure of Au-CA-TCEP to K_2PtCl_4 and cisplatin solutions causes an increase in the contact angle due to occupation of hydrophilic carboxylic acid sites, where the increase in case of cisplatin is higher as it is relatively more hydrophobic[7].

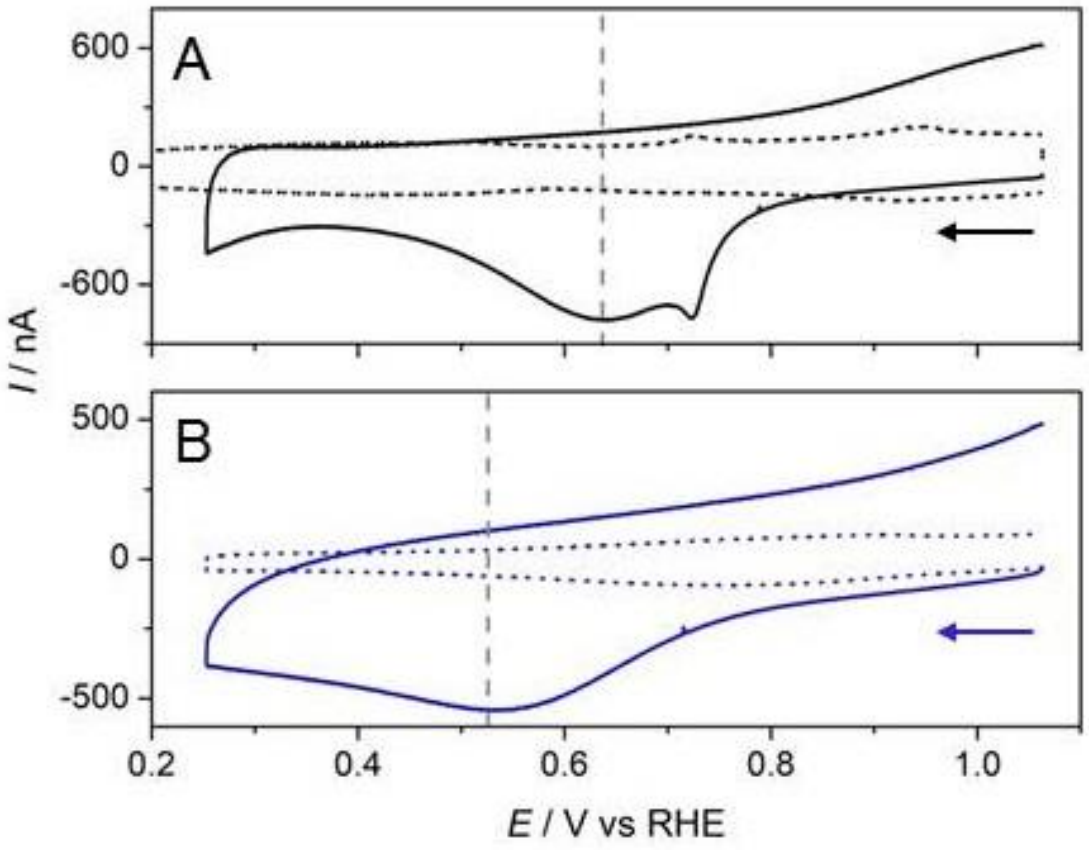

Figure SI6.16. Voltammetric profiles of Au (A), Au-CA-TCEP (B) before (⋯) and after (—) exposure to 10 mM solution of K_2PtCl_4 in DPBS over 15 minutes. Scan rate υ = 0.05 V s^{-1}.

In the case of bare gold (A) K_2PtCl_4 irreversibly adsorbs on the surface and gets reduced in the first scan and it is visualised by the peak at 0.63 V vs RHE (dashed black vertical line). Similar observations have been reported in the literature[8, 9]. The voltammetric profile of Au-CA-TCEP (B) shows a broad cathodic peak at 0.53 V vs RHE (dashed blue vertical line) after exposure to 10 mM K_2PtCl_4 solution. This feature can be attributed to the reduction of Pt^{2+} to Pt^0, and 100 mV shift with respect to similar process on bare gold (dashed black vertical line) suggests this reaction takes place onto the surface modification. Similar observations were made by Kolb et al. on the deposition of metal onto thiol-modified electrode through pre-adsorption step.[10, 11]

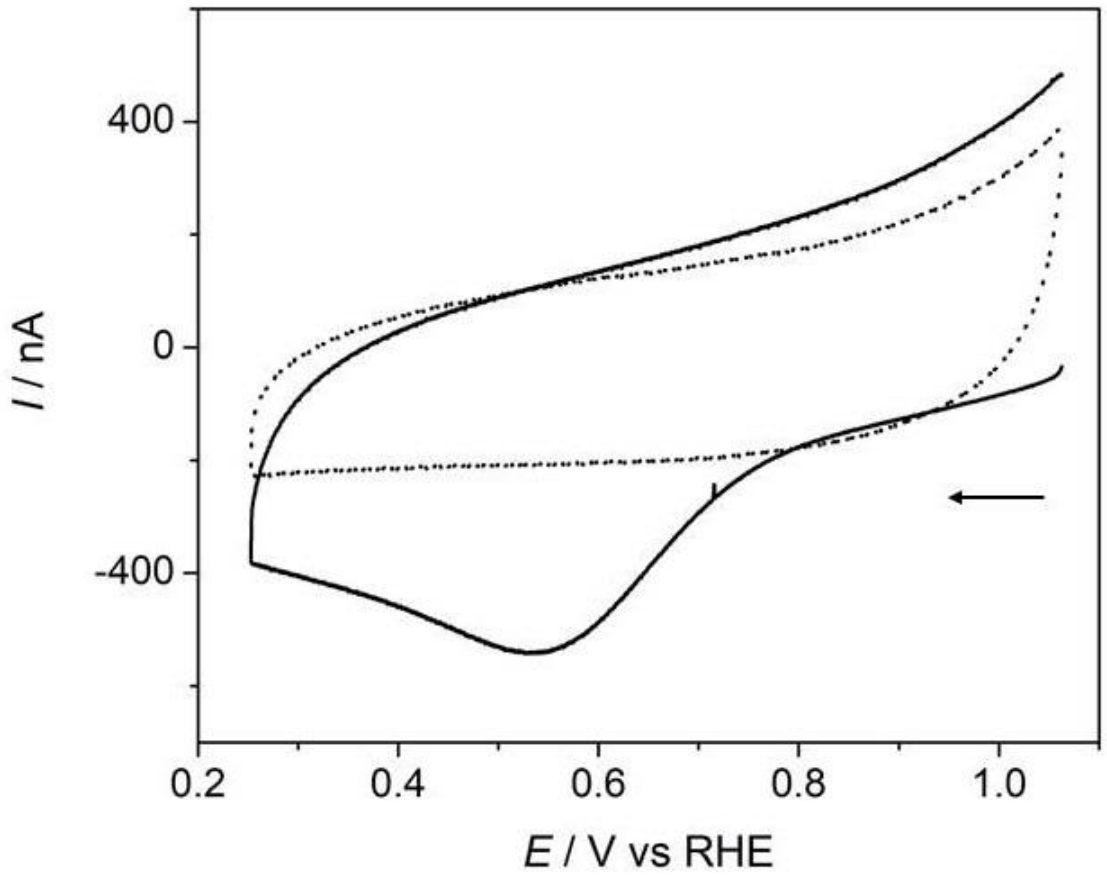

Figure SI6.17. Voltammetric profile of Au-CA-TCEP exposed to 10 mM solution of K_2PtCl_4 in DPBS over 15 minutes and transferred to Pt-free electrochemical cell filled with DPBS. (—) and (···) lines correspond to the first and the second scan, respectively. Scan rate υ = 0.05 V s^{-1}.

The first scan (solid black line) shows a defined reductive peak that corresponds to the irreversible reduction of Pt^{2+} to Pt^0. The second scan (dotted black line) does not show any reactivity in this potential range suggesting that reduction has been quantitatively performed during the first scan. This open doors for the quantification of the amount of Pt species on the electrode surface, and therefore, quantification in the solution based on the integration of charge involved in the reductive process (when using voltammetric methods) as shown in Fig. SI6.18, or the direct application of chronocoulometry[12].

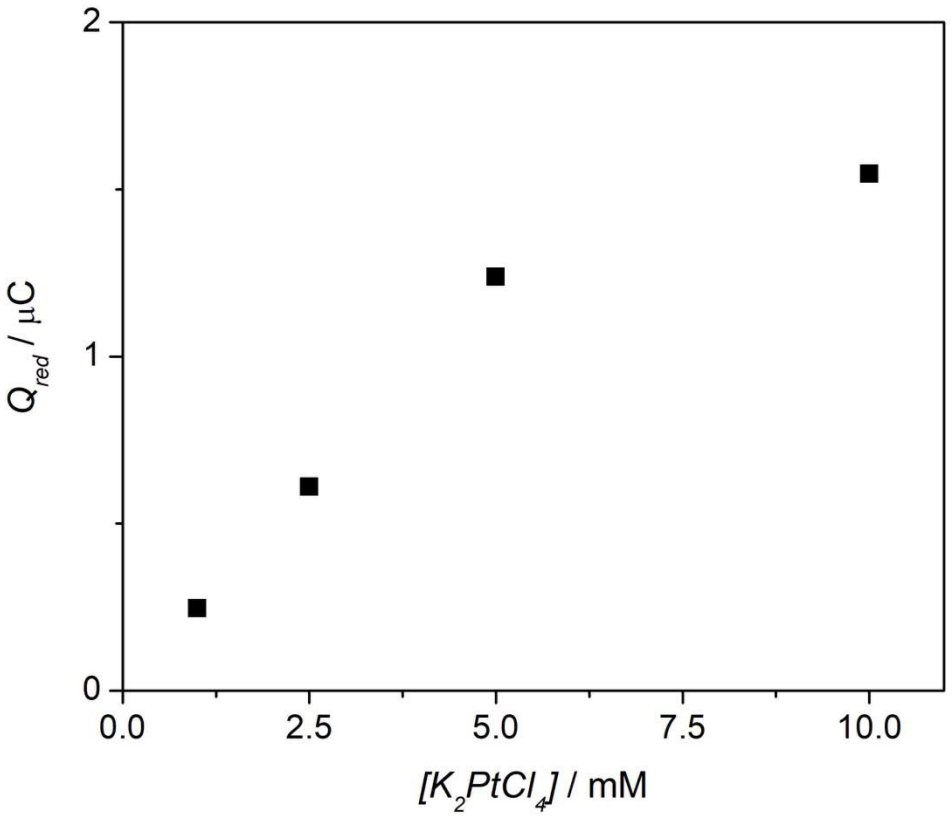

Figure SI6.18. Charge involved in the reductive process on Au-CA-TCEP after immersion in differently concentrated solutions of K_2PtCl_4 in DPBS for 15 minutes at open circuit potential.

6.9. References

1. A. Krezel, R. Latajka, G. D. Bujacz and W. Bal, *Inorg. Chem.*, 2003, **42**, 1994-2003.
2. S. O. Grim, R. L. Keiter and McFarlan.W, *Inorg. Chem.*, 1967, **6**, 1133-1137.
3. S. Chen, H. Jiang, K. Wei and Y. Liu, *Chem. Commun.*, 2013, **49**, 1226-1228.
4. A. Pidcock, in *Catalytic Aspects of Metal Phosphine Complexes*, American Chemical Society, 1982, vol. 196, ch. 1, pp. 1-22.
5. A. Kolodziej, M. C. Figueiredo, M. T. M. Koper, F. Fernandez-Trillo and P. Rodriguez, *Electrochim. Acta*, 2017, **248**, 409-415.
6. L. V. Protsailo and W. R. Fawcett, *Electrochim. Acta*, 2000, **45**, 3497-3505.
7. J. A. Platts, D. E. Hibbs, T. W. Hambley and M. D. Hall, *J. Med. Chem.*, 2001, **44**, 472-474.
8. Y. Nagahara, M. Hara, S. Yoshimoto, J. Inukai, S.-L. Yau and K. Itaya, *J. Phys. Chem. B*, 2004, **108**, 3224-3230.
9. I. Bakos, S. Szabó and T. Pajkossy, *J. Solid State Electrochem.*, 2011, **15**, 2453-2459.
10. V. Ivanova, T. Baunach and D. M. Kolb, *Electrochim. Acta*, 2005, **50**, 4283-4288.
11. M. Manolova, V. Ivanova, D. M. Kolb, H. G. Boyen, P. Ziemann, M. Büttner, A. Romanyuk and P. Oelhafen, *Surf. Sci.*, 2005, **590**, 146-153.
12. L. Shen, Z. Chen, Y. Li, P. Jing, S. Xie, S. He, P. He and Y. Shao, *Chem. Commun.*, 2007, 2169-2171.

Chapter 7: Conclusions

The aim of this PhD project was to design and create the electrochemical system for the filtration of toxic anticancer drugs from blood. The removal of toxic drugs is of utmost importance for patients undergoing chemotherapy since the excess of introduced drugs is not metabolised. This leads to the accumulation of toxic species in body tissues and lowers the quality of life. This disadvantage was particularly extensively reported for cisplatin; therefore, this molecule was the main target of the thesis.

This challenge was approached in a unique way, not previously reported in the literature. Since this is the first-time electrochemistry was used for the removal and detection of Pt-based drugs, many aspects of the proposed system were studied.

The main findings of this dissertation are:

i) Chapter 4 provides the evidence for cisplatin adsorption on the surface of gold. It is proposed that the process is mediated by phosphate anions that are known to be prone to adsorb on gold and to coordinate Pt^{2+} species. Therefore, the amount of adsorbed Pt is governed by the amount of adsorbed phosphate anions. Additionally, cisplatin adsorbs on the surface of gold in the potential range from 0.85 V to 1.65 V vs RHE. At lower potential values cisplatin gets electrochemically reduced to Pt particles. If higher potential is applied, no interaction between cisplatin and gold is observed due to surface of gold being covered with an oxide layer.

This is of great importance for the project as it determines a safe potential range where cisplatin does not get reduced on bare gold was determined.

ii) Chapter 5 describes factors that affect the electrochemical stability of thiols and disulfides assembled on gold. It is dependent on the number sulfur atoms the molecule is chemisorbed through, although the structure of a thiol (length of carbon chain, functional groups) has an impact on it as well.

Chapter 4 also demonstrates that monolayers are more stable on Au(100) surface as compared to Au(111) due to the difference in value of the potential of zero total charge for differently oriented gold surfaces.

This is of great importance for the project since a safe potential range where thiol- and disulfide-based modifications are stable was determined with an outlook into the future on how to modulate the modifying molecule and/or the underlying surface to achieve better stability.

iii) One of the main findings of the Chapter 6 is that TCEP coordinates to cisplatin in physiological medium much quicker than natural chelators such as glutathione or DNA, reaching a plateau within an hour. Introduction of TCEP molecule to the modification of gold electrode can be achieved through EDC-catalysed on-surface coupling reaction. No change in the integrity of the monolayer was observed upon TCEP introduction.

Gold electrodes modified with TCEP functionality reproduce its affinity from heterogeneous phase towards Pt^{2+} species. A well-defined signal corresponding to the reduction of Pt^{2+} to Pt^{0} was recorded following the

immersion of modified electrode in the solution of K_2PtCl_4 in a physiological medium. Similar observations were not made for the case of adsorption of cisplatin, due to higher energy required for its transformation to Pt^0.

It is of great importance for the project because a time-efficient ligand coordinating cisplatin was found and introduced as a surface modification. It was shown to be Pt-responsive what gives a great promise to the use of surface-confined scavenging of Pt species.

Along with many important developments that were achieved over the course of this project, number of challenges were faced. A future work would have to address them:

i) *Electrode material:* although gold serves as an excellent platform for the modification via thiol/disulfide self-assembly, it strongly interacts with cisplatin. This may cause adsorption the drug, and if a sufficiently negative potential is applied – a reduction to metallic platinum. Pt is known to possess high catalytic properties and its exposure to blood components could lead to undesired and potentially harmful transformations. To overcome these disadvantages, other types of conductive platforms could be applied. The most obvious choice, carbon, offers multiple modification strategies to prepare functional interfaces.[1] Nevertheless, rather complex surface chemistry of carbon materials would make it difficult to be homogeneously functionalised. Another opportunity is represented by doped silicon surfaces. They were extensively reported for the broad scope of possible functionalisations[2] and applications in electrochemical sensing[3]. Moreover,

unmodified surface of silicon is covered with a native oxide which is known to be inert and no article on its interactions with Pt complexes was reported.

ii) *Surface modification:* even though thiols are extensively reported as excellent modifiers of gold surfaces, their applicability is a subject of discussions. They were reported to be chemically unstable.[4] Moreover, their electrochemical stability is limited with a very recent results from Bizzotto Group (University of British Columbia, Canada) showing that the integrity of monolayers is affected at much earlier potential than the apparent cathodic peak.[5] This instability could be overcome by the application of different modification strategy. An electrografting of diazonium salt was reported for number of substrates and is believed to form much more stable layers as compared to self-assembled monolayers of thiols but the preparation procedure is more demanding and may lead to the formation of multi-layered structures.[6] A very promising approach was reported in 2014 when N-heterocyclic carbenes (NHCs) were self-assembled on gold electrodes.[7] These were shown to be extremely stable under various conditions and further applications proved their usefulness. Moreover, this solution gained interest of biosensor manufacturing companies as the one providing reproducible products. This strategy could be of great use for this project as provides stable underlying structure preventing from non-specific interactions.

iii) *Enhancement of adsorption capacity:* the work presented in this thesis was performed on a flat bead-type electrode. Considering the applied, yet fundamental nature of this PhD project, introduction of high surface area platform is a natural step forward. Such a platform could be made of nanoparticles that offer some tunability in terms of size[8] and shape[9] while remaining their modification potential.

iv) *Interferences:* the work presented in this thesis was fully performed in a physiological phosphate buffer. Even tough it is known to be a competitive medium, especially when it comes to the coordination to various species, it does not reflect on the composition of blood – a medium that would be used in the real-life application. Therefore, future work needs to address the effect of the presence of haemoglobin, proteins and sugars in the electrolyte on the performance of the system.

v) *Flow effects:* the work presented in this thesis was performed in the stationary conditions. It is of great relevance to transform these results to the system that work in flow. Certain aspects, such as diffusion of cisplatin to the surface of the electrode are expected to improve. Nevertheless, to my knowledge, no article has reported the stability of thiol-modified electrode exposed to the constant flow. This would certainly be an important aspect of future developments of the electrochemical hemofiltration system.

7.1. References

1. P. Allongue, M. Delamar, B. Desbat, O. Fagebaume, R. Hitmi, J. Pinson and J. M. Saveant, *J. Am. Chem. Soc.*, 1997, **119**, 201-207.
2. A. Langner, A. Panarello, S. Rivillon, O. Vassylyev, J. G. Khinast and Y. J. Chabal, *J. Am. Chem. Soc.*, 2005, **127**, 12798-12799.
3. M. J. Schoning, A. Kurowski, M. Thust, P. Kordos, J. W. Schultze and H. Luth, *Sensor. Actuat. B-Chem.*, 2000, **64**, 59-64.
4. C. Vericat, M. E. Vela, G. Benitez, P. Carro and R. C. Salvarezza, *Chem. Soc. Rev.*, 2010, **39**, 1805-1834.
5. K. K. Leung, A. D. Gaxiola, H. Z. Yu and D. Bizzotto, *Electrochim. Acta*, 2018, **261**, 188-197.
6. J. J. Gooding, *Electroanalysis*, 2008, **20**, 573-582.
7. C. M. Crudden, J. H. Horton, Ebralidze, II, O. V. Zenkina, A. B. McLean, B. Drevniok, Z. She, H. B. Kraatz, N. J. Mosey, T. Seki, E. C. Keske, J. D. Leake, A. Rousina-Webb and G. Wu, *Nat. Chem.*, 2014, **6**, 409-414.
8. T. K. Sau, A. Pal, N. R. Jana, Z. L. Wang and T. Pal, *J. Nanoparticle Res.*, 2001, **3**, 257-261.
9. Y. G. Sun and Y. N. Xia, *Science*, 2002, **298**, 2176-2179.